Antenna Laboratory Report No. 69-5

MULTIPLE SCATTERING BY SPHERES

by

John H. Bruning
Y. T. Lo

Technical Report

May 1969

Sponsored by

National Science Foundation
Washington, D.C. 20550
Grant No: NSFGK-4161

Antenna Laboratory
Department of Electrical Engineering
Engineering Experiment Station
University of Illinois
Urbana, Illinois

ERRATA SHEET

Page in thesis

19 in equation (2.27), the terms sin mϕ inside the two brackets should be preceded by i, i.e., should read:

$$\begin{bmatrix} \cos m\phi \\ i \sin m\phi \end{bmatrix}\hat{\theta} \quad \& \quad \begin{bmatrix} i \sin m\phi \\ \cos m\phi \end{bmatrix}\hat{\phi}$$

21 equation (2.31) should read:

$$A^{mn}_{m\nu} = -B^{mn}_{m\nu} \approx \ldots .$$

22 Second to last line, the term B^{11}_{11} should read:

$$B^{11}_{11} = -3e^{iz}(1-iz)/2z^2$$

23 3rd line, p(1,1) should read: $p(1,1) = -i\frac{3}{4}$

24 3rd line, A_{E_1} should read: $A_{E_1} = -\frac{3i}{4}\left[\ldots \frac{(\quad)}{1-u(ka)A_1}\right]^{-1}$

43 equation (4.1) all signs are +

44 2nd line should be $i\hat{\phi}$ instead of $-i\hat{\phi}$

157 equation (A24) should read:

$$+ \frac{ikd \sin \theta_o}{2\nu(\nu+1)} \quad [\ \ldots\ ]$$

158 equation (A28) should be $\begin{bmatrix} r \leq d \\ r \geq d \end{bmatrix}$

164 equation (A47) should read:

$$A^{mn}_{\mu\nu} = -B^{mn}_{\mu\nu} \approx \ldots$$

MULTIPLE SCATTERING BY SPHERES

Abstract

Multiple scattering of electromagnetic or acoustic waves by two or three spheres is studied in great detail using three different approaches: the multipole expansion, ray optics, and experimental measurements. The first method requires a translational addition theorem, the complexity of which has till now severely restricted its numerical usefulness. In this connection an important recursion relation is derived which allows routine calculation of the required translation coefficients. Incorporating this with other simplifications has decreased computation times by several orders of magnitude and has increased the usable range of the solution so that multiple scattering can be accurately computed for spheres of any material as large as 10 wavelengths in radius at any separation (even in contact). Particularly simple forms are presented for the special cases of Rayleigh scattering and far multiple scattering. Extensive numerical results are presented and compared, whenever possible, with the experimental results; the agreement is remarkably good in all cases. Multiple scattering by two spheres using this method is also discussed from the point of view of depolarization.

The ray optical approach is formulated in terms of pure geometric optics rays, creeping wave rays, and hybrid rays. This approach is basically restrictive to large spheres, but it is shown to yield excellent results even for spheres as small as 1/2 wavelength radius. This method (at present limited to perfectly conducting spheres) provides a simple

physical picture of the scattering mechanism and can be used to predict many interesting phenomena. The limitations and applications are discussed with the aid of a large number of examples.

Acoustic scattering by two spheres is treated using the modal expansion and incorporates many of the simplifications used in the electromagnetic problem. A closed form for far multiple scattering is derived and a unique correspondence to the electromagnetic problem is noted. This problem is discussed with the aid of numerical results. Finally the three sphere problem is formulated and numerical and experimental results are presented for a few special cases.

General remarks concerning the various approaches are summarized and suggestions for future research are made.

TABLE OF CONTENTS

LIST OF FIGURES

1. INTRODUCTION

Over the past century scattering by a sphere has been one of the most widely studied problems in diffraction theory. The widespread interest in this problem, aside from its practical value, stems from the fact that the sphere is one of the very few bodies for which the complete scattering behavior is known. This makes the sphere an ideal candidate for testing approximate solutions to more complex scattering problems.

The more difficult problem of multiple scattering, the scattering by many objects, has interested investigators for an equally long period of time, but progress has been slower. The reason for this is that one must know not only the solution for the component scatterers (when isolated), but how the presence of each object affects the scattering by all the others (i.e., coupling effects). There is a great body of literature on the subject which has recently been surveyed by Twersky (1960) and Burke and Twersky (1964).

The motivation for extensive research in this area has been the better understanding of problems associated with: propagation through rain, the study of sols, air polution, meteorology, to name only a few.

It seems only natural that together with some very general formulations for rigorous and approximate multiple scattering theory (Twersky, 1962, 1967; Zitron and Karp, 1961a and 1961b) there must also be a thorough investigation of some very basic problems in multiple scattering; i.e., one that plays an analogous role to the isolated sphere in single body scattering theory. Such a fundamental problem in two dimensions is the scattering by two parallel circular cylinders. This has

been studied by Twersky (1952) and Row (1955). The very simplest three dimensional multiple scattering problem involving the scattering by bodies of finite extent is the two sphere scattering problem. Certainly then, this very fundamental multiple scattering problem deserves a thorough investigation.

In 1935 Trinks presented the solution to the boundary value problem of electromagnetic scattering by two spheres. His solution employed an "addition theorem" which allowed him to expand the field of each sphere about the spherical coordinate origin of the other and thereby satisfy the boundary conditions on each sphere in the presence of the other. Due to the extreme complexity of the addition theorem, he was able to give explicit results only for spheres of radius much less than a wavelength. His solution was later reviewed by Mevel (1960) and Lillesaeter (1964) but with no attempt made for solution (numerical or otherwise) beyond the Rayleigh region. While Trinks' results were presented only for plane wave incidence on two identical spheres from the endfire and broadside directions, Germogenova (1963) extended his results to the case of an arbitrary angle of incidence and spheres of unequal size. More recently, Liang and Lo (1967), and Crane (1967) reformulated the two sphere problem using a newly derived form of the addition theorem given by Stein (1961) and Cruzan (1962). While Crane gave no numerical results, Liang and Lo presented numerical results for a few special cases of metallic spheres. They indicate their method to be applicable for spheres of radius less than 3/4 wavelength at wide spacing. Bonkowski, et al., (1953), using geometric optics, found the backscattered field from a pair of identical metallic spheres at broadside incidence. Angelakos and Kumagai (1964) extended

their results to an array of spheres and gave some experimental results.

None of these treatments are unified to the extent that multiple scattering by spheres of arbitrary size can be computed. The modal expansion solution of the problem is, in pricipal, exact for spheres of all sizes, but the complexity of the problem has thwarted even the most recent attempt at numerical solution on a high speed digital computer for spheres larger than a wavelength in radius. The advent of the computer has allowed us to solve, numerically, many problems that have not been possible any other way. This has forced us to view theoretical analysis in a somewhat new light. In other words, the value of a theoretical solution must now also be judged on the basis of its ability to yield to numerical solution.

The objective of this thesis is to present a complete investigation of the problem of multiple scattering by two spheres. The problem is studied using the multipole expansion technique, a ray optical formulation, and scattering experiments.

In Chapter 2 the classical multipole expansion technique is introduced and the appropriate addition theorem is given. With this, the boundary conditions on each sphere in the presence of the other are satisfied. Numerous simplifications are noted in the analysis, particularly for special geometries. Additionally, when the sphere separation is large, the form of the addition theorem is shown to reduce to a particularly simple form. This gives rise to the far multiple scattering approximation. The Rayleigh approximation for small spheres is given in closed form.

Chapter 3 is concerned with the problem of the numerical analysis of the modal expansion solution. The various functions involved are discussed in terms of efficient techniques for generation in this particular

problem. Then an important recursion relation is introduced which allows routine calculation of the coefficients involved in the translational addition theorem. With the introduction of this and previously referred to symmetries, calculation times have been reduced by several orders of magnitude, and the range of sphere sizes to which the method is applicable has been extended to spheres nearly 10 wavelengths in radius. Furthermore, the sphere materials are arbitrary.

In Chapter 4 the basic structure of the computer programs is discussed and some computer times are given. These programs are used to compute radar cross-sections of many different cases which are compared with experimental results obtained using the methods discussed in Chapter 7. These results include radar cross-sections for spheres of different sizes and materials for the following three basic configurations:

Endfire incidence—variable separation

Broadside incidence—variable separation

Variable angle of incidence—fixed separations.

The agreement between experiment and theory in all these cases is remarkably good. Numerical results are also obtained for bistatic cross-sections and backscattering from two spheres in contact for fixed orientations and variable sphere size. Multiple scattering is also discussed in the context of depolarization with illustrative numerical examples.

Chapter 5 discusses the fundamentals of geometric optics and creeping wave theory and introduces hybrid rays. Numerous examples are considered using this ray optics method for two perfectly conducting spheres and comparison is made with the modal expansion approach. Although this is a high frequency approach, it is shown that results can be quite

accurately predicted even for spheres as small as 1/2 wavelength in radius. The advantages, limitations and extensions of the method are discussed.

In Chapter 6 the modal expansion technique is applied to cover the additional case of acoustic scattering by two spheres. Refinements made in the addition theorem for the vector problem are also applicable to this scalar case. In addition to the scalar character of the problem, the solution may be simplified further in cases involving symmetries. The scalar addition theorem, when applied to widely separated spheres is shown to yield a closed form solution for two spheres involving only scattering functions of the individual spheres. A unique connection between this problem and the electromagnetic problem is cited for particular configurations. Numerical results are given for equal spheres at broadside and endfire incidence for soft and hard spheres at ka = 2 and 10. Chapter 6 is concluded with a brief discussion of the three sphere problem with a few numerical results and experimental verifications.

The experimental measurement technique is discussed in detail in Chapter 7. There the problems associated with supporting two spheres and making dynamic radar cross-section measurements are discussed and several techniques are described and evaluated.

General conclusions are drawn in Chapter 8 and recommendations for further research are made.

2. MODAL OR MULTIPOLE EXPANSION APPROACH TO THE TWO SPHERE BOUNDARY VALUE PROBLEM

The solution of the problem of scattering of scalar or vector waves by two or more spherical bodies requires the satisfaction of appropriate boundary conditions on the surfaces of all scatterers simultaneously. Unfortunately there is no separable coordinate system for the wave equation whose coordinate surfaces coincide with all the surfaces in question. The modal or multipole expansion for the scattered field of each sphere in the presence of the others can still be made to satisfy the boundary conditions on each sphere provided we have an appropriate "addition theorem." The required translational addition theorem relates the scalar or vector wave functions with respect to one origin in terms of those with respect to another. By imposing the boundary conditions on each sphere there results a set of simultaneous equations. In the case of two dimensional problems involving circular cylinders, the translational addition theorem is elementary and there involves no coupling between the TE and TM waves. In the case of the three dimensional problem involving spheres, the theorem becomes so complicated that it is difficult to render even numerical solution, despite the many theoretical analyses that have appeared over the past thirty years. Even recently available numerical results were restricted to relatively small spheres at large spacings.

In this chapter the classical multipole expansion technique is reviewed and the vector spherical wave addition theorem is introduced. Several special cases of interest are considered and as a result, great simplification can be achieved. Later, an important recursion relation

is discussed, from which the scattering can be accurately and economically computed from spheres of diameters as large as fifteen wavelengths and as close as physical contact. With this recursion relation, the computational effort is reduced by several orders of magnitude.

2.1 Multipole Expansion Technique

Consider two spherical bodies A and B of arbitrary material of radii a and b whose centers lie at the origins of two spherical coordinate systems 0 and 0' separated by a distance d. With no loss in generality one may assume 0 and 0' to lie along the z-axis, with a point in space having the coordinates (r,θ,ϕ) and (r',θ',ϕ) with respect to the two systems respectively. Further let there be incident on these two spheres a uniform plane wave of unit strength whose propagation vector $\hat{k}$ lies in the xz plane and makes an angle α with the z axis as shown in Figure 2.1. The incident electric field is assumed to be plane polarized at an angle γ with a line in xz perpendicular to $\hat{k}$. The problem is then to find the scattered electromagnetic field everywhere in space after satisfying the boundary conditions on each sphere in the presence of the other.

The electric and magnetic fields in a source free homogenous medium satisfy Maxwell's equations

$$\nabla \times \bar{E} = i\omega\mu\bar{H}$$
$$\nabla \times \bar{H} = - i\omega\epsilon\bar{E} \qquad (2.1)$$

and hence the vector Helmholtz equation

$$\nabla \times \nabla \times \bar{A} - k^2\bar{A} = 0 \qquad (2.2)$$

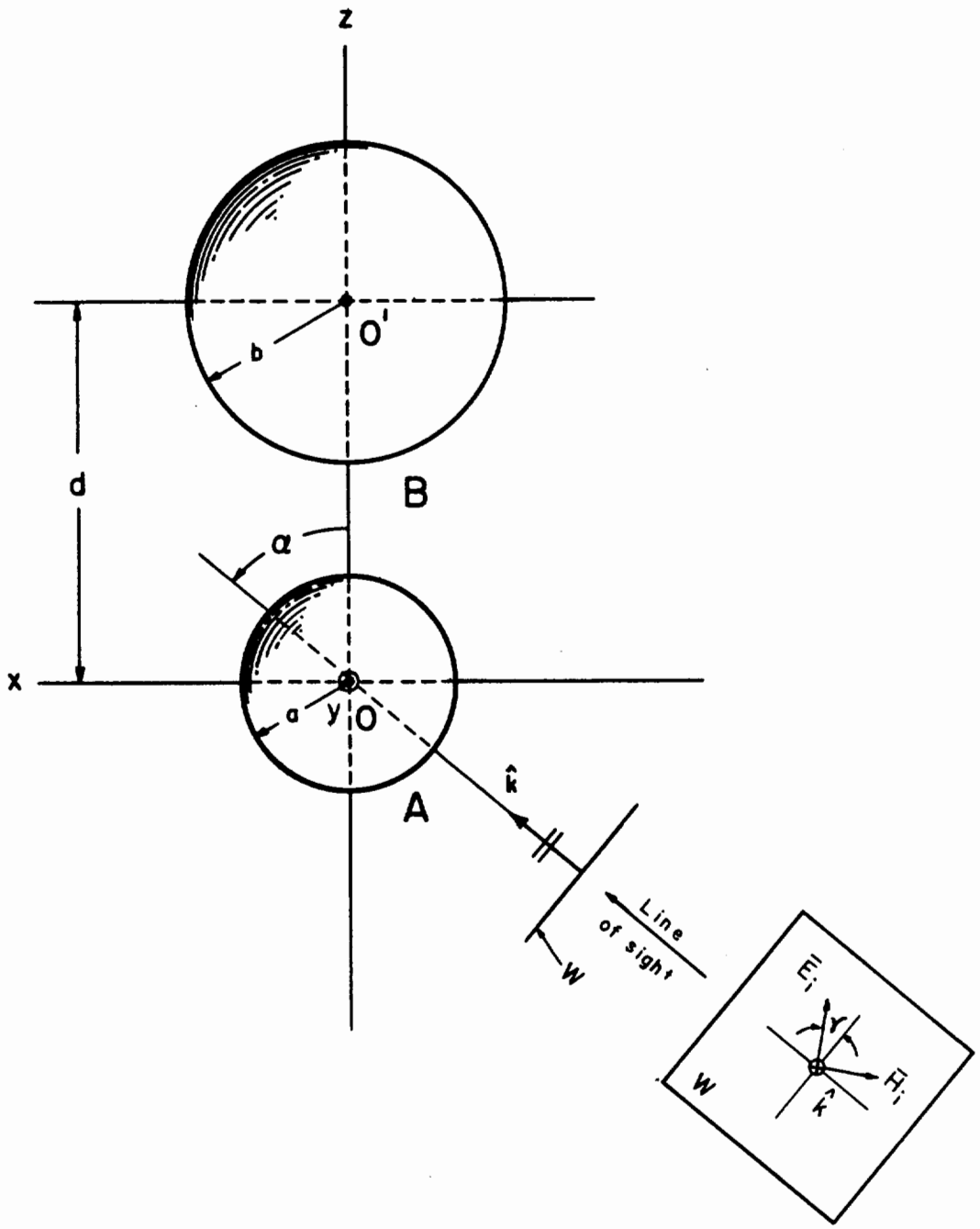

Figure 2.1 Geometry of Two Sphere Problem.

where $k^2 = \omega^2\mu\varepsilon$ and $\bar{A}$ is the vector field $\bar{E}$ or $\bar{H}$.[†]

Stratton (1941) shows that there are two independent vector solutions to equation (2.2):

$$\bar{M}_{mn}^{(j)} = \nabla u_{mn}^{(j)} \times \bar{r}$$

and (2.3)

$$\bar{N}_{mn}^{(j)} = \frac{1}{k} \nabla \times \bar{M}_{mn}^{(j)}$$

where $\bar{r}$ is the position vector for the spherical coordinate system 0 with coordinates (r,θ,ϕ) and the scalar potentials $u_{mn}^{(j)}$ are characteristic solutions of the scalar wave equation

$$\nabla^2 u + k^2 u = 0 \tag{2.4}$$

and are given by:

$$u_{mn}^{(j)} = z_n^{(j)}(kr) P_n^m(\cos\theta) e^{im\phi}; \quad 0 \leq n < \infty, \ |m| \leq n. \tag{2.5}$$

$z_n^{(j)}$ represents the appropriate spherical Bessel function j_n, n_n, $h_n^{(1)}$, or $h_n^{(2)}$, to be denoted respectively by the superscripts j = 1,2,3, and 4; P_n^m is the associated Legendre function as defined by Stratton. From (2.3) and (2.5) can be written the explicit forms for the vector spherical waves:

$$\bar{M}_{mn}^{(j)} = z_n^{(j)}(kr) \frac{im}{\sin\theta} P_n^m(\cos\theta) e^{im\phi} \hat{\theta} - z_n^{(j)}(kr) \frac{\partial}{\partial\theta} P_n^m(\cos\theta) e^{im\phi} \hat{\phi}$$

[†] A harmonic time factor $e^{-i\omega t}$ is assumed throughout this work and is suppressed hereafter.

$$\bar{N}_{mn}^{(j)} = \frac{1}{kr} z_n^{(j)}(kr)n(n+1)P_n^m(\cos\theta)e^{im\phi}\hat{r} \qquad (2.6)$$

$$+ \frac{1}{kr}\frac{\partial}{\partial r}[rz_n^{(j)}(kr)]\frac{\partial}{\partial\theta}P_n^m(\cos\theta)e^{im\phi}\hat{\theta}$$

$$+ \frac{1}{kr}\frac{\partial}{\partial r}[rz_n^{(j)}(kr)]\frac{im}{\sin\theta}P_n^m(\cos\theta)e^{im\phi}\hat{\phi}$$

Clearly $\bar{M}_{mn}^{(j)}$ has no radial component and hence all radial fields must be represented by $\bar{N}_{mn}^{(j)}$ alone. Therefore, H modes (TE) which have only a magnetic radial component, have $\bar{H}$ represented by $\bar{N}_{mn}^{(j)}$ and $\bar{E}$ by $\bar{M}_{mn}^{(j)}$; for E modes (TM), the opposite is true. An arbitrary electromagnetic field, which generally involves both types of modes, can then be written as (Stratton, 1941):

$$\bar{E} = \sum_{n=1}^{\infty}\sum_{m=-n}^{n}(A_{mn}\bar{M}_{mn}^{(j)} + B_{mn}\bar{N}_{mn}^{(j)})$$

$$\bar{H} = -\frac{ik}{\omega\mu}\sum_{n=1}^{\infty}\sum_{m=-n}^{n}(A_{mn}\bar{N}_{mn}^{(j)} + B_{mn}\bar{M}_{mn}^{(j)}) \qquad (2.7)$$

This is usually referred to as a multipole, modal, or partial wave expansion. From (2.6) it is clear that the n = 0 term vanishes and hence this is omitted in (2.7). The unknown coefficients A_{mn} and B_{mn} and the superscripts (j) are determined by the boundary conditions and the incident field.

2.2 Vector Spherical Wave Addition Theorem

In the case of two spheres, in order to satisfy the boundary conditions on each sphere in the presence of the other, an "addition theorem" is needed so that all the multipole fields about 0 can be expressed in terms of multipole fields about 0' and vice versa. For example, to satisfy

the boundary conditions on sphere B at 0', outgoing spherical waves from 0 must be expressible in terms of standing spherical waves about 0'. The addition theorem for this case is a specialization of the more general rigid translation discussed in the Appendix. Here translation is confined to the z axis with no loss in generality and is given by:

$$\begin{aligned} \bar{M}^{(3)'}_{mn} &= \sum_{\nu=(1,m)}^{\infty} (A^{mn}_{m\nu}\bar{M}^{(1)}_{m\nu} + B^{mn}_{m\nu}\bar{N}^{(1)}_{m\nu}) \\ \bar{N}^{(3)'}_{mn} &= \sum_{\nu=(1,m)}^{\infty} (A^{mn}_{m\nu}\bar{N}^{(1)}_{m\nu} + B^{mn}_{m\nu}\bar{M}^{(1)}_{m\nu}). \end{aligned} \tag{2.8}$$

Here (and everywhere in the text) the prime indicates only association with the coordinate system with origin 0', and (1,m) symbolizes the larger of 1 and m. As implied above, the radial dependence on the LHS of (2.8) is $h^{(1)}_n(kr')$ and $j_\nu(kr)$ on the RHS. For translation from 0' to 0 the theorem corresponding to (2.8) is given by:

$$\begin{aligned} \bar{M}^{(3)}_{mn} &= \sum_{\nu=(1,m)}^{\infty} (-1)^{n+\nu}(A^{mn}_{m\nu}\bar{M}^{(1)'}_{m\nu} - B^{mn}_{m\nu}\bar{N}^{(1)'}_{m\nu}) \\ \bar{N}^{(3)}_{mn} &= \sum_{\nu=(1,m)}^{\infty} (-1)^{n+\nu}(A^{mn}_{m\nu}\bar{N}^{(1)'}_{m\nu} - B^{mn}_{m\nu}\bar{M}^{(1)'}_{m\nu}) \end{aligned} \tag{2.9}$$

This simple relationship between translation in opposite directions has not been noted by previous authors. The form of the translation coefficients $A^{mn}_{m\nu}$ and $B^{mn}_{m\nu}$ is very complicated and hence is left to the Appendix (see equations (A8), (A28), and (A.29)). Their computability is discussed in Chapter 3.

2.3 Expansion of the Incident Field

Before the boundary conditions can be applied to the spheres, the incident field must also be cast into a multipole expansion form. For an incident plane wave of unit strength with the geometry shown in Figure 2.1 we have

$$\begin{aligned} \bar{E}_i &= e^{i\bar{k}\cdot\bar{r}}\hat{e} \\ \bar{H}_i &= \frac{1}{\eta_o} e^{i\bar{k}\cdot\bar{r}}\hat{h} \end{aligned} \tag{2.10}$$

where

$$\begin{aligned} \hat{e} &= -\cos\alpha\cos\gamma\,\hat{x} + \sin\gamma\,\hat{y} + \sin\alpha\cos\gamma\,\hat{z} \\ \hat{h} &= -\cos\alpha\sin\gamma\,\hat{x} - \cos\gamma\,\hat{y} + \sin\alpha\sin\gamma\,\hat{z} \end{aligned} \tag{2.11}$$

and η_o is the impedance of free space. Using the scalar plane wave expansion for the incident vector $\hat{k}$ in the xz plane (Stratton, 1941):

$$e^{i\bar{k}\cdot\bar{r}} = \sum_{n=0}^{\infty}\sum_{m=-n}^{n} i^n(2n+1)\frac{(n-m)!}{(n+m)!}P_n^m(\cos\alpha)u_{mn}^{(1)} , \tag{2.12}$$

one can find the multipole coefficients of the expansion:

$$\bar{E}_i = \sum_{n=1}^{\infty}\sum_{m=-n}^{n}\left[p(m,n)\bar{N}_{mn}^{(1)} + q(m,n)\bar{M}_{mn}^{(1)}\right] \tag{2.13}$$

by using the orthogonality properties of the vector spherical wave functions and the trigonmetric functions with the results:

$$p(m,n) = -\, i^n \frac{2n+1}{n(n+1)} \frac{(n-m)!}{(n+m)!} [\tau_{mn}(\alpha)\sin\gamma + i\pi_{mn}(\alpha)\cos\gamma]$$

$$q(m,n) = i^n \frac{2n+1}{n(n+1)} \frac{(n-m)!}{(n+m)!} [\pi_{mn}(\alpha)\sin\gamma + i\tau_{mn}(\alpha)\cos\gamma] \qquad (2.14)$$

where

$$\tau_{mn}(\alpha) = \frac{m}{\sin\alpha} P_n^m(\cos\alpha)$$

$$\pi_{mn}(\alpha) = -\frac{\partial}{\partial\alpha} P_n^m(\cos\alpha). \qquad (2.15)$$

The coefficients for the case of an infinitesimal dipole source lying in the xz plane, at a finite distance from the spheres, may also be found from (2.14), however, in this case the functions in (2.15) contain an additional factor related to the distance to origin 0. This case is cited only for completeness and will not be discussed further. For details see Jones (1964).

The expansion (2.13) of $\bar{E}_i$ was made about 0 and we also need an expansion about 0'. For the latter case, all quantities on the right of (2.13) become primed where the coefficients p'(m,n) and q'(m,n) (for a plane wave source) differ from those in (2.14) only by the multiplicative phase factor $e^{ikd\cos\alpha}$.

2.4 Expansion of the Total Field

Before boundary conditions on the spheres can be satisfied, the incident and scattered field from both spheres must be expressed alternately in the two coordinate systems. About 0 the scattered field of sphere A in the presence of sphere B is (for $r \geq a$):

$$\bar{E}_S^A = \sum_{n=1}^{\infty} \sum_{m=-n}^{n} [A_E(m,n)\bar{N}_{mn}^{(3)} + A_H(m,n)\bar{M}_{mn}^{(3)}] \tag{2.16}$$

and the scattered field about 0' of sphere B in the presence of sphere A is (for $r' \geq b$):

$$\bar{E}_S^{B'} = \sum_{n=1}^{\infty} \sum_{m=-n}^{n} [B_E(m,n)\bar{N}_{mn}^{(3)'} + B_H(m,n)\bar{M}_{mn}^{(3)'}] \tag{2.17}$$

where $A_E(m,n)$, $A_H(m,n)$, $B_E(m,n)$ and $B_H(m,n)$ are respectively the unknown multipole coefficients for the E and H modes of spheres A and B. With (2.8), (2.9), (2.13), (2.16), and (2.17), the total field about 0 and 0' can be written. About 0 the result is:

$$\begin{aligned}\bar{E}_T = \sum_{nm} [&p(m,n)\bar{N}_{mn}^{(1)} + q(m,n)\bar{M}_{mn}^{(1)} + A_E(m,n)\bar{N}_{mn}^{(3)} + A_H(m,n)\bar{M}_{mn}^{(3)} \\ &+ B_E(m,n) \sum_{\nu} (A_{m\nu}^{mn}\bar{N}_{m\nu}^{(1)} + B_{m\nu}^{mn}\bar{M}_{m\nu}^{(1)}) \\ &+ B_H(m,n) \sum_{\nu} (A_{m\nu}^{mn}\bar{M}_{m\nu}^{(1)} + B_{m\nu}^{mn}\bar{N}_{m\nu}^{(1)})]\end{aligned} \tag{2.18}$$

Similarly, the total field about 0' is:

$$\begin{aligned}\bar{E}_T' = \sum_{nm} [&p'(m,n)\bar{N}_{mn}^{(1)'} + q'(m,n)\bar{M}_{mn}^{(1)'} + B_E(m,n)\bar{N}_{mn}^{(3)'} + B_H(m,n)\bar{M}_{mn}^{(3)'} \\ &+ A_E(m,n) \sum_{\nu} (-1)^{n+\nu}(A_{m\nu}^{mn}\bar{N}_{m\nu}^{(1)'} - B_{m\nu}^{mn}\bar{M}_{m\nu}^{(1)'}) \\ &+ A_H(m,n) \sum_{\nu} (-1)^{n+\nu}(A_{m\nu}^{mn}\bar{M}_{m\nu}^{(1)'} - B_{m\nu}^{mn}\bar{N}_{m\nu}^{(1)'})]\end{aligned} \tag{2.19}$$

The magnetic fields are obtained from above by interchanging the $\bar{N}_{mn}$'s and $\bar{M}_{mn}$'s and multiplying the result by $-ik/\omega\mu$.

2.5 Application of the Boundary Conditions

For spheres of arbitrary homogeneous composition the boundary conditions to be satisfied at the surface of each sphere in the presence of the other are continuity of the tangential electric and magnetic fields. Points interior to a sphere must of course be characterized by the vector wave functions $\overline{M}_{mn}^{(1)}$ and $\overline{N}_{mn}^{(1)}$ since the field quantities are finite there; the radiation condition requires that we choose $\overline{M}_{mn}^{(3)}$ and $\overline{N}_{mn}^{(3)}$ for points exterior to both spheres. Lastly it is understood that in equations (2.16) through (2.19) the coefficients $A_E(m,n)$, $A_H(m,n)$, $B_E(m,n)$ and $B_H(m,n)$ are different depending respectively on whether $\overline{r}$ and $\overline{r}'$ lie inside or outside of spheres A and B. With this in mind, the required continuity conditions are:

$$\hat{r} \times \overline{E}_T\Big|_{a^+} = \hat{r} \times \overline{E}_T\Big|_{a^-}$$

$$\hat{r} \times \overline{H}_T\Big|_{a^+} = \hat{r} \times \overline{H}_T\Big|_{a^-}$$

$$\hat{r}' \times \overline{E}'_T\Big|_{b^+} = \hat{r}' \times \overline{E}'_T\Big|_{b^-}$$

$$\hat{r}' \times \overline{H}'_T\Big|_{b^+} = \hat{r}' \times \overline{H}'_T\Big|_{b^-}$$

where the superscripts + and - indicate respectively outside and inside the surface of the spheres. Applying these conditions to (2.16) through (2.19) and using the orthogonality relation

$$\int_0^{\pi} \left(\frac{dP_n^m}{d\theta} \frac{dP_\ell^m}{d\theta} + \frac{m^2}{\sin\theta} P_n^m P_\ell^m \right) \sin\theta d\theta = \frac{2n(n+1)}{2n+1} \frac{(n+m)!}{(n-m)!} \delta_{\ell n} \qquad (2.20)$$

gives rise to four sets of coupled, linear, simultaneous equations in the unknown multipole coefficients:

$$
\begin{aligned}
A_E(m,n) &= v_n(ka)\{p(m,n) + \sum_{\nu} [A_{mn}^{m\nu} B_E(m,\nu) + B_{mn}^{m\nu} B_H(m,\nu)]\} \\
A_H(m,n) &= u_n(ka)\{q(m,n) + \sum_{\nu} [A_{mn}^{m\nu} B_H(m,\nu) + B_{mn}^{m\nu} B_E(m,\nu)]\} \\
B_E(m,n) &= v_n(kb)\{p'(m,n) + \sum_{\nu} (-1)^{n+\nu} [A_{mn}^{m\nu} A_E(m,\nu) - B_{mn}^{m\nu} A_H(m,\nu)]\} \\
B_H(m,n) &= u_n(kb)\{q'(m,n) + \sum_{\nu} (-1)^{n+\nu} [A_{mn}^{m\nu} A_H(m,\nu) - B_{mn}^{m\nu} A_E(m,\nu)]\}
\end{aligned}
\tag{2.21}
$$

where

$$
\begin{aligned}
v_n(\rho) &= -\frac{\mu_1 j_n(\rho) \frac{d}{d\rho}[N\rho j_n(N\rho)] - \mu_2 N^2 j_n(N\rho) \frac{d}{d\rho}[\rho j_n(\rho)]}{\mu_1 h_n^{(1)}(\rho) \frac{d}{d\rho}[N\rho j_n(N\rho)] - \mu_2 N^2 j_n(N\rho) \frac{d}{d\rho}[\rho h_n^{(1)}(\rho)]} \\
u_n(\rho) &= -\frac{\mu_1 j_n(N\rho) \frac{d}{d\rho}[\rho j_n(\rho)] - \mu_2 j_n(\rho) \frac{d}{d\rho}[N\rho j_n(N\rho)]}{\mu_1 j_n(N\rho) \frac{d}{d\rho}[\rho h_n^{(1)}(\rho)] - \mu_2 h_n^{(1)}(\rho) \frac{d}{d\rho}[N\rho j_n(N\rho)]}
\end{aligned}
\tag{2.22}
$$

and $\rho = kx = 2\pi x/\lambda$; x = a or b, the radius of the sphere. μ_1 and μ_2 are the permeabilities of the surrounding medium and the sphere material respectively and N^2 is the relative dielectric constant of the sphere material with respect to the surrounding medium; if the material is lossy, N^2 is complex.

The above coefficients are the well known coefficients for the external field of a single homogeneous dielectric sphere which have been tabulated as early as 1908 (Mie).

At this point it should be emphasized that the expressions in equation (2.21) are valid for determination of the multipole coefficients of any two spheres, equal or unequal in size, having the same or different material as long as the appropriate single sphere coefficients $u_n(\rho)$ and

$v_n(\rho)$ for each sphere are known.† In the case of a perfectly conducting sphere, the coefficients (2.22) reduce to

$$u_n(\rho) = -\frac{j_n(\rho)}{h_n^{(1)}(\rho)}$$

$$v_n(\rho) = -\frac{\frac{d}{d\rho}[\rho j_n(\rho)]}{\frac{d}{d\rho}[\rho h_n^{(1)}(\rho)]} \qquad (2.23)$$

The computation of the coefficients (2.22) involves some special considerations which will be elaborated upon in a later section.

Returning momentarily to the coupled sets of equations (2.21), it is clear that there is no coupling through the azimuthal modes (i.e., modes with different index m), hence, this system of equations may be solved independently for each m where $-n \leq m \leq n$, which represents in general, $2n+1$ sets of equations. As shown below there are several important special cases in which the form of (2.21) can be simplified considerably.

2.6 The Far Field Approximation

Of practical interest is the scattered field in the far zone. This can be obtained from (2.21), (2.16) and (2.17) and the asymptotic forms of the vector spherical wave functions when $r, r' \gg d$.†† The vector

---

† The precise form for $u_n(\rho)$ and $v_n(\rho)$ is also known for spheres composed of several concentric layers of different materials (Aden and Kerker, 1951) and even concentric layers of non-uniform dielectric constant (Levine and Kerker, 1963).

†† It is assumed that $d \geq a + b$, the case of coalescing spheres is not considered here.

spherical wave functions (2.6) in this case reduce to:

$$\bar{M}_{mn}^{(3)} \approx i^{-n} \frac{e^{ikr}}{kr} [\tau_{mn}(\theta)\hat{\theta} - i\pi_{mn}(\theta)\hat{\phi}]e^{im\phi}$$

$$\bar{N}_{mn}^{(3)} \approx i^{-n} \frac{e^{ikr}}{kr} [-\pi_{mn}(\theta)\hat{\theta} + i\tau_{mn}(\theta)\hat{\phi}]e^{im\phi} \tag{2.24}$$

where the functions π_{mn} and τ_{mn} have been previously defined in (2.15). Since $r' \approx r - d\cos\theta$, $\bar{M}_{mn}^{(3)'}$ and $\bar{N}_{mn}^{(3)'}$ differ from (2.24) only by the phase factor $e^{-ikd\cos\theta}$. With the above, (2.16) and (2.17) are combined with the result:

$$\bar{E}_S \approx \frac{e^{ikr}}{kr} \sum_{n=1}^{\infty} \sum_{m=-n}^{n} i^{-n} e^{im\phi} \Big(-[e(m,n)\pi_{mn}(\theta) - h(m,n)\tau_{mn}(\theta)]\hat{\theta}$$

$$+ i[e(m,n)\tau_{mn}(\theta) - h(m,n)\pi_{mn}(\theta)]\hat{\phi} \Big) \tag{2.25}$$

where

$$e(m,n) = A_E(m,n) + B_E(m,n)e^{-ikd\cos\theta}$$

$$h(m,n) = A_H(m,n) + B_H(m,n)e^{-ikd\cos\theta}. \tag{2.26}$$

By using the symmetry properties of the addition theorem coefficients, which in turn are obtained from the properties of the associated Legendre functions, the series (2.25) can be transformed into one involving only non-negative values of the index m if the scattered field is produced by a source whose E vector is polarized either parallel or perpendicular to the common axis of the two spheres,† i.e., $\gamma = 0$ or $\pi/2$. Then for

† This same transformation could of course be applied to (2.16) through (2.19). Liang and Lo (1967) considered only the polarization $\gamma = \pi/2$ but did not note the symmetry in the functions for positive and negative m.

$\gamma = \begin{bmatrix} 0 \\ \pi/2 \end{bmatrix}$, (2.25) becomes:

$$\bar{E}_s \approx \frac{e^{ikr}}{kr} \sum_{n=1}^{\infty} \sum_{m=0}^{n} i^{-n} \epsilon_m \Big(-[e(m,n)\pi_{mn}(\theta) - h(m,n)\tau_{mn}(\theta)] \times \begin{bmatrix} \cos m\phi \\ \sin m\phi \end{bmatrix} \hat{\theta} + i[e(m,n)\tau_{mn}(\theta) - h(m,n)\pi_{mn}(\theta)] \times \begin{bmatrix} \sin m\phi \\ \cos m\phi \end{bmatrix} \hat{\phi} \Big) \tag{2.27}$$

where $\epsilon_m = 1$ if $m = 0$ and 2 if $m > 0$. It should be stressed, however, that the scattering coefficients $e(m,n)$ and $h(m,n)$ are different for the two polarizations by virtue of (2.14) and (2.21).

2.7 Analytical Simplifications for Special Geometries

There are several configurations that deserve special consideration as these all lead to some simplification in the analysis.

2.7.1 Endfire Illumination

Perhaps the greatest simplification results when the direction of propagation of the incident wave coincides with the axis of the two spheres ($\alpha = 0,\pi$). In this case (say $\alpha = 0$) the coefficients of the incident wave become from (2.14):†

$$p(m,n) = q(m,n) = -i^n \frac{2n+1}{2n(n+1)} \delta_{m,1} \tag{2.28}$$

† Equation (2.27) demonstrates that we need consider only non-negative values of m hereafter, since an arbitrarily polarized incident field can be synthesized from two orthogonal linear polarizations.

This means the system (2.21) need be solved only for m = 1, which in turn means that only the translation coefficients $A_{mn}^{m\nu}$ and $B_{mn}^{m\nu}$ for m = 1 need be calculated. Furthermore, in this case, the coefficients can be reduced to simple forms (see (A28) and (A36)).

2.7.2 Broadside Illumination - Identical Spheres

When the source impinges upon two identical spheres at broadside incidence ($\alpha = \pi/2$) with either parallel or perpendicular polarization ($\gamma = 0, \pi/2$) another simplification results. For perpendicular polarization

$$\begin{aligned} B_E(m,n) &= (-1)^{n+m} A_E(m,n) \\ B_H(m,n) &= -(-1)^{n+m} A_H(m,n) \end{aligned} \tag{2.29}$$

and (2.21) becomes:

$$\begin{aligned} A_E(m,n) &= v_n(ka)\Bigg(p(m,n) + \sum_{\nu=(1,m)}^{\infty} (-1)^{\nu+m} \\ &\qquad \times \left[A_{mn}^{m\nu} A_E(m,\nu) - B_{mn}^{m\nu} A_H(m,\nu)\right]\Bigg) \\ A_H(m,n) &= u_n(ka)\Bigg(q(m,n) - \sum_{\nu=(1,m)}^{\infty} (-1)^{\nu+m} \\ &\qquad \times \left[A_{mn}^{m\nu} A_H(m,\nu) - B_{mn}^{m\nu} A_E(m,\nu)\right]\Bigg) \end{aligned} \tag{2.30}$$

For horizontal polarization ($\gamma = 0$), a simple sign change is introduced on the RHS of (2.29) and preceding the summations in (2.30).

2.7.3 Asymptotic Form for Large Separation

In the Appendix a simple asymptotic form for the translation coefficients $A_{m\nu}^{mn}$ and $B_{m\nu}^{mn}$ is derived which is valid when the translational

distance kd is sufficiently large. From the series expansion of the Hankel function $h_p^{(1)}(kd)$ it is shown that $kd > 0(n+\nu)^2$ is the required condition for the asymptotic form where $n,\nu \leq 0(\max\{ka,kb\})$.† If $a > b$, this criterion becomes $\frac{d}{a} > 0(ka)$. It is interesting to note at this point, that this is also the familiar far field criterion for a circular aperture of radius a. If the above criterion is satisfied, the translation coefficients become (A47):

$$A_{m\nu}^{mn} = B_{m\nu}^{mn} \approx i^{n-\nu-1} \frac{2\nu+1}{2\nu(\nu+1)} n(n+1) \frac{e^{ikd}}{kd} \delta_{m,1} \qquad \begin{cases} m \geq 0 \\ \frac{d}{a} > 0(ka) \end{cases} \tag{2.31}$$

This says that when the sphere separation is sufficiently large, the only contribution to the coupling of energy between the spheres is through the azimuthal mode m = 1. In regard to the addition theorem, say from 0 to 0', which reads:

$$\begin{aligned} \bar{M}_{mn}^{(3)'} &= \sum_{\nu=(1,m)}^{\infty} (A_{m\nu}^{mn} \bar{M}_{m\nu}^{(1)} + B_{m\nu}^{mn} \bar{N}_{m\nu}^{(1)}) \\ \bar{N}_{mn}^{(3)'} &= \sum_{\nu=(1,m)}^{\infty} (A_{m\nu}^{mn} \bar{N}_{m\nu}^{(1)} + B_{m\nu}^{mn} \bar{M}_{m\nu}^{(1)}) , \end{aligned} \tag{2.8}$$

(2.31) says that $\bar{M}_{mn}^{(3)'}$ (at 0') is constructed only from vector wave functions of the type $\bar{M}_{l\nu}^{(1)}$ and $\bar{N}_{l\nu}^{(1)}$ (from 0) each appropriately weighted by (2.31). This weighting (for each ν) is seen to be the strength of a spherical wave which originated at 0.

†This inequality for n and ν is based on the truncation point of the Mie series.

Another intuitively pleasing aspect of the above result is that the Kronecker delta δ_{m1} in (2.31) selects the only vector wave functions ($\bar{N}_{1\nu}$ and $\bar{M}_{1\nu}$) which have a non-zero value in the direction connecting the two sphere centers, which in the present problem is the z-axis.

Numerical results employing this approximation are given in Chapter 4 and indicate that in some cases the criterion $\frac{d}{a} > 0(ka)$ may be relaxed somewhat.

2.7.4 Rayleigh Scattering by Two Spheres

The preceding analysis to this point may be easily specialized to the Rayleigh region where we assume that ka and kb are so small that only the term for n = 1 contributes, the others being taken as zero. Certainly for this case we must assume ka,kb $\ll$ 1. This situation, for equal spheres at endfire and broadside incidence, was considered in detail by Trinks (1935) and later generalized to arbitrary angle of incidence and dissimilar spheres by Germogenova (1963). In the interest of completeness, the Rayleigh approximation is presented using the present formulation.

Consider first the coupled equations (2.21) in light of assuming $u_n(kx)$, $v_n(kx) = 0$ for $n > 1$, where x = a or b (cf. (2.22)). For definiteness, assume the vertical polarization $\gamma = \pi/2$. Equation (2.21) may then be written explicitly after listing the coefficients $A_{mn}^{m\nu}$ and $B_{mn}^{m\nu}$. For the case at hand only the following are required:

$$A_{01}^{01} = -3e^{iz}(z+i)/z^3 \qquad B_{01}^{01} = 0$$

$$A_{11}^{11} = 3e^{iz}[z+i(1-z^2)]/2z^3 \qquad B_{11}^{11} = -3e^{iz}(1-iz)/2z^3$$

where $z \equiv kd$ has been introduced for brevity. For the assumed vertical

polarization, (2.14) becomes:

$$p(0,1) = 0 \qquad q(0,1) = i\frac{3}{2}\sin\alpha$$

$$p(1,1) = i\frac{3}{4} \qquad q(1,1) = -i\frac{3}{4}\cos\alpha$$

Using these results in (2.21) and leaving only one subscript to denote m = 0 or 1 we have:

m = 0:

$$\begin{aligned} A_{E_o} &= B_{E_o} = 0 \\ A_{H_o} &= u(ka)(q_o + A_o B_{H_o}) \\ B_{H_o} &= u(kb)(q_o' + A_o A_{H_o}) \end{aligned} \tag{2.32}$$

m = 1:

$$\begin{aligned} A_{E_1} &= v(ka)(p_1 + A_1 B_{E_1} + B_1 B_{H_1}) \\ A_{H_1} &= u(ka)(q_1 + A_1 B_{H_1} + B_1 B_{E_1}) \\ B_{E_1} &= v(kb)(p_1' + A_1 A_{E_1} - B_1 A_{H_1}) \\ B_{H_1} &= u(kb)(q_1' + A_1 A_{H_1} - B_1 A_{E_1}) \end{aligned} \tag{2.33}$$

The problem then reduces to solving two sets of equations with at most four unknowns. A simple case for illustration occurs for a pair of identical spheres at broadside incidence, where we may use the result (2.30) and obtain for (2.32) and (2.33)

$$
\begin{aligned}
A_{E_o} &= 0 \\
A_{H_o} &= \frac{3i}{2}\, u(ka)\left[1-u(ka)A_o\right]^{-1} \\
A_{E_1} &= \frac{3i}{4}\, v(ka)\left[1+v(ka)A_1 + \frac{u(ka)v(ka)B_1^2}{1-u(ka)A_o}\right]^{-1} \\
A_{H_1} &= -u(ka)B_1A_{E_1}\left[1-u(ka)A_1\right]^{-1}
\end{aligned}
\tag{2.34}
$$

The results for horizontal polarization are obtained similarly. Further approximations may be made if restrictions are placed on kd. The fields may then be simply calculated using the previous results.

3. NUMERICAL ANALYSIS

The possibility of obtaining accurate numerical results for the scattering by two spheres beyond the Rayleigh region using the multipole expansion technique requires much more than just the availability of a large scale computer; it requires the most efficient computational techniques available. This means maximum use of recursive and iterative techniques.

3.1 Special Functions

Inspection of the functions in the various multipole expansions (e.g. (2.5) and (2.6)), and the expansions themselves, indicates that any field calculation involves series of functions in which is required the summation of many orders of functions which have the same argument.

As is well known there is a large class of special functions of mathematical physics which satisfy three-term recurrence relations of the form:

$$w_{n+1} + a_n w_n + b_n w_{n-1} = 0 \qquad (3.1)$$

where $n = 1,2,\ldots$, and a_n and b_n are known constants. The Bessel and Legendre functions which appear in the analysis here are members of this class. Recursion formulas for these or any other functions must not, however, be used indiscriminately since each cycle of a recursive process not only generates its own rounding errors, but inherits those committed in all previous cycles. This aspect of recursion relations — stability — must be known for each of the cases for which they are to be used. This will be discussed in what follows with respect to the functions used in

this analysis. An excellent review of the computational aspects of three-term recursion relations is given by Gautschi (1967).

3.1.1 Spherical Bessel Functions

The spherical Bessel functions $z_n^{(j)}(x)$ satisfy the recurrence relation:

$$z_{n+1}^{(j)} - \frac{2n+1}{x} z_n^{(j)} + z_{n-1}^{(j)} = 0 \qquad (3.2)$$

where $z_n^{(j)}$ may be j_n, n_n, $h_n^{(1)}$, or $h_n^{(2)}$ referred to respectively as spherical Bessel functions of the first, second, third, and fourth kind ($j = 1,2,3,4$). The first two are linearly independent solutions to (3.2). Consider the case of generating $j_n(x)$ with the computer using (3.2) for fixed x and $n = 0,1,2,\ldots$, given $j_o(x)$ and $j_1(x)$ as starting values. $j_o(x)$ and $j_1(x)$ can of course be given only to a finite number of significant figures. If we now try to obtain $j_n(x)$ from (3.2), starting with the approximate values $\tilde{j}_o(x)$ and $\tilde{j}_1(x)$, after recursion with <u>infinite precision</u> to some $n = N > x$, the result $\tilde{j}_N(x)$ will bear no resemblance to the correct value $j_N(x)$. This is because any error made in either of the starting values (due to the finite number of digits carried) may be regarded as a component of the other linearly independent solution $n_n(x)$. This is then carried along at every cycle and hence the error becomes arbitrarily large as n becomes infinite since $n_n(x)$ does. Gautschi (1967) shows that this disastrous accumulation of error can be anticipated whenever one tries to calculate by straightforward recursion the solution f_n of the pair of linearly independent solutions f_n and g_n which satisfies (3.1) and has the property

$$\lim_{n \to \infty} \frac{f_n}{g_n} = 0.$$

The solution f_n in this case is termed *minimal at infinity*. For $j_n(x)$, this trouble can be obviated by using backward recursion in (3.2) by starting at some sufficiently large $n = N \ni j_{N+1}(x) \approx 0$. Then letting $\hat{j}_N(x)$ equal some constant C, (3.2) implies $\hat{j}_{N-1}(x) = \frac{2N+1}{x} C$. By continuing recursion backward to $n = 0$, we arrive at $\hat{j}_o(x)$. Comparing this with $j_o(x) = \frac{\sin x}{x}$ uniquely determines C which then determines $j_n(x)$, $n = 0,1,2,\ldots,N$. The proper choice of the starting point N for a given relative error ϵ in $j_n(x)$ for the largest n of interest has been determined by Carbató and Uretsky (1959). It has been pointed out by Logan (1965) that Lord Rayleigh in a paper published in 1904 was the first to realize the necessity of reversing the direction of recursion for Bessel functions of the first kind (when the order is larger than the argument) in order to control the propagation of error.

In summary then, $j_n(x)$ must be generated by backward recurrence; $n_n(x)$ may be generated in either direction. Once j_n and n_n are generated $h_n^{(1)}$ and $h_n^{(2)}$ follow by linear combination. To get from $n = 0 \rightarrow N$ or from $N \rightarrow 0$, all intermediate values of $z_n^{(j)}$ are generated (and saved in storage) — this is the principal advantage in recursion techniques.

3.1.2 Associated Legendre Functions

The associated Legendre function $P_n^m(x)$ is defined by:

$$P_n^m(x) = \frac{(1-x^2)^{m/2}}{2^n n!} \frac{d^{n+m}}{dx^{n+m}} (1-x^2)^n \qquad (3.3)$$

One would not, however, dream of using this definition for calculation purposes.

For the general case, x is fixed and the set of functions $P_n^m(x)$ is needed for degrees $n = 0,1,2,\ldots,N$ and orders $m \leq n$. These functions, fortunately, do not have the minimal property at infinity (in the range $|x| \leq 1$) as do the Bessel functions of the first kind. This then permits us to use the well known recursion formulas for $P_n^m(x)$ in order and degree, in either direction, without the worry of disastrous error accumulation. The same applies to recursive generation of the functions π_{mn} and τ_{mn} which can be shown to satisfy nearly identical recurrence relations.

It was actually found to be most effective to use only backward recursion in order, using the relation:

$$(n+m-1)(n-m+2)P_n^{m-2} + 2mx\, P_n^{m-1}/\sqrt{1-x^2} - P_n^m = 0 \qquad (3.4)$$

with the starting points

$$P_o^o(x) = 1,\ P_1^o = x, \text{ and } P_1^1(x) = \sqrt{1-x^2}\ ,$$

and the auxiliary relations:

$$\begin{aligned} P_{n+1}^{n+1}(x) &= (2n+1)\sqrt{1-x^2}\ P_n^n(x) \\ P_{n+1}^n(x) &= x\, P_n^n(x)/\sqrt{1-x^2} \end{aligned} \qquad (3.5)$$

This then defines an algorithm which generates and stores P_n^m for all degrees $n = 0,1,2,\ldots,N$ and orders $m \leq n$. The derivatives of the associated Legendre functions are also generated at the same time since they are related to the same quantities which are used in the calculation of the P_n^m's; this avoids redundant calculation.

3.2 Translational Addition Theorem Coefficients

Unquestionably, the most challenging problem regarding numerical solution of the two sphere problem is the calculation of the translation coefficients $A_{\mu\nu}^{mn}$ and $B_{\mu\nu}^{mn}$ which appear in the addition theorems (2.8) and (2.9). For $r \leq d$ they are given by (A28) and (A29) as:

$$A_{m\nu}^{mn} = (-1)^m i^{\nu-n} \frac{2\nu+1}{2\nu(\nu+1)} \sum_p i^{-p}[n(n+1)+\nu(\nu+1)-p(p+1)] \times a(m,n,-m,\nu,p) h_p^{(1)}(kd) \tag{3.6}$$

$$B_{m\nu}^{mn} = (-1)^m i^{\nu-n} \frac{2\nu+1}{2\nu(\nu+1)} \sum_p i^{-p}(-2imkd) a(m,n,-m,\nu,p) h_p^{(1)}(kd)$$

Fortunately the index p extends only over the range $n+\nu, n+\nu-2, \ldots, |n-\nu|$, which means that the series may consist of a minimum of one term but no more than $1 + \max\{\nu,n\}$ terms. The computational aspects of the spherical Bessel functions of the third kind was discussed previously; what remains are the coefficients $a(m,n,-m,\nu,p)$. These coefficients are defined by the linearization expansion

$$P_n^m(x) P_\nu^{-m}(x) = \sum_p a(m,n,-m,\nu,p) P_p(x) \tag{3.7}$$

where from Cruzan (1962) and Liang and Lo (1967)

$$a(m,n,-m,\nu,p) = (2p+1) \left[\frac{(n+m)!(\nu-m)!}{(n-m)!(\nu+m)!} \right]^{1/2} \begin{pmatrix} n & \nu & p \\ 0 & 0 & 0 \end{pmatrix} \begin{pmatrix} n & \nu & p \\ m & -m & 0 \end{pmatrix} \tag{3.8}$$

and $\begin{pmatrix} j_1 & j_2 & j_3 \\ m_1 & m_2 & m_3 \end{pmatrix}$ is the Wigner 3-j coefficient. As shown in the Appendix each one of these coefficients involves a rather complex summation of

multitudinous factorials (equation (A8)). If the number of the coefficients $a(m,n,-m,\nu,p)$ required for solution of the two sphere problem were small, then tabulated values (Rotenberg, et al., 1959) could be used and read directly into the computer subroutine for determining the $A_{m\nu}^{mn}$'s and $B_{m\nu}^{mn}$'s. Such is the case only for very small spheres (considerably less than a wavelength in radius).

If the scattering by a single sphere of size $ka = 2\pi a/\lambda$ is to be calculated numerically using the multipole expansion technique, the series must be truncated at some $n = N$; this value of N, which depends on ka, is determined so as to insure that the resultant error incurred by this truncation is less than some ϵ. An empirical formula for this truncation point for an error of less than .01% in the radar cross-section is:

$$N \approx [1 + ka + 3(ka)^{1/3}] \tag{3.9}$$

Senior and Goodrich (1964) state nearly the same result. If we now consider two spheres, (say both of size ka) the same truncation point for the index n is applicable when the spheres are not too close to each other, or touching. Taking this also as the truncation point for the index ν, we may determine the number of coefficients $a(m,n,-m,\nu,p)$ which need to be calculated to give an accurate result for the scattered field say. Since the limits on all the indices n, m, ν and p are defined in relation to each other, and the truncation point N, for n and ν, then it is a simple matter to show that this total number of required coefficients is:

$$N_a = N^2(N+1)(N+2)/6 + N^2 \tag{3.10}$$

This number is shown plotted in Figure 3.1 vs. ka for N given by (3.9). For large ka it is clear that N_a approaches asymptotically the value

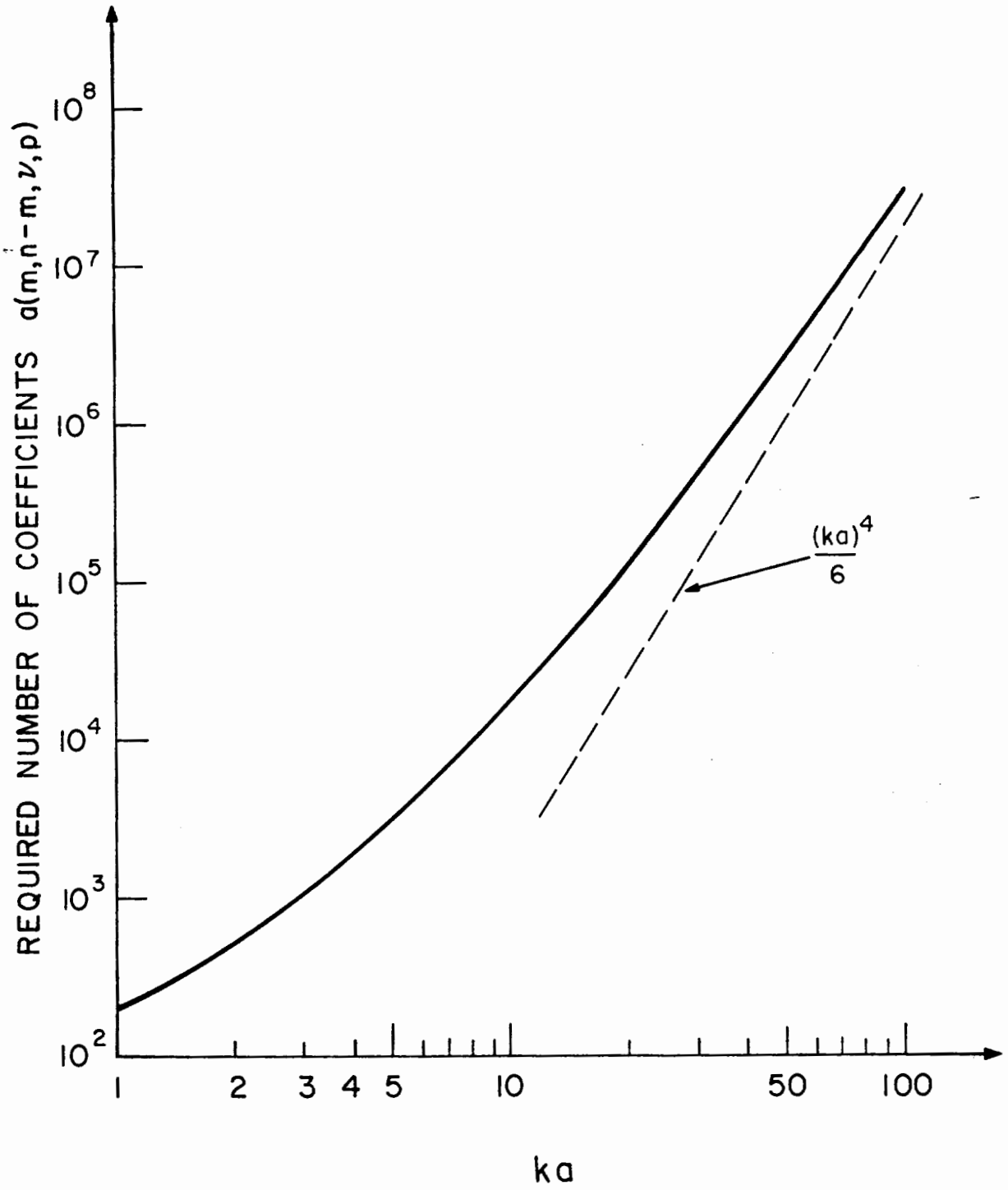

Figure 3.1 Minimum Number of Coefficients, a(m,n,-m,ν,p), Required for Calculation of Scattering by Two Spheres of Size ka.

$(ka)^4/6$. It is also evident that for all but the smallest pair of spheres the calculation of the required number of coefficients represents a tremendous expenditure of effort, in view of the complicated definition of the 3-j coefficients (A9). To give some sort of feeling for the computation involved, consider the case of computation of the scattered field from a pair of spheres both of size ka = 4. This will require about 10 terms (in n) in the multipole expansion of the scattered field (2.27), while (3.10) indicates that 2300 of the coefficients $a(m,n,-m,\nu,p)$ must be calculated! Furthermore, using Liang's form for the coefficients (3.8) with (A9) means that for the computation of a single coefficient $a(\cdot)$, as many as 156 factorials will have to be evaluated with the largest one being 41!. This clearly demonstrates that if any practical computations are to be made of the scattering by two spheres in this size range or larger, the efficiency of the computation of the coefficients $a(m,n,-m,\nu,p)$ must be radically improved.

Inspection of the form of the coefficients $A_{m\nu}^{mn}$ and $B_{m\nu}^{mn}$ in (3.6) indicates that if recursion techniques can be applied, a recursion relation for the $a(\cdot)$'s in which only the index p cycles would be the most desirable. Such a recursion formula is derived in the Appendix with the results reproduced below:

$$\alpha_{p-3}a_{p-4} - (\alpha_{p-2} + \alpha_{p-1} - 4m^2)a_{p-2} + \alpha_p a_p = 0 \qquad (3.11)$$

where

$$a_p \equiv a(m,n,-m,\nu,p),\ p = n+\nu, n+\nu-2, \ldots, |n-\nu|$$

and

$$\alpha_p = [(n+\nu+1)^2 - p^2][p^2 - (n-\nu)^2]/(4p^2-1). \qquad (3.12)$$

The recursion relation (3.11) is most conveniently used in the backward direction since simple starting values result for $p = n+\nu$ and $n+\nu-2$. These are:

$$a_{n+\nu} = \frac{(2n-1)!!(2\nu-1)!!}{(2n+2\nu-1)!!} \frac{(n+\nu)!}{(n-m)!(\nu+m)!}$$

$$a_{n+\nu-2} = \frac{(2n+2\nu-3)}{(2n-1)(2\nu-1)(n+\nu)} [\nu n - m^2(2n+2\nu-1)] a_{n+\nu} \tag{3.13}$$

The form of (3.11) displays vividly the inherent efficiency of this recurrence technique — every new coefficient calculated makes use of all previously calculated quantities and requires only two additional evaluations of the quantity α_p. Furthermore, when generating the set of coefficients $a(\cdot)$ for all n, m, ν, and p, by starting from $\nu = 1$ and $m = 0$ (3.13) becomes

$$a_{n+\nu} = \frac{n+1}{2n+1} \; ; \; a_{n+\nu-2} = \frac{n}{2n+1} \; .$$

All other starting values for the various indices n, ν, and m are then found from the above and the obvious recurrent forms implied by (3.13). The question of stability of the recursion formula (3.11) is trivial since all quantities involved in (3.11) are rational numbers. That is, if need be, the recursion process (3.11) could be carried out entirely in integer arithmetic after rationalization with no attendent loss in accuracy at any step. If (3.11) is not rationalized, there are several checks which can be made after the set of coefficients $\{a(\cdot)\}$ is generated to test stability. The first is obvious from (3.7), i.e.:

$$\sum_p a(m,n,-m,\nu,p) = \delta_{m,o} \; . \tag{3.14}$$

Secondly, (3.11) must be applied most often for the cases when $\nu = n$. In these cases, the end coefficients $a(m,n,-m,n,0)$ are known explicitly as simply $(-1)^m/(2n+1)$, a very convenient quantity to check with.

There are two special cases of (3.11) which deserve mention, namely, the cases for m = 0 and 1. When m = 0 (3.11) reduces to

$$\alpha_{p-1}a_{p-2} = \alpha_p a_p \ . \tag{3.15}$$

This corresponds to the azimuthally symmetric case in the acoustic two sphere problem where the incident vector lies along the common axis of the two spheres (see 6.1). The case m = 1 is the azimuthally symmetric case for the electomagnetic problem where the coefficients $a(1,n,-1,\nu,p)$ are related to those for m = 0 by (A35), i.e.:

$$a(1,n,-1,\nu,p) = - a(0,n,0,\nu,p)\beta_p/2\nu(\nu+1)$$

where $\beta_p = n(n+1) + \nu(\nu+1) - p(p+1)$. The m = 1 case then has the two term recursion formula

$$\alpha_{p-1}\beta_p a_{p-2} = \alpha_p \beta_{p-2} a_p$$

which is valid when $\beta_p \neq 0$. In case $\beta_p = 0$, a_{p-2} may be found from (3.11) as

$$a_{p-2} = - \frac{\alpha_{p+2}}{\alpha_{p-1}} a_{p+2} \ .$$

3.3 Solution of the Coupled Equations for the Multipole Coefficients

The possibility of obtaining numerical results of the rigorous solution of electromagnetic scattering by two spheres rests on the ability to solve the system of equations (2.21) which is repeated here for convenience:

$$
\begin{aligned}
A_E(m,n) &= v_n(ka)\{p(m,n) + \sum_\nu [A_{mn}^{m\nu} B_E(m,n) + B_{mn}^{m\nu} B_H(m,n)]\} \\
A_H(m,n) &= u_n(ka)\{q(m,n) + \sum_\nu [A_{mn}^{m\nu} B_H(m,n) + B_{mn}^{m\nu} B_E(m,n)]\} \\
B_E(m,n) &= v_n(kb)\{p'(m,n) + \sum_\nu (-1)^{n+\nu} [A_{mn}^{m\nu} A_E(m,n) - B_{mn}^{m\nu} A_H(m,n)]\} \\
B_H(m,n) &= u_n(kb)\{q'(m,n) + \sum_\nu (-1)^{n+\nu} [A_{mn}^{m\nu} A_H(m,n) - B_{mn}^{m\nu} A_E(m,n)]\}.
\end{aligned}
\tag{2.21}
$$

It is more convenient to comment on numerical solution of this system when it is written in the matrix form given below. With the following identifications (2.21) becomes:

$$
\mathcal{M} = \mathcal{F} + \mathcal{C}\mathcal{M} \tag{3.16}
$$

where $\mathcal{M}$ is the multipole coefficient matrix

$$
\mathcal{M} = \begin{pmatrix}
A_E(m,1) \\
A_E(m,2) \\
\vdots \\
\hline
A_H(m,1) \\
\vdots \\
\hline
B_E(m,1) \\
\vdots \\
\hline
B_H(m,1) \\
\vdots
\end{pmatrix} \tag{3.17}
$$

The matrix $\mathcal{F}$ is given by:

$$\mathcal{F} = \begin{pmatrix} C_a & 0 \\ 0 & C_b \end{pmatrix} \mathcal{A} \qquad (3.18)$$

where

$$C_x = \begin{pmatrix} V_x & 0 \\ 0 & U_x \end{pmatrix} , \qquad x = a \text{ or } b$$

and

$$V_x = \left(v_1(kx)v_2(kx)\ldots\right)$$
$$U_x = \left(u_1(kx)u_2(kx)\ldots\right) ,$$

with $\mathcal{A}$ the incident wave coefficient matrix

$$\mathcal{A} = \begin{pmatrix} p(m,1) \\ p(m,2) \\ \vdots \\ \hline q(m,1) \\ \vdots \\ \hline p'(m,1) \\ \vdots \\ \hline q'(m,1) \\ \vdots \end{pmatrix}$$

Finally, the matrix $\mathcal{C}$, termed the coupling matrix, is given by

$$\mathcal{C} = \left(\begin{array}{c|c} 0 & C_a \begin{pmatrix} A & B \\ A & B \end{pmatrix} \\ \hline C_b \begin{pmatrix} A_{\pm} & -B_{\pm} \\ A_{\pm} & -B_{\pm} \end{pmatrix} & 0 \end{array}\right) \tag{3.20}$$

where

$$A = \overset{n}{\downarrow}\overset{\nu \rightarrow}{\left(A_{mn}^{m\nu}\right)}, \quad B = \overset{n}{\downarrow}\overset{\nu \rightarrow}{\left(B_{mn}^{m\nu}\right)}$$

$$A_{\pm} = \overset{n}{\downarrow}\overset{\nu \rightarrow}{\left((-1)^{n+\nu} A_{mn}^{m\nu}\right)}, \quad B_{\pm} = \overset{n}{\downarrow}\overset{\nu \rightarrow}{\left((-1)^{n+\nu} B_{mn}^{m\nu}\right)}.$$

The solution to the system (3.16) is then formally given by:

$$\mathcal{H} = (I - \mathcal{C})^{-1} \mathcal{F} \tag{3.21}$$

Equations (3.16) and (3.21) suggest the two modes of solution — iteration and direct matrix inversion. While the later method can always be applied, the former requires that all eigenvalues of the matrix $\mathcal{C}$ be of modulus less than one. Only under this condition does the following expansion for $(I - \mathcal{C})^{-1}$ become meaningful:

$$(I - \mathcal{C})^{-1} = I + \mathcal{C} + \mathcal{C}^2 + \ldots$$

When this is not the case, direct matrix inversion must be used. Returning to the previous example of the calculation of the scattering from a pair of spheres ka = 4; where for the case of moderate separation 10 terms are needed in the multipole expansion in n and ν, eleven 40 X 40 complex, non-symmetric, matrices will have to be inverted to obtain a solution

for one particular choice of parameters (a, b, d, α, and the material of each). When conditions are met, the iterative technique is preferable as this tends to minimize error accumulation and can take full advantage of all the zero entries in $\mathcal{C}$. Furthermore when the spacing is not too small, the iteration process should converge rapidly. There are various iterative schemes available; probably the two best known are the Jacobi method (method of simultaneous displacements) and the Gauss-Seidel method (method of successive displacements). In the first method, one does not use improved values until after one complete iteration, whereas the second method uses improved values as soon as they are available. The latter method is thus more naturally suited for computer application. Furthermore it can be shown (Todd, 1962) that the Gauss-Seidel process converges exactly twice as fast as the Jacobi method regardless of initial values. The "orders of scattering" iteration technique employed by Twersky (1952) and Liang and Lo (1967) is precisely the Jacobi method.

The question of where to truncate the matrix or terminate the series is of considerable practical importance for numerical calculation. This is answered by (3.9) for the case of the single sphere. For two spheres it seems quite unlikely that such a clear cut truncation point can be specified since this depends on the sphere sizes, separation, composition, and even polarization. Intuition tells us that the stronger the mutual coupling the more terms we will need. Crane (1967) shows that the elements of $\mathcal{C}$ decrease in magnitude with increasing n (or ν) as $(4ab/d^2)^{2n+1}/n^3$, which indicates that the worst case involves two identical spheres that touch. Generally this is true, however, this does not say

anything about sphere composition or polarization of the incident wave, the latter being extremely important near contact. Numerically the question of how many terms to take is left up to the computer — keep taking more terms until the result doesn't change within some prescribed amount. Numerical results indicate that for all but a very few cases, a few more terms than given by (3.9) is usually sufficient even at contact. One exceptional case involves a pair of identical metallic spheres in contact at broadside incidence for horizontal polarization ($b = a$, $d = 2a$, $\alpha = \pi/2$, $\gamma = 0$).

4. COMPUTER PROGRAM DESCRIPTION AND NUMERICAL RESULTS

Numerical results have been reported for scattering by two spheres in the Rayleigh region using the modal expansion technique by several authors, and hence will not be repeated here (Trinks, 1935, Germogenova, 1963, Lillesaeter, 1964). Here the emphasis is on scattering by larger spheres, of which the only available numerical results appear in Liang and Lo (1967). Their numerical results, however, are restricted to relatively small spheres at large separation.

By making use of the symmetries in the analysis outlined in Chapter 2, and the recursion relations for the coefficients and special functions described in Chapter 3, very general, fast, and efficient programs may be written. The basic structure of the programs used for the following results is outlined below and some computer times are quoted.

4.1 General Program Structure and Description

Nearly all of the programs were written in the FORTRAN IV language for the IBM 360/75 in single precision arithmetic (about 6 significant figures). The special functions, the coefficients u_n and v_n, and the coefficients $A_{mn}^{m\nu}$ and $B_{mn}^{m\nu}$ involving the $a(\cdot)$'s are generated outside of the main program in subroutines which are called, as needed, from the main program. These subroutines for a particular choice of parameters (a,b, d,α,θ, and the material of each sphere) when called, return the entire block of functions (for the various orders) and coefficients needed for the calculation so that only manipulation of these functions and coefficients is carried out in the main program. The calling sequence of

course depends on which parameter(s) change between subsequent calculations. Only those subroutines are re-called which involve a parameter change.

It was pointed out in Section 2.7 that when the incident electric field was polarized in a direction either parallel or perpendicular to the common axis of the spheres, that only n+1 sets of coupled equations (2.21) for the multipole coefficients had to be solved, since in those cases the index m assumed only non-negative values. For arbitrary polarization, it is more efficient to simply solve the problem twice for the above two polarizations, otherwise new coefficients and functions would have to be calculated which involve negative values of m. This procedure has the added advantage that with the solutions for these two component polarizations we then also have the solution for any other incident polarization.

The system of equations (2.21) is solved by iteration only, the Gauss-Seidel method chosen instead of the Jacobi method because of its more rapid convergence properties (see 3.3). The initial approximation used in the iterative solution of (2.21) is most logically chosen as $\mathcal{M}^{(0)} = \mathcal{F}$ where $\mathcal{M}^{(N)} = \mathcal{F} + \mathcal{C}\mathcal{M}^{(N-1)}$. The superscript corresponds to the iteration number, hence $\mathcal{M}^{(-1)} \equiv 0$. Thus, if the coupling is small (i.e., $\mathcal{C}$ is small) then $\mathcal{M}$ will not be very different from $\mathcal{F}$. Convergence of the iteration for the most part is quite rapid except when the spheres are in contact for the horizontal polarization. Relaxation methods (Todd, 1962) were tried in an attempt to alleviate this situation, however, with no improvement found over the Gauss-Seidel method. The

iteration process is terminated when the final answer does not change between successive iterates within some prescribed amount.

With the multitudes of calculations involved, the question of numerical accuracy arises. This was checked in several ways. First, several programs were written at different times for different computers, in the FORTRAN II langugage in one case and FORTRAN IV in the others. There was agreement to no less than five of the six significant figures carried. Second, the reciprocity principle was exploited as a check. By illuminating the spheres at an incident angle α and observing the scattered field at an angle θ, we should obtain the same result as by illuminating at θ and observing at α. This also allowed checking the endfire incidence program ($m = 1$) with the general and broadside incidence programs. In all these cases tested there was agreement to no less than four of the six places carried. Finally, the excellent agreement between the computed and experimental results places additional confidence in the results.

Before proceeding to the numerical results, some typical computer times are quoted and compared with the technique reported by Liang and Lo. It is difficult to make a direct comparison of the computation times between the present method and the one reported previously since in the latter case only the first iteration toward the solution to the system of equations (2.21) was considered, whereas the present results were obtained by iterating as many times as necessary to obtain convergence to the true solution. The number of iterations required in some cases is very large; for example, in the case of large spheres ($ka > 15$) in contact at endfire illumination, the required number exceeds 40. For comparison, calculation of a single point for spheres of radii about 2/3 of a wavelength ($ka = 4.19$)

took about 11 minutes using the previous method and only 1 second with the present method (the present method having performed an average of about six iterations — more near contact, less at large separation). The time factor between the two methods becomes rapidly larger as the sphere size increases. Calculations with the present programs have been made for two spheres in contact at endfire incidence for ka = 30. At this value, the computer time is still quite reasonable being only 40 seconds for a single point after performing about 50 iterations. The upper limit for sphere sizes depends on the price one is willing to pay for each point.

4.2 Radar Cross-Sections

It would be a difficult task to give a truly representative set of numerical results for scattering by two spheres because of the large number of parameters involved. To illustrate this, recall that for backscattering by a single sphere we have only the size and material to specify, whereas for two spheres we must specify not only the size and material of each, but also the separation between centers d, the incident wave vector $\hat{k}$ and its polarization.

Since measurements of radar cross-section can be made with relative ease (see Section 7), this will constitute the major body of the numerical results. In the backscatter direction $\theta = \pi - \alpha$ and $\phi = \pi$, hence the scattered field from the two spheres in the far zone is given by (2.27), for horizontal polarization ($\gamma = 0$):

$$\bar{E}_S = -\frac{e^{ikr}}{kr} \sum_{n=1}^{\infty} \sum_{m=0}^{n} i^n \epsilon_m [e(m,n)\pi_{mn}(\alpha) - h(m,n)\tau_{mn}(\alpha)]\hat{\theta} \qquad (4.1)$$

For the vertical polarization ($\gamma = \pi/2$) the result is the same upon interchanging π_{mn} and τ_{mn} and replacing $\hat{\theta}$ by $-i\hat{\phi}$. Note also that e(m,n) and h(m,n) are functions of α and γ. We see immediately that the vertically polarized field cannot backscatter any energy associated with the horizontally polarized field, regardless of sphere sizes or material. The same applies for the other polarization. In other words there will be no "depolarization" (Beckmann, 1968) for an incident polarization in these two directions. In any other direction, however, ($\gamma \neq n\pi/2$, n an integer) there will be a depolarizing effect. Results showing this effect will be presented shortly.

Using (4.1) we compute the radar cross-section (referred to hereafter as RCS) from the definition:

$$\sigma = \lim_{r \to \infty} 4\pi r^2 \left| E_s/E_i \right|^2 \qquad (4.2)$$

Figures 4.1 through 4.9 employ this result for various configurations, but we will discuss them separately. With the exception of Figure 4.3, experimental results are also shown here (as dotted curve) for comparison although the experimental procedures are not discussed until Section 7. The solid curves were computed using the modal expansion (exact) technique.

At this point, a few words about the preparation of the graphs are perhaps in order. In view of the oscillatory behavior of the RCS curves, and for the sake of presenting the results as accurately as possible (not to mention the savings in time to the writer), all theoretical scattering curves throughout this thesis were plotted by computer (Calcomp plotter). This was almost a necessity when comparison was made to experimental results since the scale on the chart recorder paper used in the measurements

did not match that of any available graph paper. The theoretical results (punched by the main program on data cards) were read into the plotting program and plotted to the same scale as the chart paper — this explains the somewhat unusual vertical scale as the plotting routine writes the axis values only at inch intervals. By having the theoretical curves plotted to the same scale as the experimental results (which were on chart paper), the latter could be transferred accurately simply by tracing. Generally for the broadside results, points were calculated at intervals of .5 in kd and .3 in kd for endfire results. Points between these were calculated by a piecewise cubic interpolation scheme which maintains continuity of the fitted curve and its slope at all points. Hence, no human guesswork was employed between rigorously calculated points.

4.2.1 Broadside Incidence — Variable Separation

Figure 4.1 shows the broadside RCS of a pair of identical metallic spheres for $\gamma = \pi/2$, normalized to σ_a, the RCS of sphere A alone for ka = 4.19 and ka = 6.246. The agreement is remarkably good with the exception of an apparent scale shift for the 4.19 case. This is an experimental phenomenon which is explained in Section 7. In Figure 4.2 the same configuration is shown except for dielectric spheres with relative dielectric constant 2.56 and size ka = 4.209. The mutual coupling for this case is nearly negligible for $d/a > 6$. Eight more cases involving this same geometry are shown in Figures 5.8 through 5.10 for comparison with the ray optical approach. They will be discussed later.

4.2.2 Broadside Incidence — Large Separation Approximation

When the asymptotic form of the translational addition theorem given in 2.7.3 is used, we obtain the results shown by the dot-dash curves in

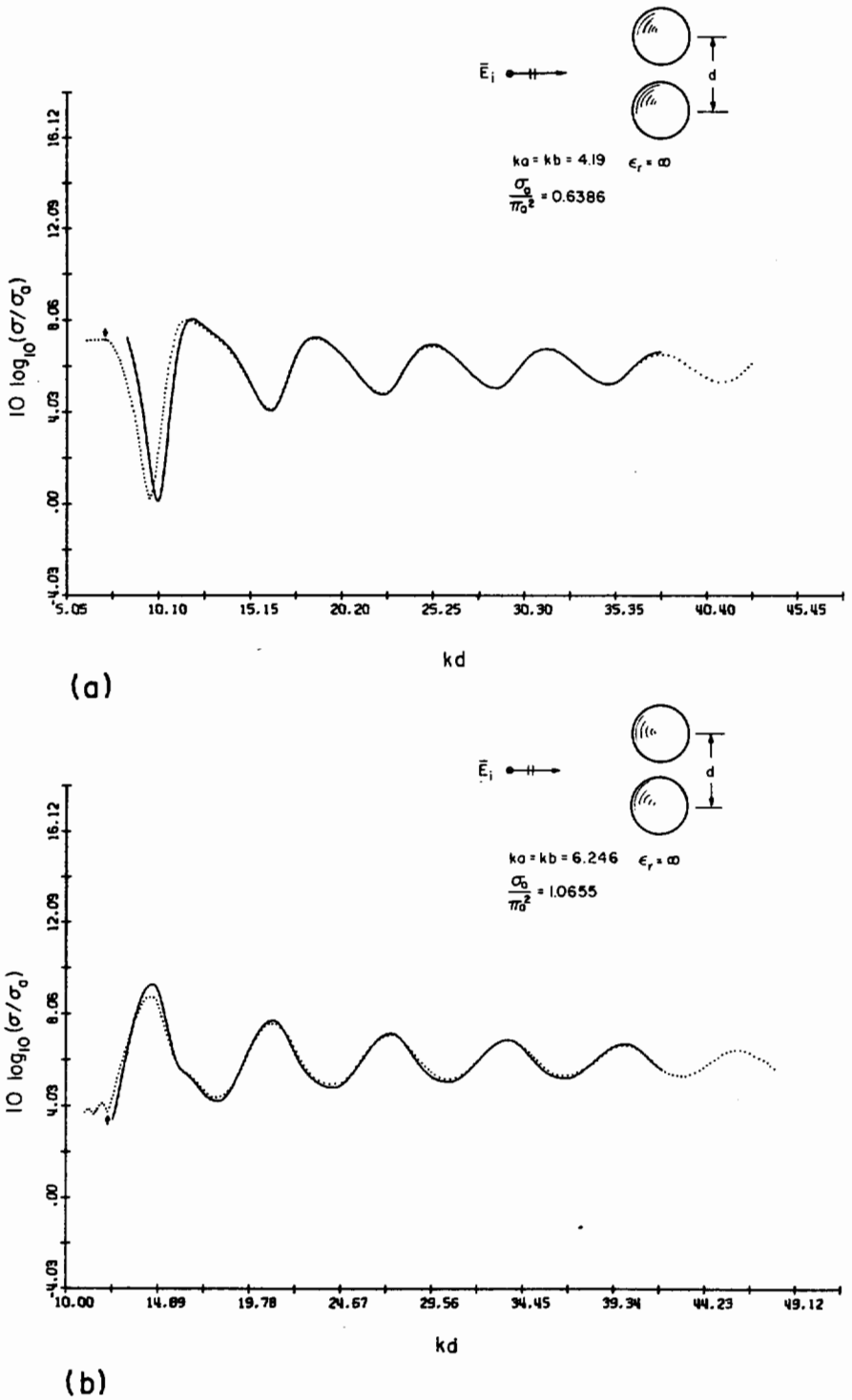

Figure 4.1 RCS of Two Equal Metallic Spheres at Broadside Incidence for (a) ka = 4.19 and (b) ka = 6.246 from Modal Approach (———) and Experiment (·····).

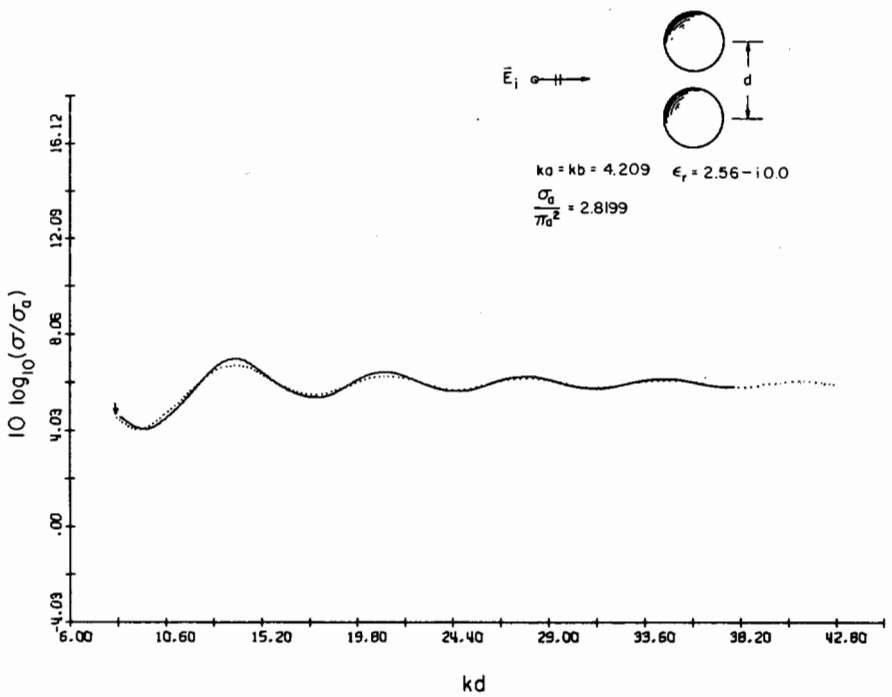

Figure 4.2 RCS of Two Equal Dielectric Spheres at Broadside Incidence for ka = 4.209 from Modal Expansion (———) and Experiment (·····).

Figure 4.3 for ka = 1, 2, and 4.19. The exact modal solution is shown for comparison. The criterion for the validity of the asymptotic solution was d/a > 0(ka), but for ka = 2 and particularly 4.19 it is seen that this restriction may be relaxed somewhat. The analogous approximation for the scalar problem is discussed in 6.1.1.

4.2.3 Endfire Incidence — Variable Separation

RCS calculations and experimental measurements are shown in Figures 4.4 through 4.6. In these cases both experimental and theoretical results were normalized to the return from the front spheres. In Figure 4.4(a) and (b) is shown the cases of identical metallic spheres for ka = 7.41 and 11.048 respectively, the former case being chosen to compare with the experimental results of Angelakos and Kumagai (1964) as indicated by the squares. These results seem to indicate very little coupling for d/a > 5. In Figure 4.5(a) and (b) is plotted the endfire RCS of two metallic spheres of different size normalized with respect to the return from the *larger* sphere. Here we see, as explained in terms of ray theory in the next section, that the larger sphere can more easily shield or "hide" a smaller sphere at close spacing than in the reverse situation. Eventually, however, at values of kd > 45 the two curves will oscillate between the same two upper and lower limits. A larger discrepency in these experimental results than in the previous cases was anticipated since it is more difficult to visually align two spheres of different size.

The RCS of two identical dielectric spheres† at endfire is shown in Figure 4.6(a) for ka = 7.44. Here we see that the interaction between the

† The relative dielectric constant used for these calculations was 2.56-i0.0. Inclusion of the actual loss term of -i.0005 in the material used in the experiment made negligible difference. At values of ka > 10, however, this does become significant.

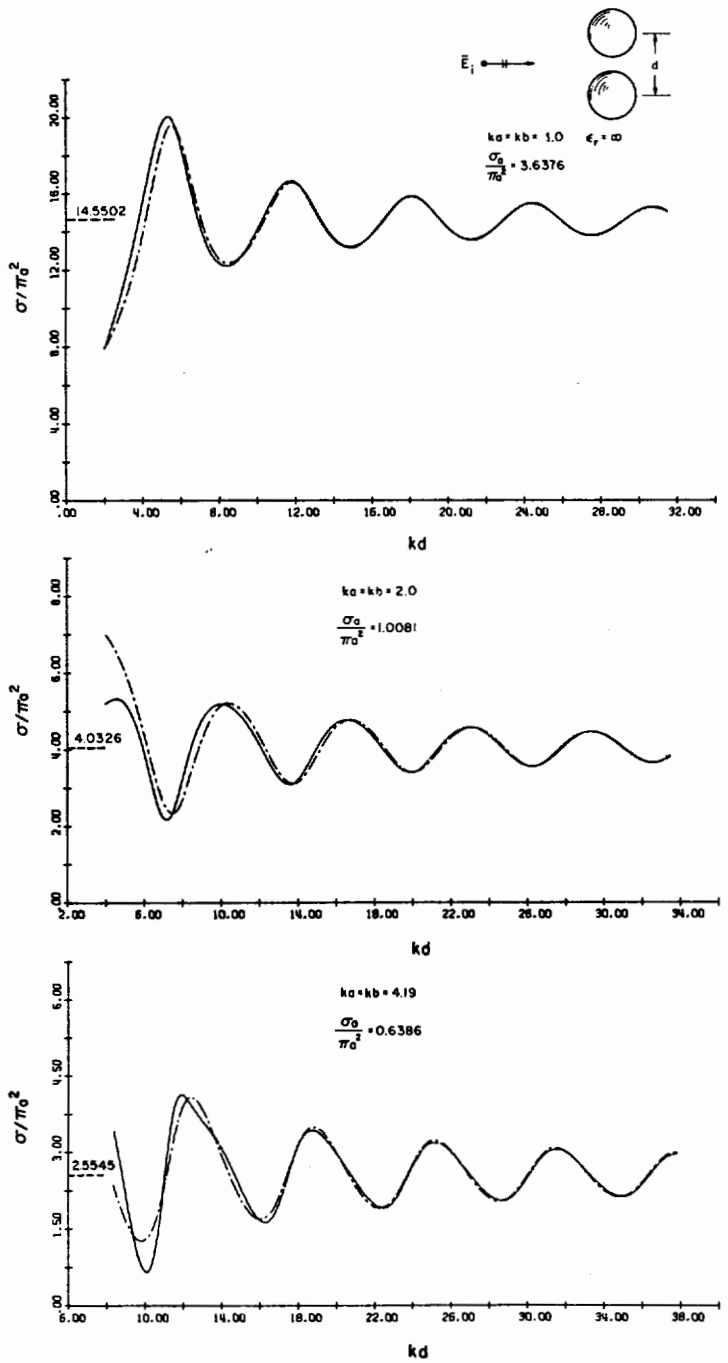

Figure 4.3 RCS of Two Equal Metallic Spheres at Broadside Incidence for ka = 1.0, 2.0, and 4.19 Using Exact (_____) and Asymptotic (__ _ __) Form of Translational Addition Theorem.

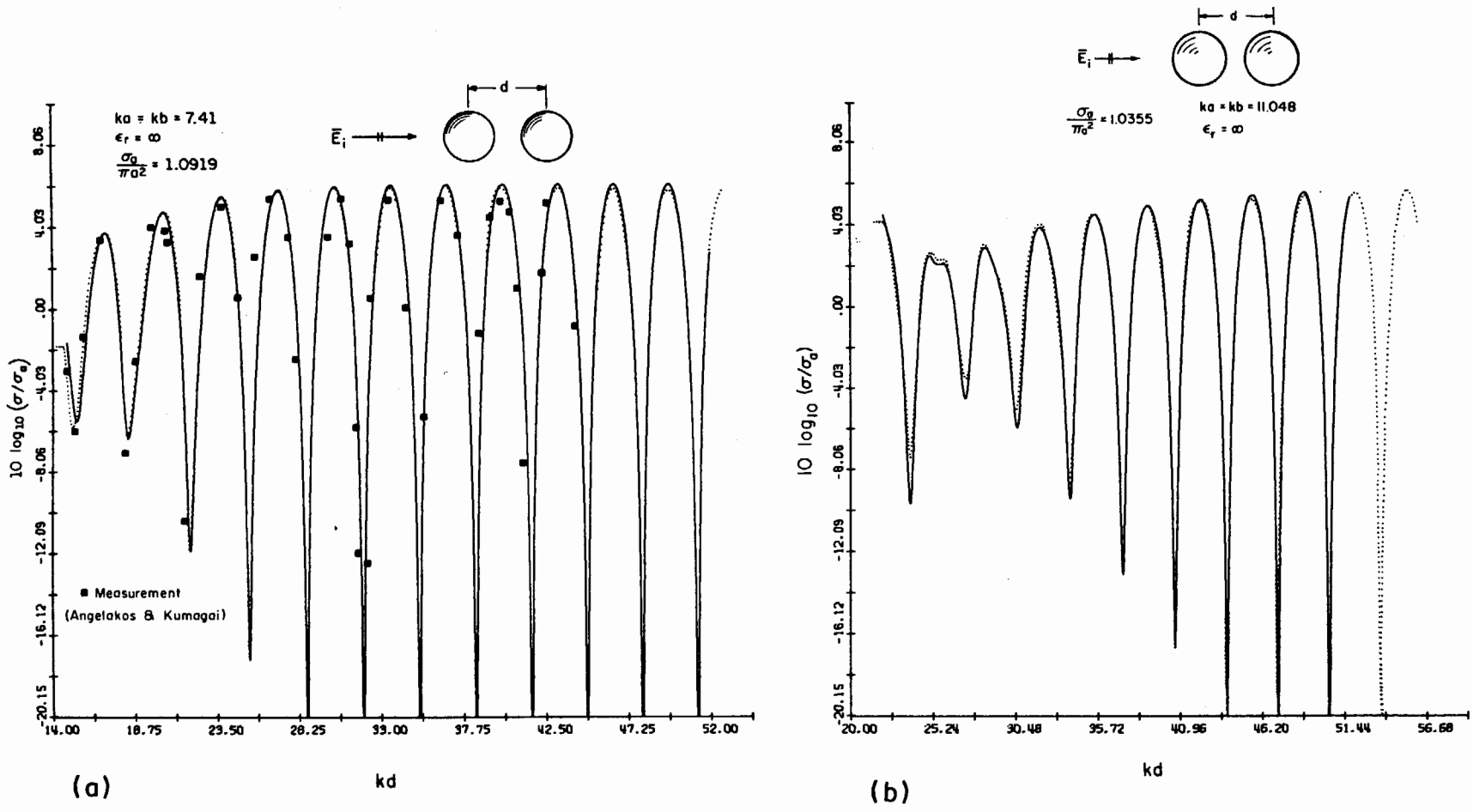

Figure 4.4 RCS of Two Equal Metallic Spheres at Endfire Incidence for (a) ka = 7.41 and (b) ka = 11.048 from Modal Approach (_____) and Experiment (·····).

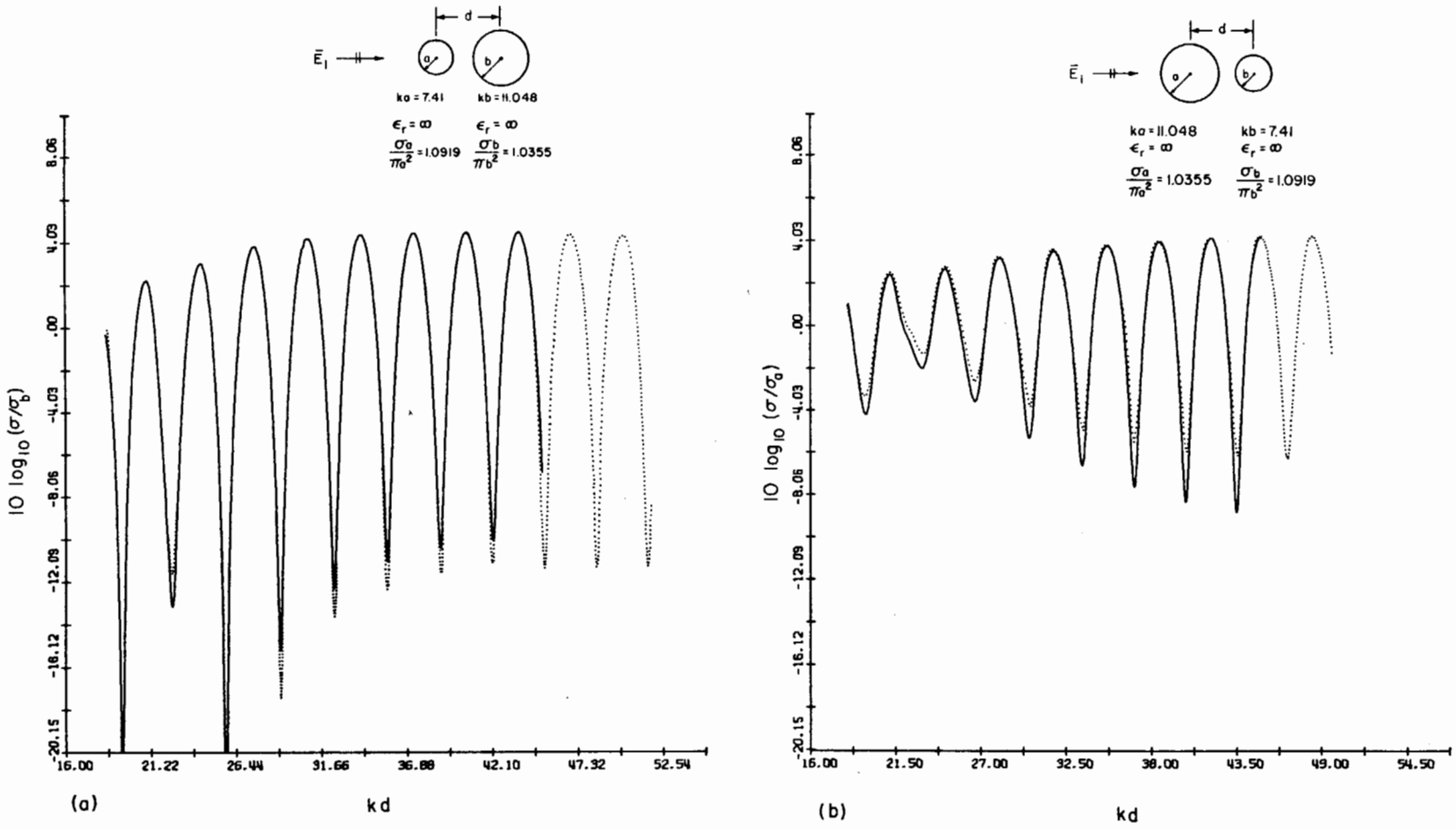

Figure 4.5 RCS of Unequal Metallic Spheres at Endfire Incidence for (a) the Smaller and (b) the Larger Sphere in Front from Modal Approach (_____) and Experiment (·····).

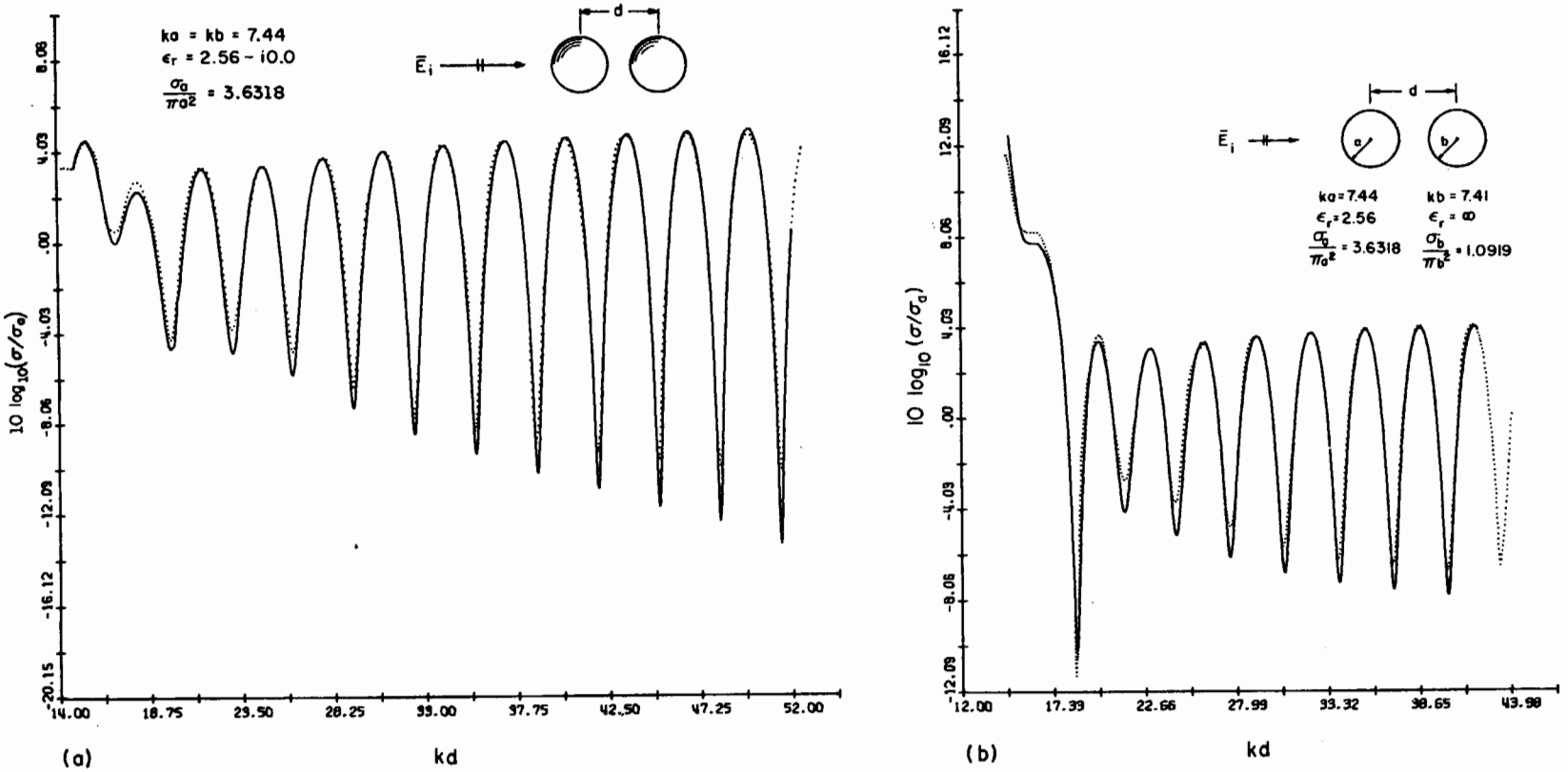

Figure 4.6 RCS of (a) Two Dielectric and (b) One Dielectric and One Metallic Sphere at Endfire Incidence from Modal Approach (———) and Experiment (·····).

spheres persists for larger kd than for the case of metallic spheres nearly the same size (cf. Figure 4.4(a)); however, in the broadside case for the same two dielectric spheres (Figure 4.2) the interaction was negligible for a much smaller value of kd. Perhaps this is due to some focusing action from the front sphere to the rear sphere. A focusing effect is clearly evident in the adjacent curve, Figure 4.6(b), where we have a metallic sphere behind a dielectric sphere, both about the same size. The quite large return at and near contact might be interpreted as due to rays focused by the front dielectric sphere, reflected by the metallic sphere and refocused by the dielectric sphere back to the observer — analogous possibly to placing a mirror behind a lens near its focal point. This same enhancement for this geometry and the same spheres was also observed both experimentally and theoretically at two other frequencies.

4.2.4 Variable Angle of Incidence — Fixed Separation

In Figures 4.7 through 4.9 the aspect angle or angle of incidence α is the independent variable. Figures 4.7(a) and (b) show the RCS of the previously discussed pair in contact, normalized to the dielectric sphere vs. α, for the horizontal and vertical polarizations respectively. The enhancement when the dielectric sphere is in front is again apparent. When the metallic sphere is in front, the return is considerably smaller than for an isolated metallic sphere of that size. The basic character is similar for the two polarizations. Note that the single sphere return for the dielectric is considerably higher than for the metallic sphere. In Figure 4.8(b) we have the same configuration as in 4.7(b) except for lower frequency. In this case we obtain large enhancement of RCS at the same place even though the RCS of an isolated dielectric sphere at this

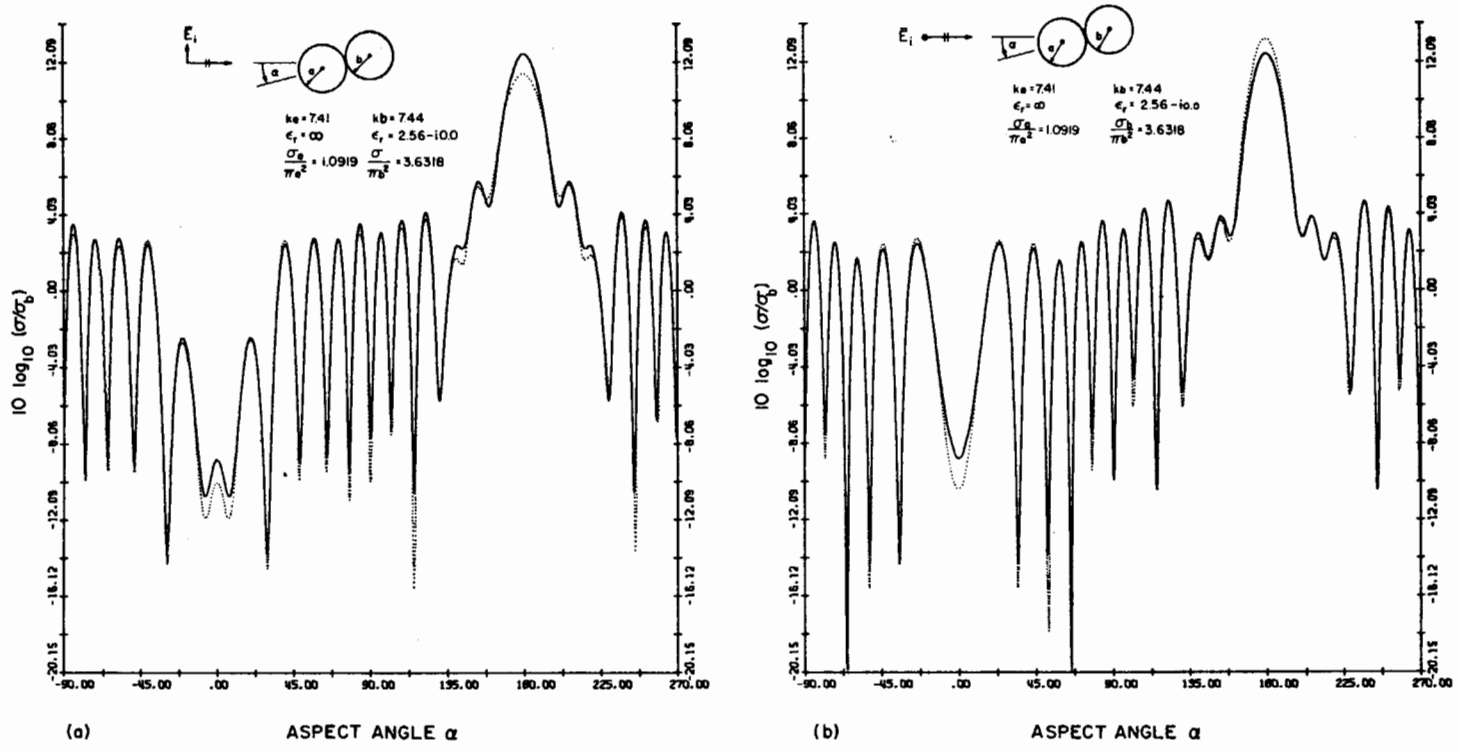

Figure 4.7 RCS of One Metallic and One Dielectric Sphere in Contact vs. Aspect Angle for (a) Horizontal and (b) Vertical Polarization from Modal Approach (_____) and Experiment (·····).

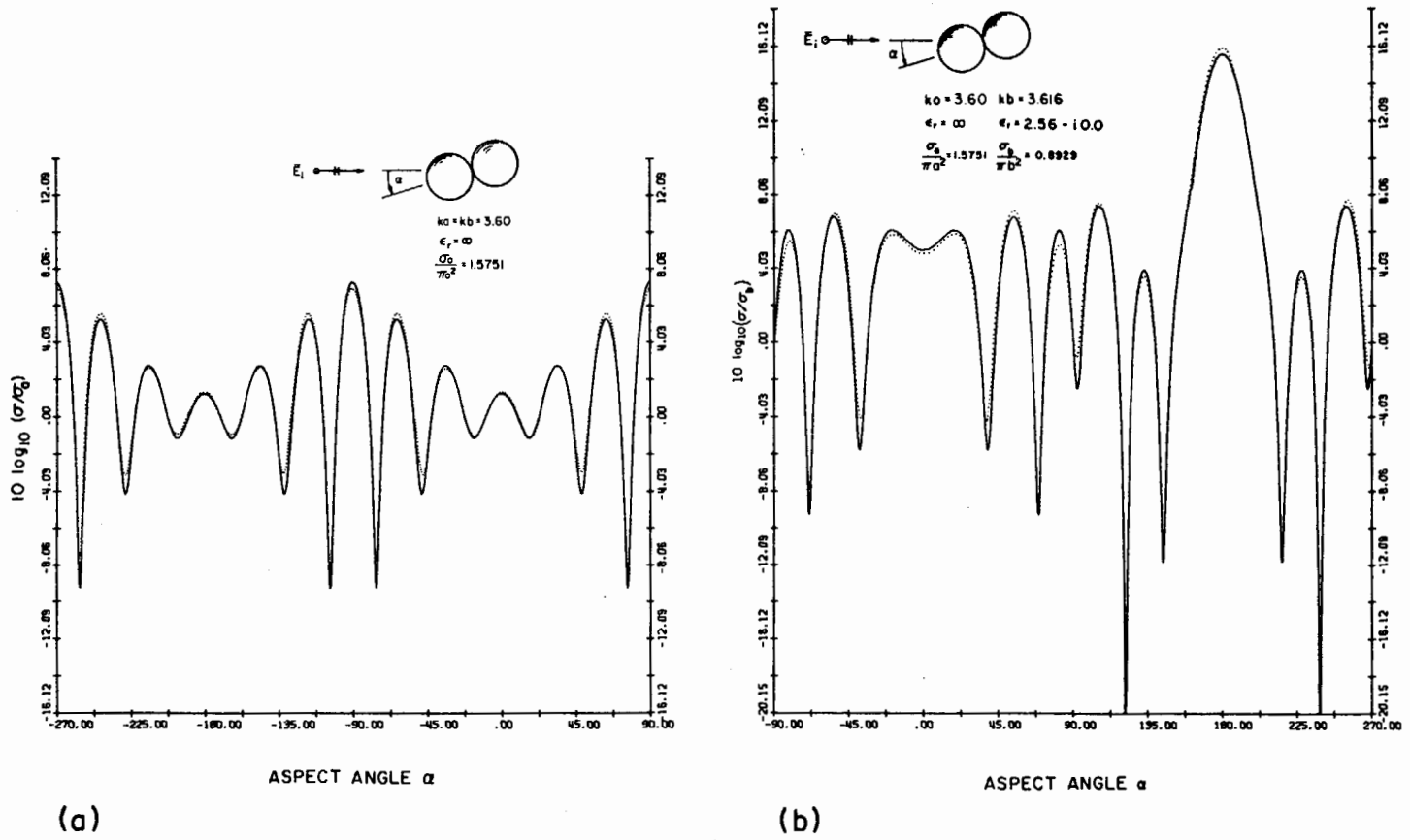

Figure 4.8 RCS of (a) Two Metallic and (b) One Metallic and One Dielectric Sphere in Contact vs. Aspect Angle from Modal Approach (_____) and Experiment (·····).

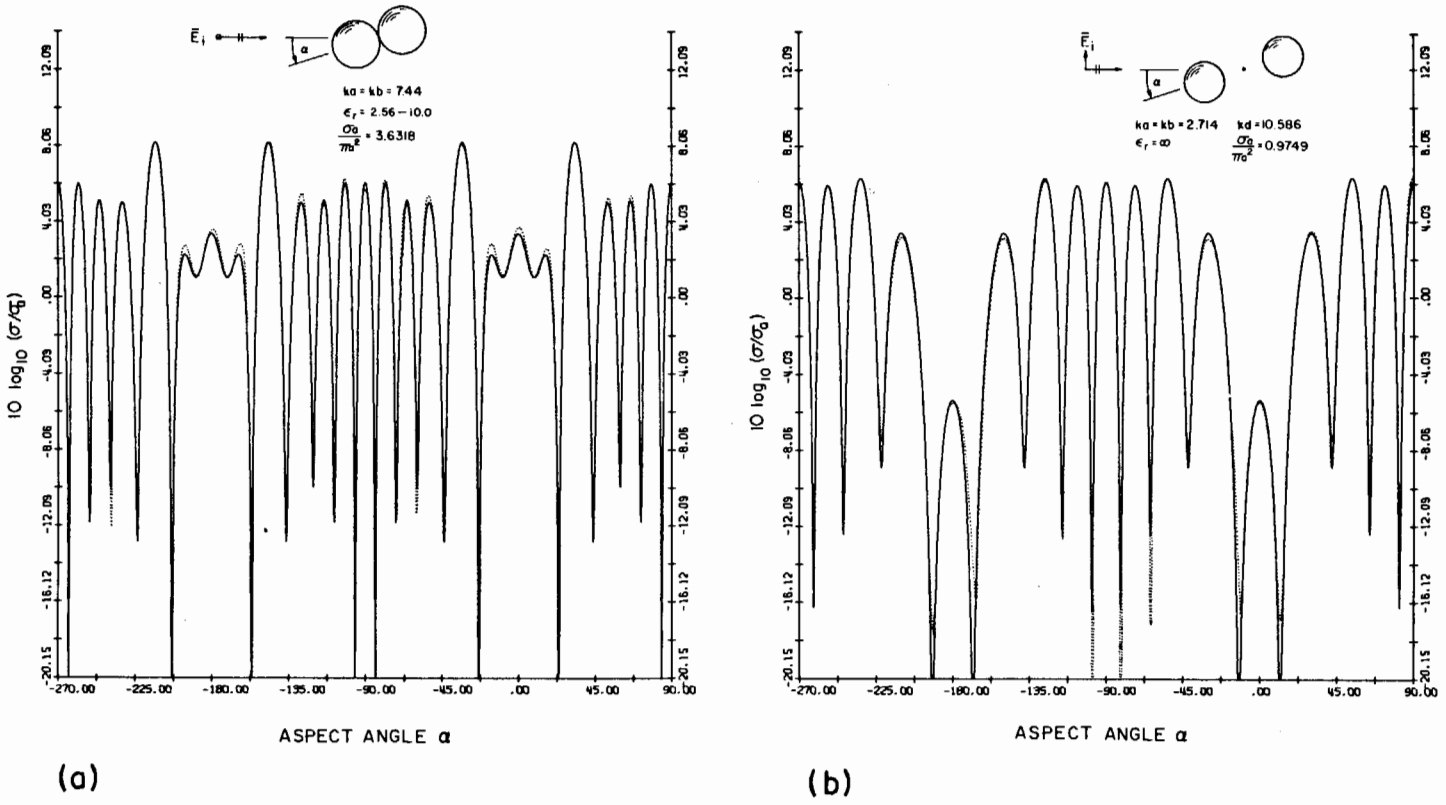

Figure 4.9 RCS of (a) Two Dielectric Spheres in Contact and (b) Two Metallic Spheres Separated by One Diameter vs. Aspect Angle from Modal Approach (_____) and Experiment (·····).

frequency is smaller than its metallic partner. In 4.8(a) is shown the RCS of a metallic pair in contact for comparison. In all these curves the agreement is nearly perfect with only very few exceptions. Two more miscellaneous examples are shown in 4.9(a) and (b).

4.3 Bistatic Cross-Sections

The multipole coefficients for the two spheres, as is clear from (2.21), depend on the angle of incidence of the plane wave and are completely independent of the point of observation. The point of observation enters into the calculation only in equations (2.26) and (2.27). Hence, once the coefficients $A_E(m,n)$, $A_H(m,n)$, $B_E(m,n)$, $B_H(m,n)$ are calculated it is relatively easy to find the scattered field in any direction. Two such examples are considered in Figure 4.10(a) and (b) where the normalized bistatic cross-sections σ_θ and σ_ϕ corresponding to E_θ and E_ϕ in the planes $\phi = 0$ and $\pi/2$ respectively have been computed for ka = 1 and 2. We see, as expected, that these two cross-sections coincide in the two directions of axial symmetry.

4.4 Depolarization Due to Multiple Scattering

As remarked previously, there is no depolarization of the back-scattered field when the incident polarization is horizontal or vertical ($\gamma = 0,\pi/2$) regardless of sphere sizes, separation or angle of incidence α (see (2.27)). This is certainly obvious in cases of symmetry, as for example, $\alpha = 0$, and $\alpha = \pi/2$ with identical spheres. The more general cases are not so obvious. Beckmann (1968) defines a polarization factor (call it P) as the quotient of the horizontal and vertical components of the electric field under consideration. Hence a horizontally polarized

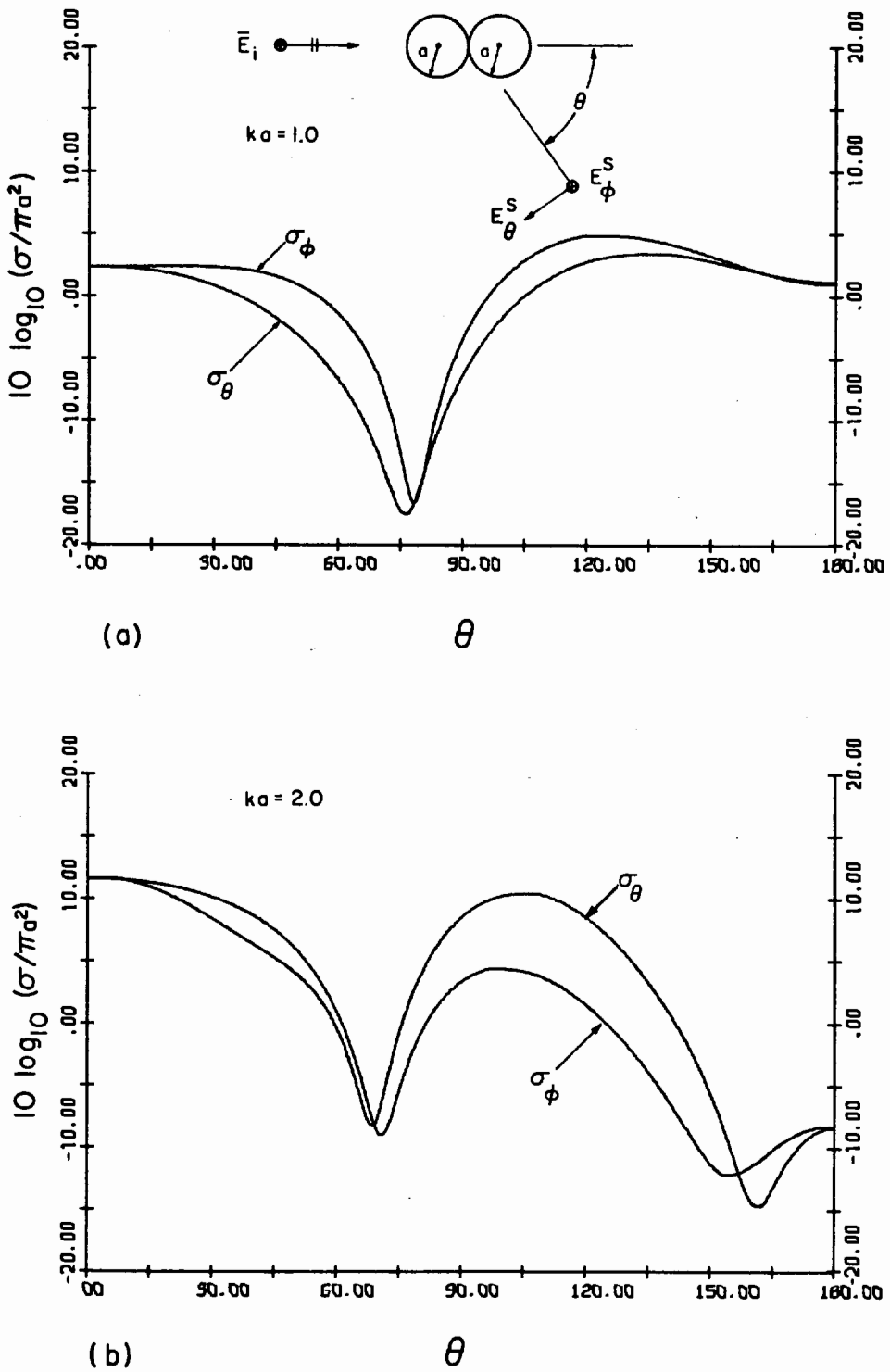

Figure 4.10 Normalized Bistatic Cross-Section in the Two Principal Planes for Two Spheres in Contact at Endfire Illumination Using Modal Expansion for (a) ka = 1.0 and (b) ka = 2.0.

incident field has the polarization factor of zero, and for vertical polarization it is infinite. All complex values of P represent elliptical polarization in general, with a right rotational sense if $Im\{P\} > 0$ and a left rotational sense if $Im\{P\} < 0$. Circular polarization is characterized by the values $\pm i$. If now, a scattered wave has the same polarization factor, then the scatterer has not "depolarized" the incident wave. The depolarization factor D is then defined as: $D = P_s/P_i$. Hence, $D = \pm 1$ when there is no depolarization. If we consider only the backscattered field, then from symmetry we know that an isolated sphere cannot depolarize an incident plane wave regardless of incident polarization. The same would also apply to any two spheres <u>if</u> there were no coupling between them. Therefore, in the absence of symmetry, the depolarization of the back-scattered field indicates the degree of the coupling between the spheres. Consider first the case of two identical spheres at broadside incidence. As we said previously there will be no depolarization at $\gamma = \ell\pi/2$, where ℓ is any integer. Consider the intermediate cases where $\gamma = (2\ell-1)\pi/4$. Here we see that since the two spheres scatter the two incident polarizations differently, depolarization of the backscattered field is therefore expected. The depolarization will be strong for close spacing and weak for large separation. Figure 4.11 shows polarization ellipses of the broadside backscattered field from two identical perfectly conducting spheres ka = 2, illuminated by a plane wave with $\gamma = \pi/4$ (P = 1). The number under each ellipse is kd and the letters L and R indicate the sense of polarization. At contact, (kd = 4) strong depolarization is evident. As the sphere separation increases, the ellipse orientation oscillates about the incident E vector direction; the ellipse itself contracts and expands, undulating and changing sense of polarization in the process, eventually

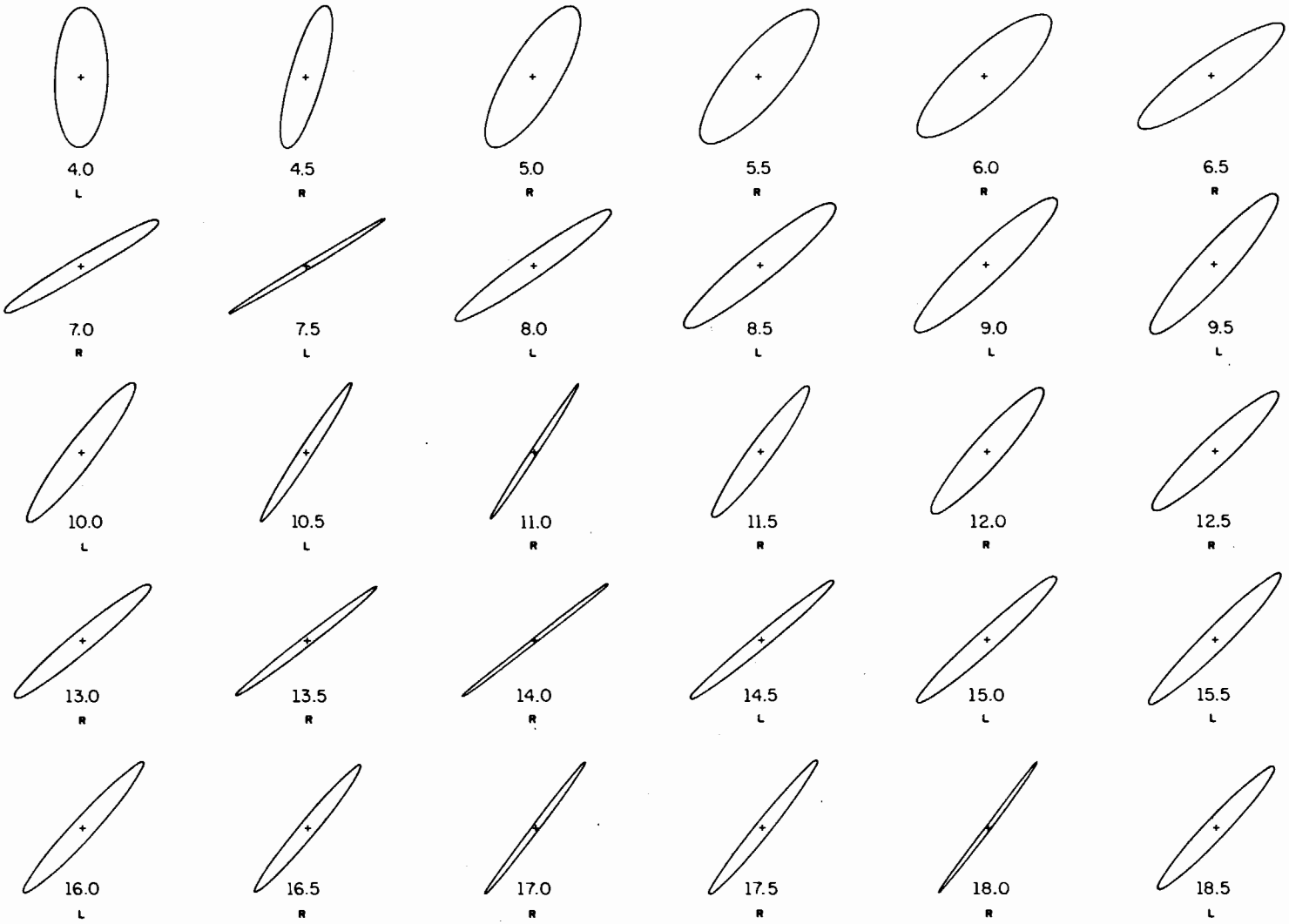

Figure 4.11 Polarization Ellipses of Backscattered Field of Two Equal Metallic Spheres ka = 2.0 vs. Separation (kd) from a Broadside Incident Plane Wave Linearly Polarized at 45°.

converging to a 45° line corresponding to no depolarization. It is rather fascinating to portray such a complex scattering process through the use of depolarization.

The depolarization effects are perhaps even more vividly seen in Figure 4.12 where the "depolarization ellipses" are shown for the back-scattered field of the same two spheres as they rotate in contact ($\alpha = 0 \rightarrow 87^{\circ}$). Here, starting at endfire where there is no depolarization, we see that the major axis of the ellipse swings from $+45^{\circ}$ to about 190° and then back to approximately 90° with wide variations in the amplitude. Several other cases of this type were investigated for different ka, with the curious result that some cases exhibited a backscattered field at particular angles with nearly perfect circular polarization.

As final examples, we compute the cross-polarized radar cross-section normalized to πa^2 for the two examples considered above. The transmitted field is polarized at $\gamma = 45^{\circ}$ and we receive at 135°. Hence, in the absence of coupling we would receive nothing at the orthogonal polarization as with the isolated sphere. The results for the broadside case are shown in Figure 4.13(a). The decrease in the cross-polarized RCS is quite rapid as kd is increased. This is to be expected since the coupling is generally related to the ratio d/a which changes more rapidly for small spheres for the same interval in kd. For large spheres, this behavior may be very simply predicted by geometric optics.

The cross-polarized RCS for two equal spheres in contact as their aspect angle changes is shown in 4.13(b). As we expect there is no cross-polarized return for the aspect angles 0 and π. It was suggested

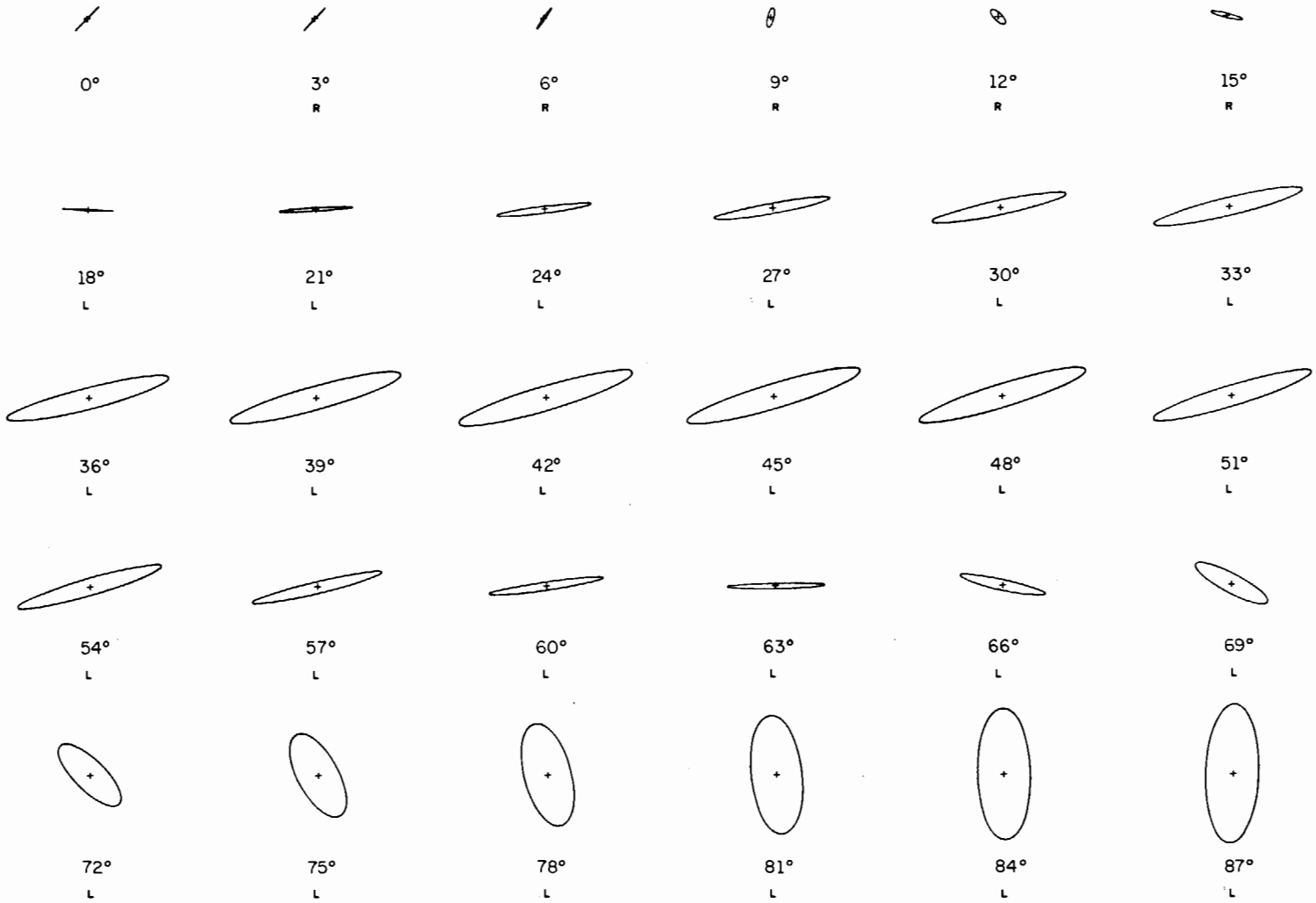

Figure 4.12 Polarization Ellipses of Backscattered Field of Two Equal Metallic Spheres ka = 2.0 in Contact vs. Aspect Angle from an Incident Plane Wave Linearly Polarized at 45°.

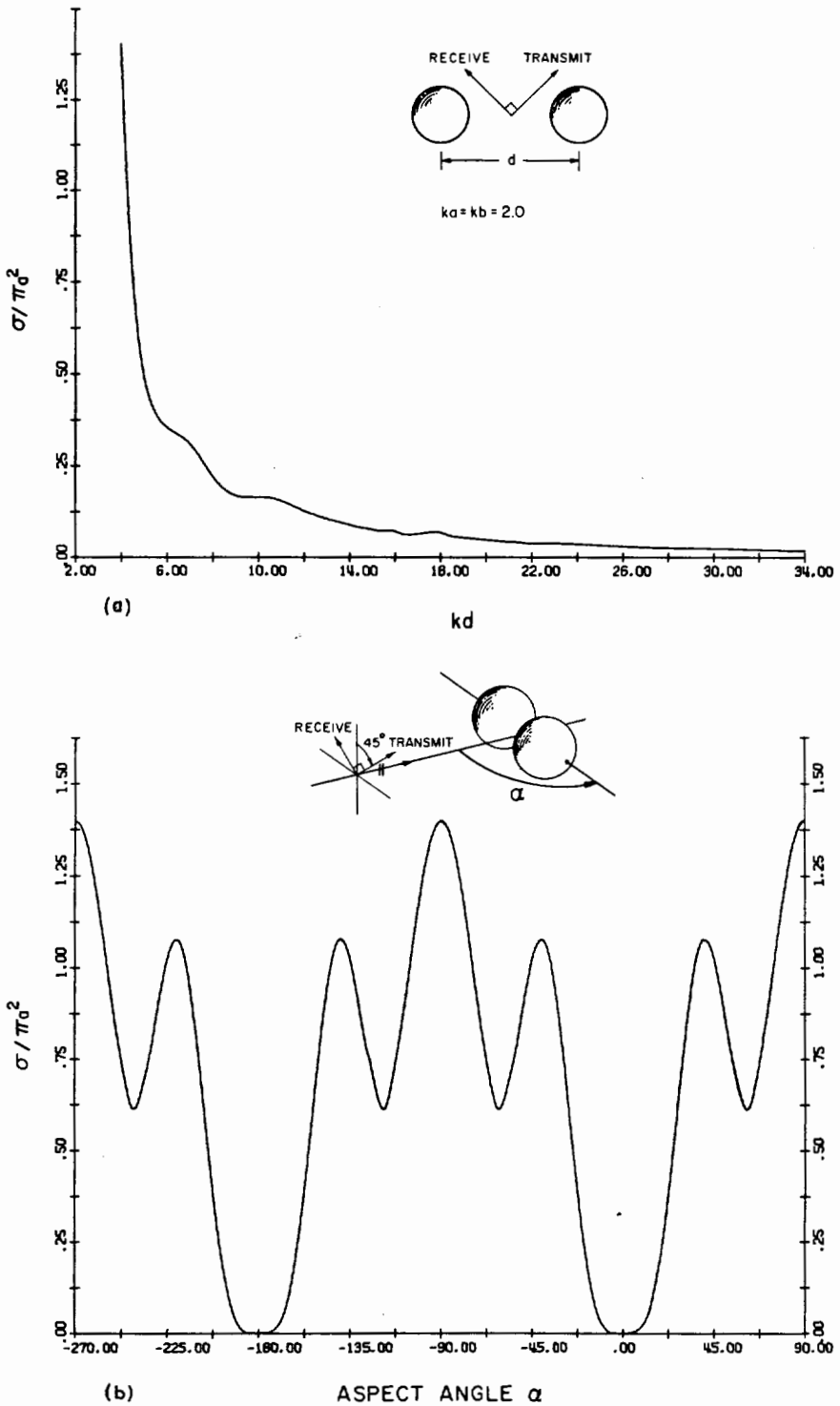

Figure 4.13 Cross-Polarized RCS of Two Equal Metallic Spheres ka = 2 (a) vs. Separation and (b) in Contact vs. Aspect Angle.

by E. Knott[†] that two spheres in either of these configurations might serve as a new means of calibration for cross-polarized RCS measurements.

4.5 Miscellaneous Results

The extinction or total scattering cross-section is a frequently discussed quantity in single body scattering theory since it is so simply related to the forward scattered field of the object (Jones, 1964). In the case of scattering by a single lossless sphere the normalized extinction cross-section approaches the asymptotic value of 2 as $ka \to \infty$, or the cross-section is twice its geometric area. As explained by Van de Hulst (1957), half of this comes from scattering by an area πa^2 and the other half from the shadow boundary of the sphere. The latter part is necessary to recover the incident field at a large distance from the sphere in the forward direction which was removed by the shadow created by the area πa^2.

We would expect that in the absence of multiple scattering, the total scattering by two bodies would be the sum of the total scattering by each, regardless of orientation. With multiple scattering it is no surprise that the total cross-section varies with changes in the parameters. As separation is increased, the total cross-section oscillates about and eventually converges to the value which is the sum of the total cross-sections of the two isolated spheres. No such general statements can be made concerning other parameter changes.

[†] Private communication (December, 1968).

The rather interesting phenomena of resonance scattering by isolated dielectric spheres also deserves some attention in relation to multiple scattering. When $\sqrt{\epsilon_r} \gg 1$, one finds very strong peaks in the scattering (Kattawar and Plass, 1967). The first peak occurs quite reliably at $ka = \pi(1-\epsilon_r^{-2})/\sqrt{\epsilon_r}$ (Jones, 1964) and is due to the very small value in the denominator of the first magnetic multipole coefficient $u_1(ka)$ (dipole). Hence, if $ka \ll 1$ then the scattering may also be called Rayleigh scattering and we need take no more than the first term in the Mie series for a single sphere. If we consider the case of Rayleigh scattering by two spheres, one or both of resonant size, we may use (2.32) and (2.33) to solve explicitly for the multipole coefficients. Clearly if one of the spheres is of resonant size and the two spheres are spaced such that there is little or no coupling, then the resonant phenomena is undisturbed. If however the spheres are in close proximity the resonant phenomena can be drastically altered. This can be understood in terms of the matrix representation of (2.21) which reads $\mathcal{M} = \mathcal{F} + \mathcal{C}\mathcal{M}$. In the case of one or two spheres at resonance $\mathcal{C}$ will be large, implying that $\mathcal{M}$ is not given by a small perturbation from $\mathcal{F}$. This also indicates that (2.21) cannot be solved by iteration.

One such case of "resonant multiple scattering" was investigated numerically for two identical lossless dielectric spheres with $\sqrt{\epsilon_r} = 50$. The first resonance for the isolated sphere occurs at $ka = .0628068$. The normalized RCS of one of these spheres at this value of ka is 2280! Multiple scattering by two spheres is usually small when the spheres are separated by several diameters ($d/a \gtrsim 6$); however, for this case, the

interaction is considerable even for $d/a \approx 50$.

It would indeed be interesting to investigate this experimentally, even for a single resonant sphere.

5. RAY OPTICAL APPROACH TO SCATTERING BY TWO SPHERES

It is quite evident from the previous work that the multipole expansion technique ceases to become useful when the spheres become very large in terms of wavelengths due to the slowness in convergence of the series and the large number of the coefficients $a(m,n,-m,\nu,p)$ which must be calculated. It is generally believed that the series solution for the single sphere cannot be efficiently used when the sphere radius exceeds several wavelengths; however, extensive calculations have been carried out using the Mie series for ka as large as 3000 (Fahlen and Bryant, 1968). The computation of the scattering by two spheres of this size, however, is out of the question since this would require in general about 1.4×10^{13} of the coefficients $a(\cdot)$. We need not cite quite so dramatic an example to make the point that eventually the series representation loses its usefulness, and that an alternative solution is needed for the case of scattering by two electrically large spheres. Such an alternative solution for the single sphere was initially provided by White (1922); he transformed the slowly converging series into a residue series by a modified Watson transformation which enabled him to separate and identify the reflected and diffracted components of the field. Later, Franz and Depperman (1952), independently,[†] recognized that the diffracted part could be interpreted as "creeping waves," i.e., waves that creep around the sphere (or cylinder). In view of the fact that, for the two sphere

[†] Logan (1962, 1965) has given an excellent historical account of this and other aspects of single sphere problem.

problem, we do not have an explicit series solution (due to the coupling of the coefficients in (6.21)), it does not appear possible to apply an analogous "Watson transformation" to the ensemble of two spheres. The alternative would then seem to be the application of the creeping wave theory developed for the single sphere and classical geometric optics.

There are very few scattering problems which possess exact solutions with which we can gauge the effectiveness and applicability of various approximate or asymptotic methods. Since we have an exact solution to the two sphere problem, including numerical results, we are in a good position to comment on several approximate methods for its solution — in particular, the following creeping wave theory and geometric optics, and the method discussed previously in 2.8.3. Application of the former method can be analyzed critically with regard to the two sphere problem and from this we may also form some conclusions regarding its applicability to other problems. There has apparently been no previous attempt to apply the creeping wave theory to a multiple scattering problem.

5.1 Creeping Wave Theory and Geometric Optics

Levy and Keller (1959) have elegantly extended Franz's (1954) creeping wave theory for the sphere to diffraction by an arbitrary smooth convex body. The canonical problems of acoustic diffraction by soft and hard cylinders provide the appropriate diffraction coefficients and decay exponents associated with the waves (or rays) that creep around the diffracting body. The ray paths associated with the creeping waves obey Fermat's principle, and hence, creep along geodesics of the surface. The diffraction and attenuation coefficients associated with the impact and

launch points are dependent on the nature of the surface at these points; and the exponential decay associated with the creeping waves is due to the continuous shedding of rays along the geodesic. The case of electromagnetic scattering by a general body is treated by appropriately combining the results for the two scalar problems (acoustically hard and soft).

The above method has been shown to be asymptotically valid when the radius of curvature of the body is sufficiently large in terms of wavelengths. When applied to the vector problem of the sphere it is found that the results are inaccurate for moderate ka. This does not mean, however, that the creeping wave concept breaks down, only that the diffraction coefficients and attenuation factors for the acoustically hard and soft cylinders (or spheres) do not accurately describe the situation for electromagnetic scattering by a sphere for moderately small ka. If instead, we use the vector problem of the sphere as the canonical problem, the results are considerably improved. Senior and Goodrich (1964) expressed the single sphere scattered field in a form which makes identification of the appropriate diffraction coefficients an easy matter.

With the above, the scattered field from two perfectly conducting spheres can be considered to be composed of essentially three types of rays (Bruning and Lo, 1967, 1968): 1) geometric optics rays, i.e., those arising from direct and multiple reflections, 2) creeping wave rays bound to a single body, and 3) "hybrid creeping wave" rays. The rays falling into the last category are those which may involve any combination of the first two types. For purposes of further classification, rays of the first type which undergo j reflections are denoted by R_j; those rays of the second type which creep over a distance equal to or less than

halfway around the body are denoted by C_-; C_+ describes the case of a larger distance. Finally the third case may be represented by any combination of the above symbols with its obvious implication. For example, a ray which creeps part way around one sphere, most of the way around the other, and reflects 5 times between the two before reaching the observer is given the symbol $C_-C_+R_5$. A particular geometry of two spheres could support any number of configurations of rays, however, generally only a few will be significant.

All these rays obey Fermat's principle and, as a result, the amplitude of the field along a ray can be deduced from the conservation of energy, properly extended to the case of a creeping wave.

Field calculations employing the geometric optics approximation are carried out using Snell's Law and the conservation of energy by calculating the change in cross-section of the tube of rays (pencil) upon each reflection from the surface of the spheres. This cross-sectional change can be calculated by following the principal radii of curvature of the wavefront through each reflection.

Consider an incident wave with radii of curvature ρ_1 and ρ_2 in the principal planes which is incident upon an arbitrary smooth perfectly conducting surface Σ at an angle θ with the normal to the surface having principal curvatures c_1 and c_2. The reflected wave after impact at point A, in the plane of the incident wave, will then have the principal curvatures (Born and Wolf, 1964):

$$\frac{1}{\rho_1^*} = \frac{1}{\rho_1} + 2c_1 \cos\theta$$
$$\frac{1}{\rho_2^*} = \frac{1}{\rho_2} + 2c_2 \sec\theta \qquad (5.1)$$

where for the sphere $c_1 = c_2 = 1/a$, a being the radius of the sphere (see Figure 5.1). Thus, if E(A) is the value of the incident field at A, then the reflected field at some point P, a distance s from A, is given by:

$$E(P) = - E(A) \left[\frac{\rho_1^* \rho_2^*}{(\rho_1^*+s)(\rho_2^*+s)} \right]^{1/2} e^{iks} \tag{5.2}$$

The bracketed term is designated the divergence factor Δ. If more than one reflection is involved, the above procedure is repeated; the field at some point P after N reflection will then assume the form:

$$E(P) = (-1)^N E(A) \prod_{r=1}^{N} \Delta_r e^{ikS_{rN}} \tag{5.3}$$

where Δ_r is the divergence factor associated with the rth reflection and S_{rN} is the ray length between the reflection points r and (r+1). The $(-1)^N$ factor is consistent with the vertical polarization assumed in Figure 5.1; for horizontal polarization, the $(-1)^N$ factor is replaced by -1. In general, the orientation of the reflected E field for each reflection is determined by the well known result of geometric optics:

$$\bar{E}_r = \bar{E}_i - 2\hat{n} \times (\bar{E}_i \times \hat{n}).$$

If the point P does not lie in the plane formed by the incident wave and the normal to the surface or if refractions are also involved, the more systematic matrix formulation of Deschamps (1967) is preferred in which the "state" of the pencil of rays is described by a curvature matrix. Each operation on the pencil (reflection, refraction, rotation, propagation) is described by a matrix; the resultant state of the pencil

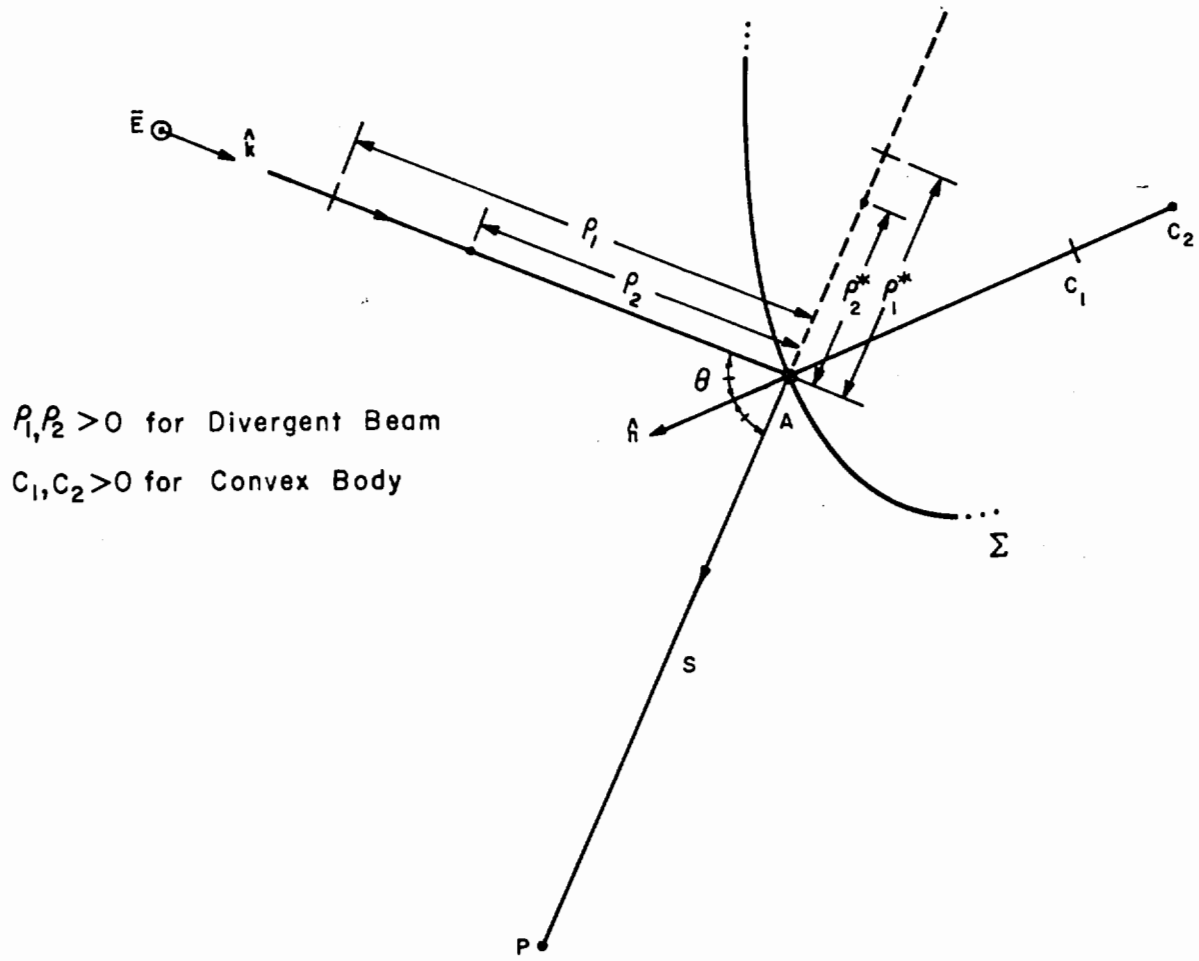

Figure 5.1 Reflection of an Astigmatic Pencil of Rays from a Curved Surface.

is obtained by multiplying together the appropriate matrices.

It is necessary next to describe the basic geometry and constituents of the creeping wave theory as it applies to the sphere. With regard to Figure 5.2, consider a source located at Q a distance R from the impact points Q_1 and Q_2. Consider next an observation point P in the geometrical shadow of Q. The field at P is due to rays which take the geodesic paths QQ_1P_1P and QQ_2P_2P in addition to those which encircle the sphere any number of additional times before leaving the sphere at P_1 and P_2, respectively. We may, however, neglect those rays which make the additional circuits since the attenuation of these rays is exponential along the surface. From Levy and Keller (1959) we find the field at P due to the ray QQ_1P_1P to be:

$$E_1(P) = E(Q_1) \left[\frac{d\sigma(Q_1)}{d\sigma(P_1)}\right]^{1/2} \left[\frac{\rho_1}{s(\rho_1+s)}\right]^{1/2} D_o^2 \times e^{ik(a\tau_1+R+s)} e^{-\alpha_o a\tau_1} \qquad (5.3)$$

The factor $[d\sigma(Q_1)/d\sigma(P_1)]^{1/2}$ is the ratio of the strip width of the surface diffracted rays at Q_1 and P_1 which for the sphere reduces to the ratio $(a_o/a_1)^{1/2}$, and ρ_1 is the secondary radius of curvature of the emerging ray P_1P which is obtained by extending a line along P_1P until intersection with the caustic line QO. With the above (5.3) becomes:

$$E_1(P) = E(Q_1) \left[\frac{aR}{\rho rs|\sin\theta|}\right]^{1/2} D_o^2 e^{ik(a\tau_1+R+s)} e^{-\alpha_o a\tau_1} \qquad (5.4)$$

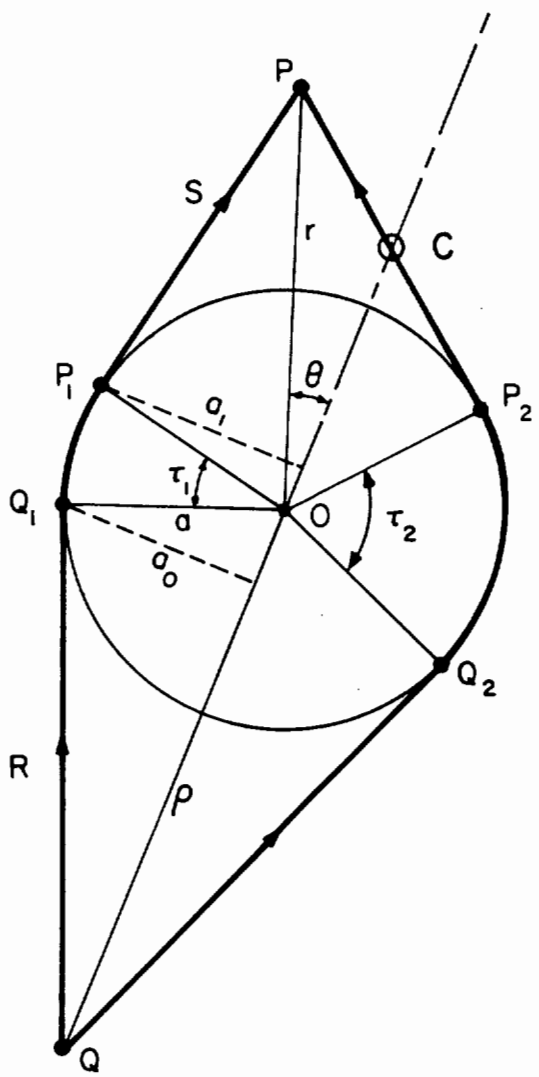

Figure 5.2 Geometry of Creeping Waves on a Sphere.

The companion ray QQ_2P_2P is found from above by replacing τ_1 by τ_2, or by replacing θ by $2\pi-\theta$ in (5.3), and multiplying the result by $e^{-i\frac{\pi}{2}}$. The $-\pi/2$ phase shift results from the fact that the ray P_2P passes through the caustic line at C (see Figure 5.2) which means that ρ_1 has changed sign resulting in an additional factor $\pm\sqrt{-1}$ in (5.3); the minus sign being chosen because of the $e^{-i\omega t}$ time convention. The factors D_o^2 and α_o are respectively the diffraction coefficients and attentuation factor of the creeping waves. We present the forms[†] for these two quantities, appropriate for the vector problem of the sphere, given by Senior and Goodrich (1964):

$$D_o^2 = \left(\frac{\pi}{2k}\right)^{1/2} e^{i\pi/12} \frac{\pi\xi}{\bar{q}_o A^2(\bar{q}_o)} (1 + e^{i\pi/3}\xi^{-2}\chi_1) \tag{5.5}$$

$$\alpha_o = a^{-1} e^{-i\pi/6}\xi\bar{q}_o(1 - e^{i\pi/3}\xi^{-2}\chi_2 + e^{i2\pi/3}\xi^{-4}\chi_3) \tag{5.6}$$

With the omission of the terms in parentheses this agrees with Levy and Keller. In the above, $\xi = (ka/6)^{1/3}$ and A(x) is the Airy integral

$$A(x) = \int_o^\infty \cos(y^2 - xy)\,dy$$

with $\bar{q}_o$ being the first zero of $\frac{d}{dx} A(x) = 0$, and is approximately given by $\bar{q}_o \approx 1.46935$. The remaining constants are:

[†] The higher order term in parentheses in the general case is a function of θ which becomes unbounded in the backscatter direction; the diffraction coefficient shown here is applicable for the backscatter direction. For large ka we have approximately, $|D_o^2/a^{1/2}| \approx (ka)^{-1/6}$, $\mathrm{Re}\{\alpha_o a\tau\} \approx .7\tau(ka)^{1/3}$.

$$A^2(\bar{q}_o) \approx 1.36142$$

$$\chi_1 = 3/20\bar{q}_o^{-2} + 8\bar{q}_o/45 \approx .330695$$

$$\chi_2 = 3/20\bar{q}_o^{-2} - \bar{q}_o/180 \approx .061313$$

$$\chi_3 = (\bar{q}_o^{-2}/9 - 7/3\bar{q}_o + 63/4\bar{q}_o^{-4})/1400 \approx .004352.$$

The diffraction coefficient and decay exponent (5.5) and (5.6) apply to the case of the electric vector propagating normal to the surface. The complimentary case of the electric vector tangential to the surface will not be discussed since it contributes negligibly in comparison to the former case.

From (5.4) it is apparent that the directions $\theta = 0$ and π are exceptional directions since (5.4) predicts an infinite value. These two directions place the observation point on the caustic line which results from the fact that in these directions there are infinitely many geodesics. Equations (5.3) and (5.4) are also not applicable in cases where the observation point lies on the shadow boundary since at these places the residue series does not converge in the first place. Furthermore, we should consider only those points at a distance $kr > (ka)^{1/3}$ (Franz, 1954). When the observation point lies in the far field the above two restrictions may be summarized by the inequality $0 < |\theta-\alpha| - \epsilon < \pi$ with $\epsilon > 0(1/ka)$ (Senior and Goodrich, 1964). The case of backscattering ($\theta = \pi-\alpha$), however, may still be included using the previous formulation if the axial caustic correction factor $(\pi ka|\sin\theta|)^{1/2}$ is supplied (Levy and Keller, 1959) along with an electromagnetic backscattering theorem which introduces an additional factor of -1/2 (Levy and Keller, 1960). The

caustic correction factor may not be used in the forward scatter direction as the residue series diverges there and the creeping wave interpretation of the solution loses its meaning.

As an illustration of the above analysis, the backscattered electric field is calculated in the far field region for an incident plane wave with the result

$$E_{\pi} = -\frac{a}{2r} e^{ik(r-2a)}\left[1 - i/2ka - D_o^2 a^{-1/2}(2\pi ka)^{1/2} \times e^{ika(\pi+2)+i\pi/4} e^{-\alpha_o a\pi}\right]. \qquad (5.7)$$

The first two terms arise from the saddle point integration of the remainder of the transformed series solution after the residue series has been split off (White, 1922); only the first term carries the geometric optics label. The third term comprises the creeping waves which creep around the backside of the sphere. If the radar cross-section (RCS) $\sigma = \lim_{r \to \infty} 4\pi r^2 |E_{\pi}|^2$, normalized to the area πa^2 is computed from (5.7) the results are found to differ from the exact solution by no more than 1% for a/λ as small as 0.3 and 3% for a/λ as small as 0.1.†

With these results for the single sphere it is quite tempting to conclude that the creeping wave theory applied to two spheres should give equally good results. As will be demonstrated shortly, application of the creeping wave theory to two spheres is critically dependent on geometry.

---

† It is interesting to note that the inclusion of the most significant creeping wave for the electric vector tangential to the surface gives consistently worse results than without it.

5.2 Application to Special Cases

Let us consider the case depicted in Figure 5.3 where we have two perfectly conducting spheres of different size (presumably large in terms of wavelengths). As in the previous approach the angle of incidence is α, and the scattering angle is θ. Using the geometric optics approach outlined in (5.1) to (5.3) we may calculate the reflected field at P which has undergone one, two or more multiple reflections. Let us introduce several notations which will be of help when a large number of rays are traced through many reflections. Let R_j be the set of rays, each member of which undergoes exactly j reflections before reaching the observer. A member of R_2 is shown in Figure 5.3, which consists of the sub-rays S_{02}-S_{12}-S_{22}. In general, a member of R_j comprises S_{0j}-S_{1j}-....-S_{jj} where S_{ij} is used to denote the length of the ray between reflection points i and (i+1). The angle between ray S_{ij} and the normal at the ith reflection point is denoted by η_{ij}.

If E_i is an incident plane wave, then from (5.1) through (5.3), for an observation point in the far field, we have for one reflection:

$$E_1 = -\frac{a}{2r} e^{ik(R+r-2a\cos\eta_{11})} \tag{5.8}$$

where

$$r = S_{11} + a\sin\eta_{11}, \quad \eta_{11} = (\pi-\theta-\alpha)/2$$

and R is the distance from the source to origin 0.

For two reflections, the situation is somewhat more difficult since we must first determine the unknowns η_{12}, η_{22}, and S_{12}. This means we must have the solution to the three simultaneous equations:

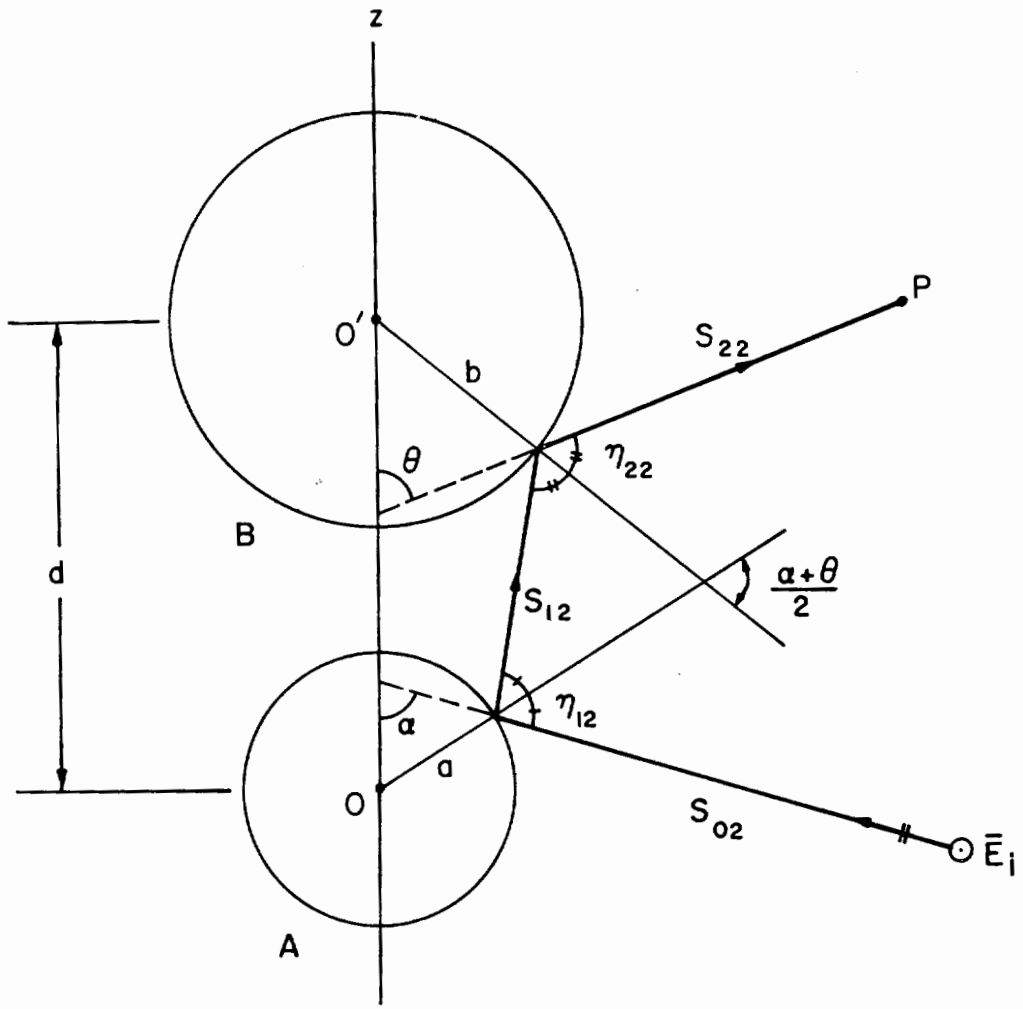

Figure 5.3 Geometry for a Ray that Undergoes Two Reflections.

$$a\cos(\alpha-\eta_{12}) + b\cos(\theta-\eta_{22}) + S_{12}\cos(\alpha-2\eta_{12}) = d$$

$$a\sin(\alpha-\eta_{12}) - b\sin(\theta-\eta_{22}) + S_{12}\sin(\alpha-2\eta_{12}) = 0 \qquad (5.9)$$

$$\eta_{12} + \eta_{22} + (\theta+\alpha)/2 = \pi.$$

This is not a trivial task since trancendental functions are involved. Numerically this can be handled with one of the gradient methods or a multidimensional form of the Newton-Raphson method (Todd, 1962). Once these parameters are determined, the divergence factors Δ_i may be calculated. The analogous result to (5.8) for two reflections using (5.1) through (5.8) is:

$$E_2 = \frac{ab}{2r}\left[\frac{\cos\eta_{12}\cos\eta_{22}}{(\ell_1\cos\eta_{22} + \ell_2\cos\eta_{12})(\tilde{\ell}_1+\tilde{\ell}_2)}\right]^{1/2}$$

$$\times\, e^{ik[R-a\cos\eta_{12} + S_{12} + r-b\cos\eta_{22}-d\cos\theta)]} \qquad (5.10)$$

where $r = S_{22} + b\cos\eta_{22} + d\cos\theta$ and the far field assumption, $S_{22} \gg d$, has been made. In addition, the following identifications apply to the above:

$$\ell_1 = a + S_{12}\cos\eta_{12} \qquad \tilde{\ell}_1 = S_{12} + a\cos\eta_{12}$$

$$\ell_2 = b + S_{12}\cos\eta_{22} \qquad \tilde{\ell}_2 = S_{12} + b\cos\eta_{22}.$$

We could carry out the same type of analysis for a field that has undergone j reflections before reaching the observer, but the analysis becomes rapidly more complicated since there will be in general 2j-1 unknowns involved in the form of simultaneous transcendental equations. The situation becomes much more meaningful if we confine our attention to a

few simple cases. Consider first the case of a pair of identical perfectly conducting spheres of radius a illuminated by a plane wave perpendicular to their common axis, i.e., broadside incidence. Furthermore, we will be interested only in the backscattered field. Some of the rays appropriate for this geometry are shown in Figure 5.4. There are many other possibilities in addition to these, for instance, using the previously defined notation we may also have rays of the type C_-R_1, R_1C_- (the same as C_-R_1 by reciprocity), C_-C_-, C_+R_1, C_-R_2, etc., the latter few can generally be excluded due to the large attenuation associated with the creeping waves combined with the divergence factors introduced by the reflections. It is difficult if not impossible to state in general which rays (particularly the hybrid rays) will be the most significant since the modulus of each depends on the incident polarization, the size of the spheres in wavelengths, and the separation of the spheres, which in turn determine the diffraction and attenuation coefficients and the divergence factors. Furthermore, this question must be reconsidered every time the angle of incidence is changed. For symmetrical configurations, however, computations are, for the most part, elementary and little effort is required to include many rays, if necessary. With these simplifications for the broadside case ($b = a$, $\alpha = \theta = \pi/2$), (5.8) becomes

$$E_1 = -\frac{a}{2r} e^{ik(R+r-2a)} \equiv R_1 \tag{5.11}$$

For two reflections, (5.9) can be solved directly giving $\eta_{12} = \eta_{22} = \pi/4$ with $S_{12} = d-a\sqrt{2}$. Using this in (5.10) yields the very simple result:

$$E_2 = \mp \frac{a^2}{4rd} (1-a/\sqrt{2}d)^{-1/2} e^{ik(R+r+d-2a\sqrt{2})} \tag{5.12}$$

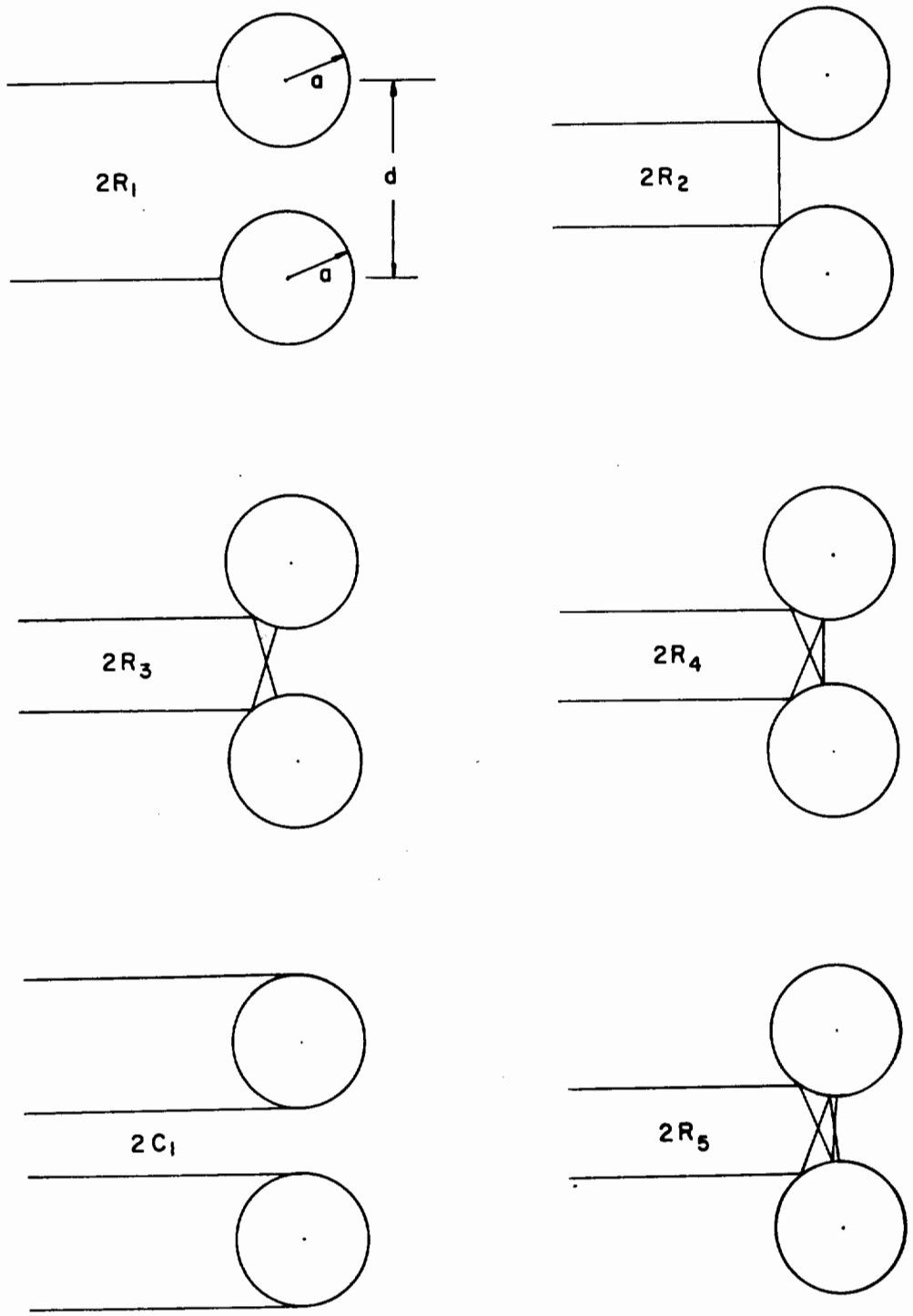

Figure 5.4 Some Possible Broadside Backscattered Rays.

Extracting the singly reflected field (5.11), equation (5.12) becomes:

$$E_2 = \pm \frac{R_1}{2\mu\sqrt{1-1/\sqrt{2}\mu}} e^{ika(\mu+2-2\sqrt{2})} \tag{5.13}$$

where μ is the ratio d/a and the upper and lower signs refer respectively to horizontal and vertical polarization ($\gamma = 0,\pi/2$). The result (5.12) was also obtained by Bonkowski et al. (1953) using a rather lengthy tensor formulation.

The calculation of the triply reflected rays shown in Figure 5.4 is quite straightforward due to the symmetry. Using the previously defined notation, we find that:

$$\begin{aligned} \eta_{23} &= 0 \\ \eta_{13} &= \eta_{33} = \sin^{-1}[(1 + \sqrt{8\mu^2+1})/4\mu] \\ S_{13} &= S_{23} = a\csc 2\theta(\mu-\sin\theta-\sin 2\theta) \equiv a\delta . \end{aligned} \tag{5.14}$$

It is worth noting that had we considered α, θ, a, and b as arbitrary, we would be confronted with the problem of solving five simultaneous equations (4 transcendental, 1 linear) not knowing a priori that a solution even exists; i.e., clearly no triply reflected ray can exist when $\alpha = 0$, regardless of the values of a, b, and θ.

Upon insertion of (5.14) into equations (5.1) through (5.3), and (5.11), we obtain the following expression for the field due to three reflections:

$$E_3 = R_1\cos\eta[(\cos\eta+2\delta)(1+2\delta\cos\eta)(\cos\eta+2\delta+2)(1+2\delta\cos\eta+2\cos\eta)]^{-1/2} \times e^{i2ka(1-\cos\eta+\delta)} \tag{5.15}$$

where for brevity we have written η for η_{13} and η_{33}.

The analogous expressions for the fields which have undergone four, five, and six reflections have also been derived, but will not be written down since the expressions become quite lengthy and the recipe for obtaining them has already been given.

The hybrid creeping waves likely to be most influential for the present broadside configuration are those of the type C_-R_1 and R_1C_-. The hybrid ray C_-R_1 is shown in Figure 5.5, from which we may ascertain the following

$$\eta_{11} = \sin^{-1}[(1 + \sqrt{1+8\mu(1+\mu)})/4\mu]$$

$$\tau_1 = 2\eta_{11}$$

$$s = a(\mu^2 - 2\mu\sin\eta_{11})^{1/2}.$$

Combining this with the previous results of the creeping wave theory and geometric optics gives us the following expression for the far field due to the hybrid wave C_-R_1

$$E(C_-R_1) = -R_1(-i)D_o^2[2/\mu(a\cos\eta_{11}+2s)]^{1/2} \times e^{ik[s-a\cos\eta_{11}+2a(1+\eta_{11})]} e^{-2\alpha_o\eta_{11}} \qquad (5.16)$$

It may be verified by direct calculation that the above result is identical to that obtained from the hybrid ray R_1C_- — as we should expect from reciprocity. This ray cannot be computed when the spheres are very close, or touch, since in this case the reflected ray at P (Figure 5.5) nearly grazes the surface; and at contact, the ray interpretation, for this hybrid ray, breaks down and (5.16) becomes unbounded. There are

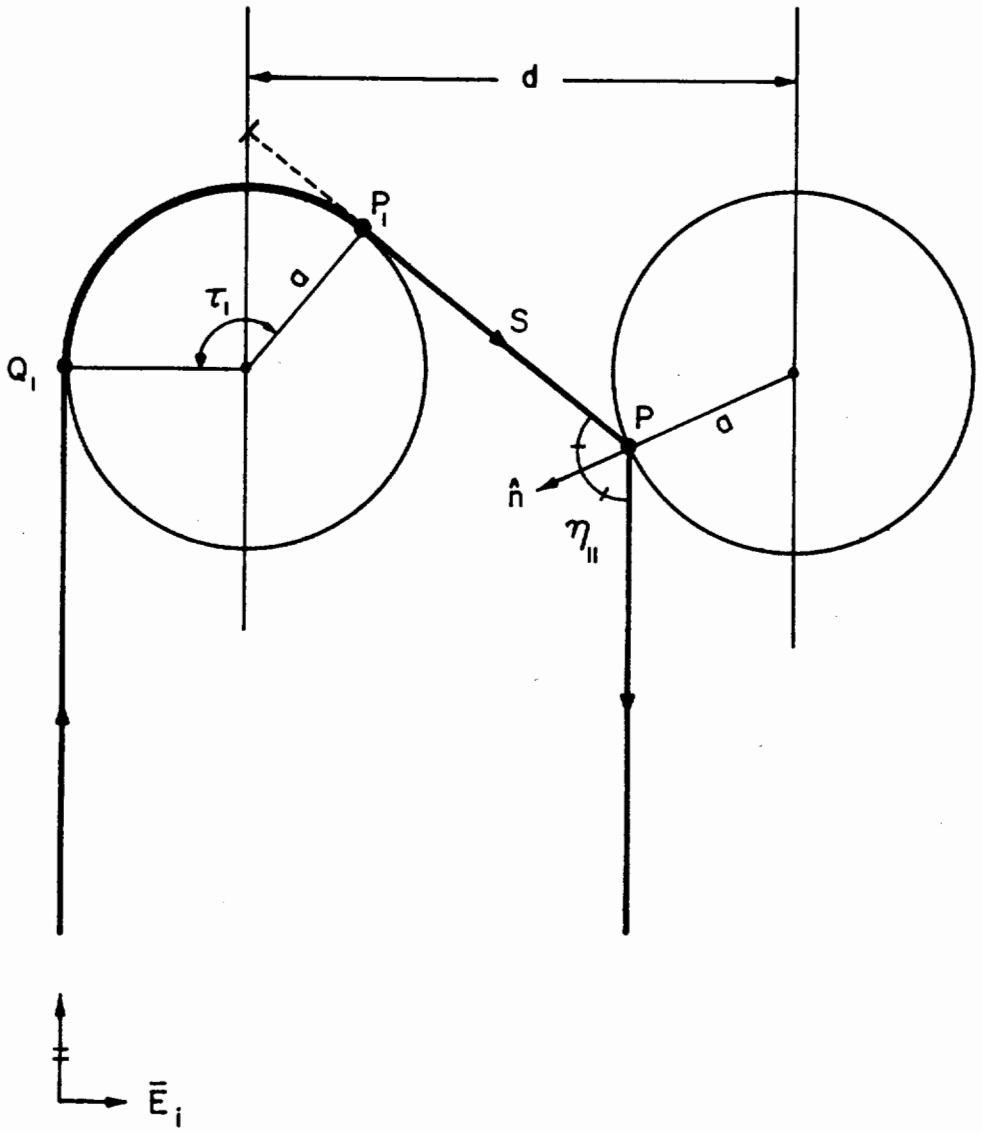

Figure 5.5 Geometry of the Hybrid Ray C_-R_1.

four such rays ($2C_-R_1 + 2R_1C_-$) which contribute to the total back-scattered field, however their effect is negligible for all but the smallest pair of spheres for the horizontal polarization and completely negligible for vertical polarization since the associated attenuation of the creeping wave is much higher. For this reason we may exclude all hybrid rays for this geometry.

We now confine our attention only to those rays C_- and R_1 through R_6 and present some numerical results. We would expect those rays which reflect more times before reaching the observer to contribute less. In Figure 5.6 the modulus of the multiply reflected rays R_2 through R_6 (normalized to R_1 as in (5.13) and (5.15)) is shown vs. the parameter $\mu = d/a$. This illustrates several important points. When the ratio d/a is large (not necessarily the sphere spacing d), each higher order reflected ray is about an order of magnitude smaller than the previous one; however, at contact (d/a = 2) even six multiple reflections may not be sufficient. Moreover, the higher order rays decrease in magnitude at a very much more rapid rate with separation. This is illustrated perhaps more vividly in Figure 5.7 where we see adjacent to each curve, plotted for particular values of the ratio d/a, the corresponding photographically recorded intensity distribution of the reflected rays of two polished silvered spheres illuminated by a point source of light. The two bright spots, common to all the diagrams, denote the specular returns R_1 from the front surface of each sphere. The remaining spots R_2, R_3, ..., (when they can be seen) are identified by counting inward from the two R_1 spots. The first spot picture (for d/a = 2) was obtained by illuminating the pair of

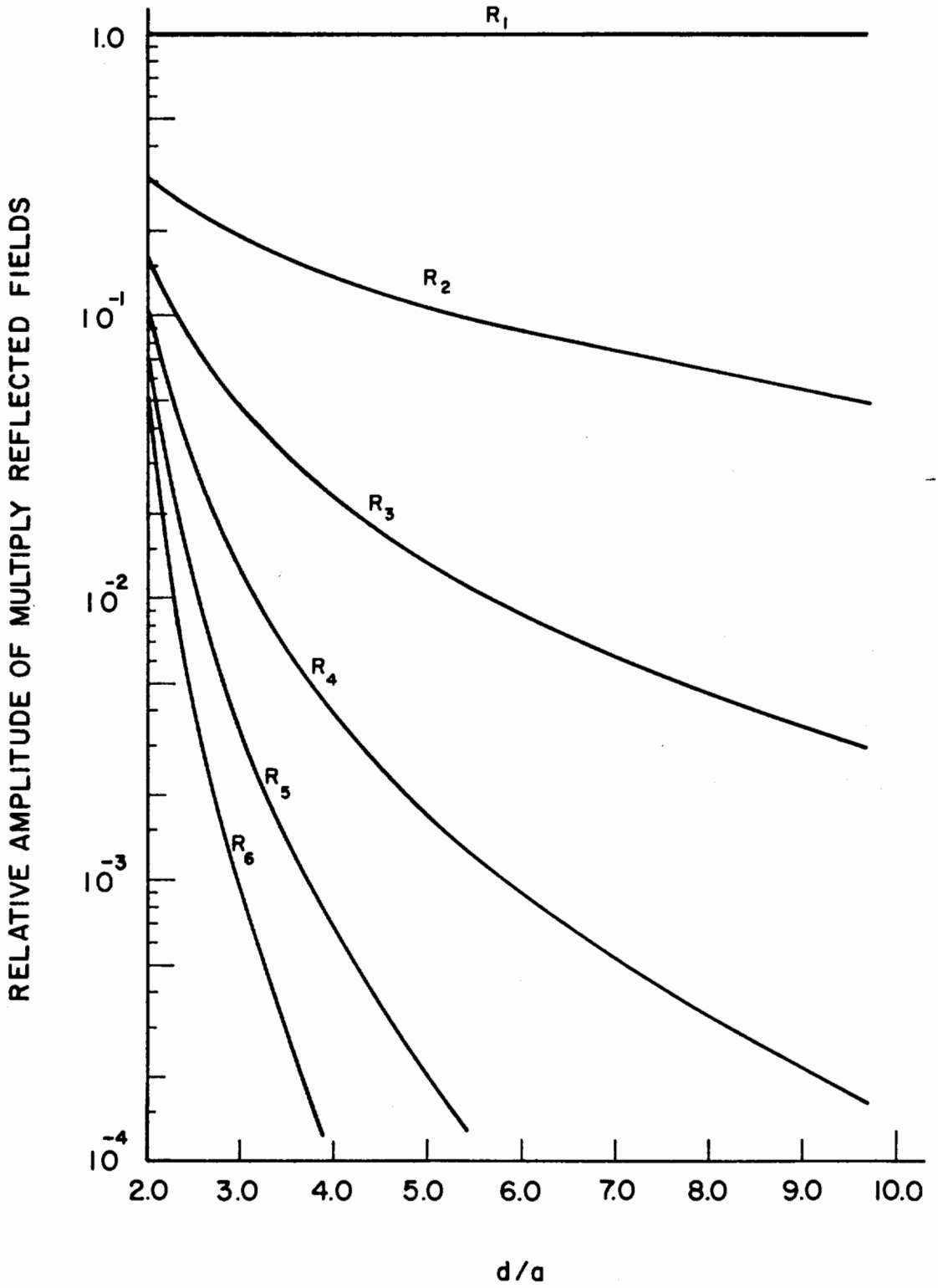

Figure 5.6 Relative Amplitude of Multiply Reflected Backscattered Fields from Two Equal Spheres at Broadside Incidence.

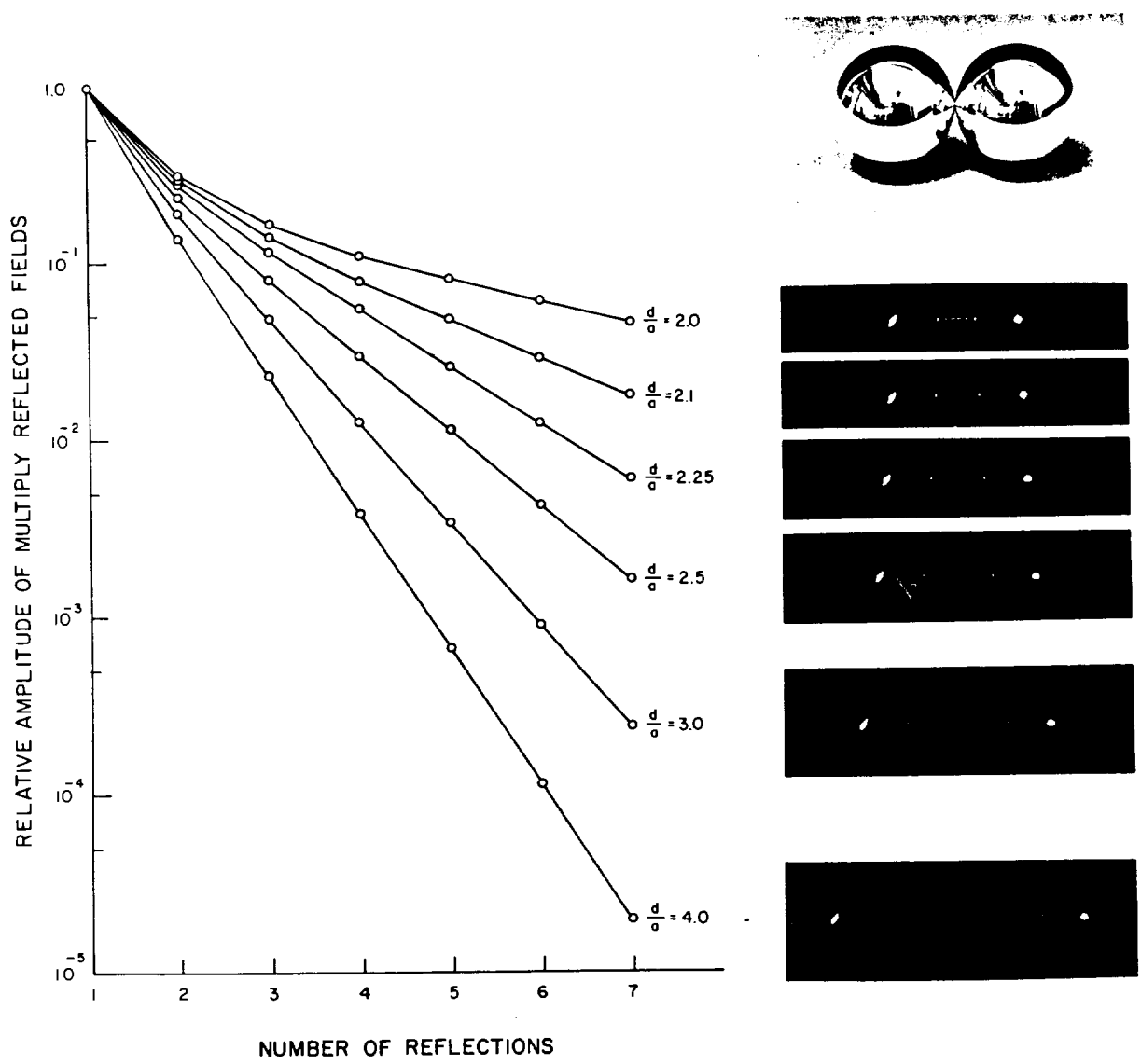

Figure 5.7 Qualitative Comparison of the Relative Amplitude of Backscattered Rays vs. the Number of Reflections, and the Corresponding Photographically Recorded Intensity Distribution.

spheres shown in the photo immediately above by a point source of ordinary light situated as close as possible to the axis of the camera and recording the reflected intensity on film when the studio lights were extinguished. The remaining diagrams were obtained under the same circumstances with increased center separation (measurable as the distance between the two bright spots). Due to the finite exposure time, only those spots of intensity greater than -30 db with respect to the specular returns R_1 can be seen. The rapid disappearance of the higher order rays with separation is quite evident (cf. Figure 5.6).

Using only the rays R_1, C_- (5.7) and R_2 through R_6, we compute the normalized radar cross-sections of pairs of identical metallic spheres for the two principal polarizations for ka = 2, 4.19, 6.246, and 10.0. This size range was chosen so that the results could be compared with the exact approach (modal expansion technique) for the purpose of determining where solutions obtained by the two approaches "overlap." These results are presented in Figures 5.8 and 5.9. Throughout this thesis, the results obtained from the modal theory will be shown by solid curves and those from the ray theory by dashed curves unless otherwise stated. With the exception of the case of horizontal polarization at ka = 2 (Figure 5.8a), the results are surprisingly good. By using no hybrid rays for this geometry, we would expect the results for vertical polarization to be slightly better than those for the companion case of horizontal polarization, since attenuation associated with hybrid waves for the former case is much higher. Figures 5.8 and 5.9 seem to demonstrate this. It is interesting, however, to make note of the fact that including the hybrid rays C_-R_1 and C_-C_- (and even C_-R_2, C_+R_1, $C_-R_2C_-$, $R_1C_+R_1$,...) does <u>not</u> improve the results for any of

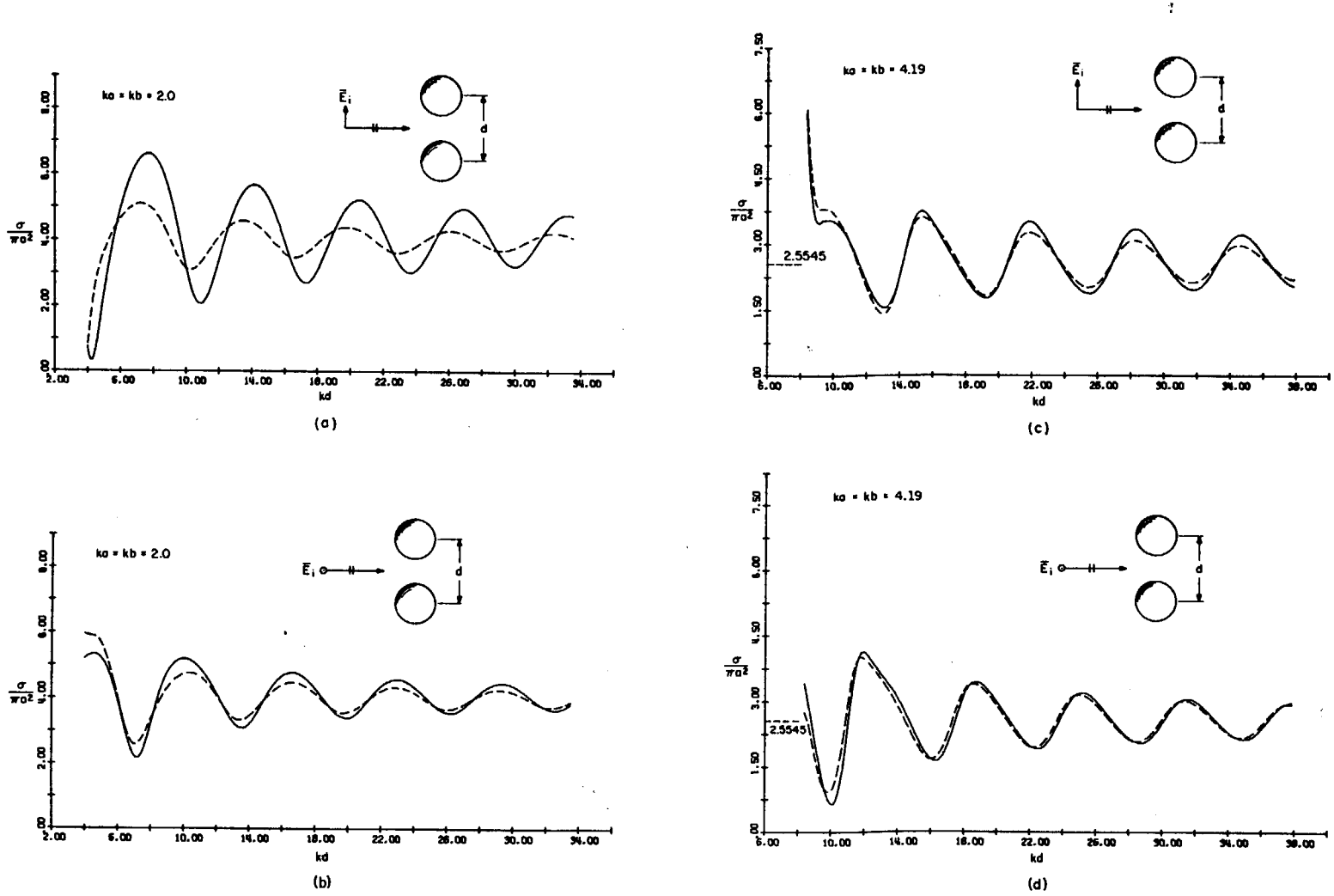

Figure 5.8 RCS of Two Equal Metallic Spheres at Broadside Incidence for the Two Principal Polarizations for ka = 2.0 and 4.19 using the Modal (———) and Ray Optics (-----) Solutions.

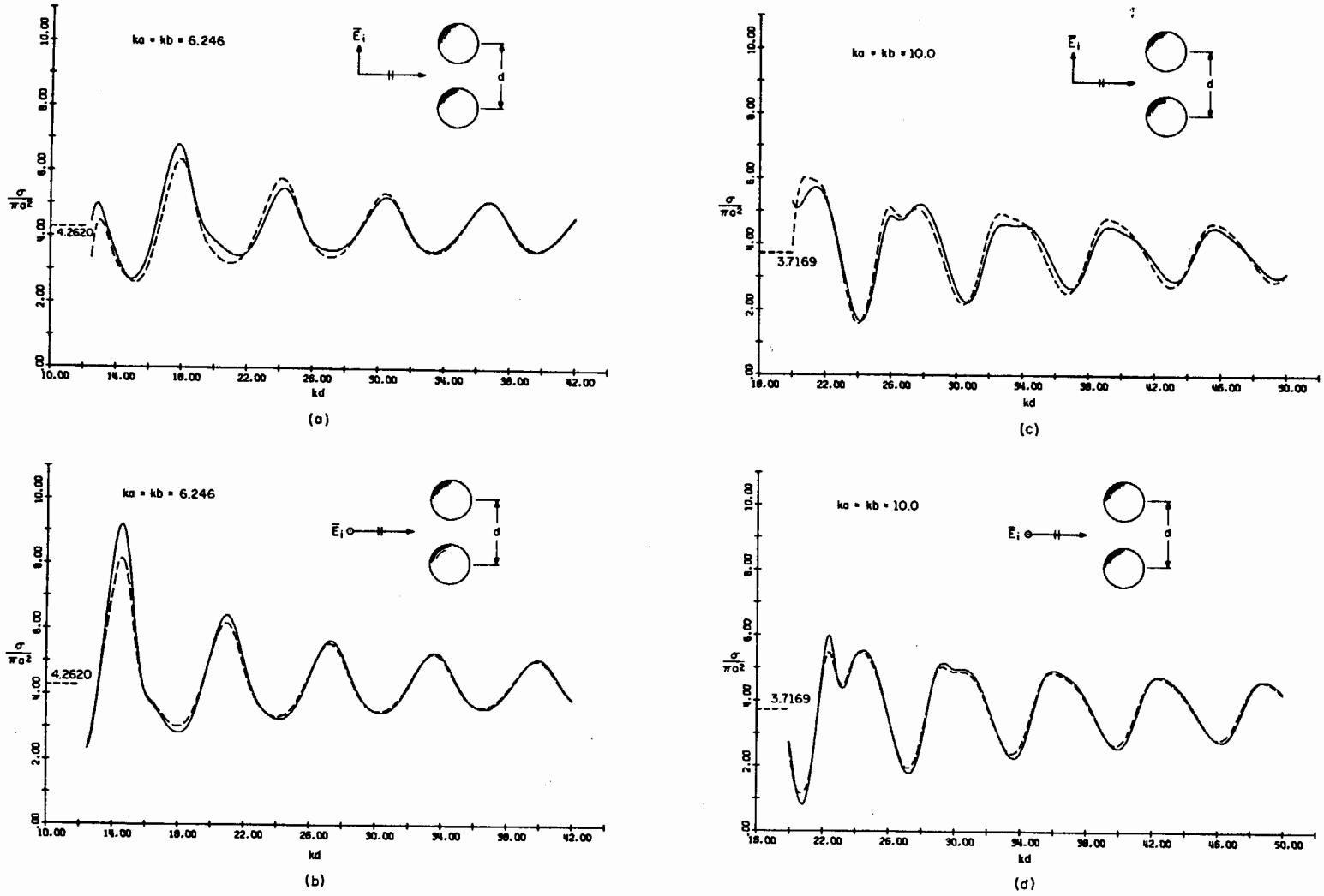

Figure 5.9 RCS of Two Equal Metallic Spheres at Broadside Incidence for the Two Principal Polarizations for ka = 6.246 and 10.0 Using the Modal (———) and Ray Optics (-----) Solutions.

these cases. From these figures we also see that as d/a becomes large (and hence the coupling small) the normalized cross-section settles down to $4(\sigma_a/\pi a^2)$ as expected.

A further example is given in Figure 5.10 which involves the radar cross-section of a pair of spheres in contact as they both grow in size for vertical polarization. Again, the same set of rays is considered as was used for computation in the previous example. The creeping wave influence for this example is apparent for ka $\lesssim$ 10 and can be identified with the local maxima in this range since we know the creeping wave C_- to add in phase with R_1 (for the single sphere) at ka $\approx 2n\pi/(2+\pi)$ with a period in ka of roughly $2\pi/(2+\pi)$. Beyond this point the radar cross-section seems almost completely dominated by the geometric optics components alone. We draw this conclusion on the basis of the good agreement of the results using ray theory with those of the rigorous modal expansion technique shown together in Figure 5.10. The normalized RCS of the pair will not, however, settle down to some constant value for large ka as it does for the single sphere. This is because d/a is constant and hence the normalized return is made up of components constant in magnitude, but whose relative phases change with ka. It should also be mentioned that this ray-optical result obtained for sets of reflected rays inclusive to R_6 is closer to the true solution than other sets of rays which involve fewer reflections. This is what we would expect intuitively. This is not necessarily true, however, as we saw in the previous examples when higher order <u>hybrid</u> rays were included. Asymptotic expansions in general are subject to both types of behavior when more terms are taken.

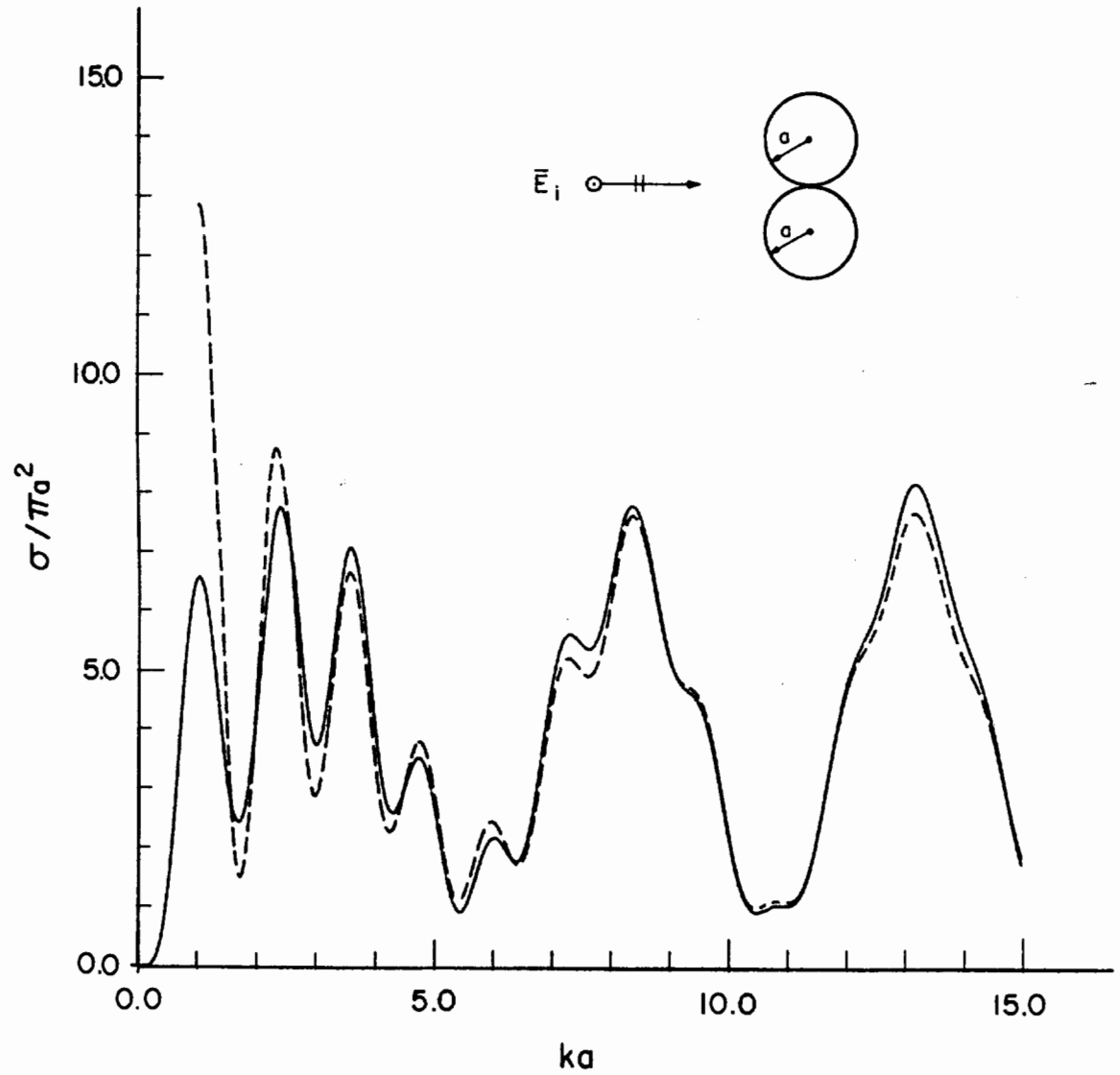

Figure 5.10 RCS of Two Equal Metallic Spheres in Contact at Broadside Incidence as They Both Grow in Size Using the Modal (———) and Ray Optics (-----) Solutions.

Another case study involves the scattering by two spheres when the incident vector is colinear with the common axis of the two spheres, i.e., endfire incidence. This is a rather interesting case since sphere B lies in the geometric shadow of A ($b < a$), hence the only purely geometric optics return is the specular reflection from sphere A. If $b = a$ we have the creeping waves C_- on sphere A in addition to hybrid rays which graze the shadow boundary of sphere A, creep around B, and again graze A. These grazing rays do not reflect off of A, nor do they actually creep over A, since a zero creeping path length is involved. Let us assign this ray the symbol G, even though we may not be able to compute its true value. The rays to consider for this geometry when $b = a$ are then: R_1, C_-, GC_-G, those shown in Figure 5.11: $C_-R_1^NC_-$, $C_-R_1C_-$, $C_-R_3^NC_-$, $C_-R_3C_-$, and possibly others such as $C_-R_2C_+G$, $C_-C_+C_-$, etc. R_j^N means that of j multiple reflections, one is a normal reflection. For backscattered rays this implies $S_{oj} = S_{jj}$, $S_{1j} = S_{j-1,j}, \ldots, S_{j-1/2,j} = S_{j+1/2,j}$. There are several drawbacks of the ray approach for this configuration. Geometric optics dictates that the shadowed sphere will never see the incident field which we know it should eventually at very large spacing — i.e., for large d/a, the backscattered field of two identical spheres should approach the single sphere value times the array factor $1 + e^{2ikd}$. This indicates that we will have to be content with the case of two rather closely spaced spheres for this geometry. Furthermore, the larger the separation, the closer the hybrid rays are to the shadow boundary where the representation breaks down. Finally, precisely at contact, we must exclude the rays C_- on A, $C_-R_1C_-$ and $C_-R_3C_-$ since their passage through the caustic line is blocked by B. The ray GC_-G still presents a problem.

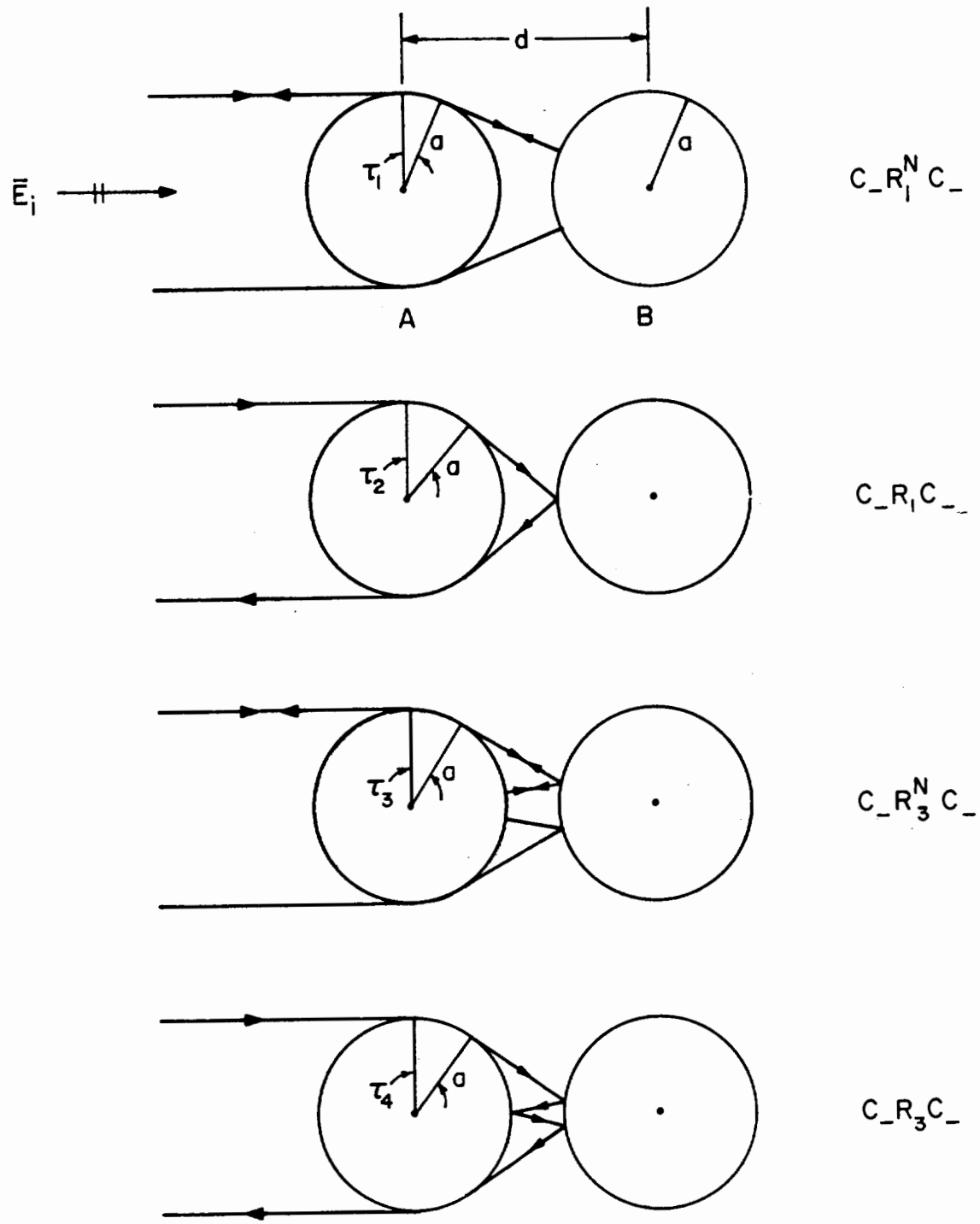

Figure 5.11 Some Possible Endfire Backscattered Hybrid Waves.

When $b < a$ this becomes the ray $C_-C_-C_-$, and C_- on B when $b > a$. To get some sort of a crude estimate of the importance of GC_-G, we consider the former case ($b < a$) and let b approach a. When we do this, we obtain for the backscattered field GC_-G:

$$E(GC_-G) = \frac{D_o^4}{d} E(C_-)e^{2ikd} \tag{5.17}$$

The effect of a glancing ray can then be estimated as $D_o^2 e^{ikd}/d^{1/2} \approx e^{ikd}/\mu^{1/2}(ka)^{1/6}$ for large ka. Hence at contact and $ka \approx 10$, (5.17) implies that the modulus of E_{GC_-G} is at most 20% of E_{C_-}; hence, a small error in GC_-G will not have a large overall effect.

We expect the largest contributions, next to R_1, to be of the type $C_-R_1^NC_-$ and $C_-R_1C_-$ at close spacing. The field due to these hybrid rays is calculated in a manner similar to the others with the results for arbitrary a and b:

$$E(C_-R_1^NC_-) = R_1(D_o^4/a)[\lambda\pi ka/(\mu^2-1-\lambda\sqrt{\mu^2-1})]^{1/2}$$
$$\times e^{2ika[1-\lambda+\sqrt{\mu^2-1}+\csc^{-1}\mu]-i\pi/4} e^{-2\alpha_o a \csc^{-1}\mu} \tag{5.18}$$

$$E(C_-R_1C_-) = R_1(-i)(D_o^4/a)[\pi ka/\sqrt{(\mu-\lambda)^2-1}]^{1/2}$$
$$\times e^{2ika[1+\sqrt{(\mu-\lambda)^2-1}+\csc^{-1}(\mu-\lambda)]-i\pi/4} e^{-2\alpha_o a \csc^{-1}(\mu-\lambda)} \tag{5.19}$$

where $\lambda = b/a$ and $\mu = d/a$.

If b and/or d is considerably larger than a, then the ray $C_-R_1^NC_-$ will lie very close to the shadow boundary of sphere A and we would not expect to obtain very good results. The size of sphere A in wavelengths determines how close we may approach the shadow boundary and still use

the results of the creeping wave theory of the single sphere; the sharpness of the shadow boundary and darkness of the shadow region are related to ka.

Figure 5.12 shows the normalized RCS of two identical metallic spheres for ka = 7.41, 11.048, and 20.0. These computations were made using the rays R_1, C_-, GC_-G, $C_-R_1^NC_-$, and $C_-R_1C_-$, computed from equations (5.7) and (5.17) through (5.19), respectively. The exact solution (multipole expansion) is shown for comparison. In the absence of coupling, the normalized radar cross-section will oscillate between 0 and $4\sigma_a/\pi a^2$, the latter being indicated by the dashed line on the ordinate of each curve. The agreement does get better (for small to moderate d/a) with increasing ka as we expect and is best for ka = 20. The results even at close spacing, for ka = 7.41, however, are not very satisfactory. The fact that the position of the peaks and nulls can be predicted with reasonable accuracy seems to indicate that perhaps we have made a judicious choice for the sets of rays. The amplitude discrepency, however, can be attributed, at least in part, to the inaccuracy in the canonical creeping wave problem near a shadow boundary. This conjecture was tested with the following additional examples. Endfire radar cross-section was computed for the case ka = 7.41, kb = 11.048 and the case ka = 11.048, kb = 7.41. The dominant contribution (next to R_1) for close spacing in both cases is the ray $C_-R_1^NC_-$. The results for the former case were worse than the case when both spheres were of size 7.41; and the results of the latter example were better than the case when both spheres were of size 11.048. In the first case the ray $C_-R_1^NC_-$ was closer to the shadow boundary, whereas in the second case it was further from the shadow boundary. In the previous

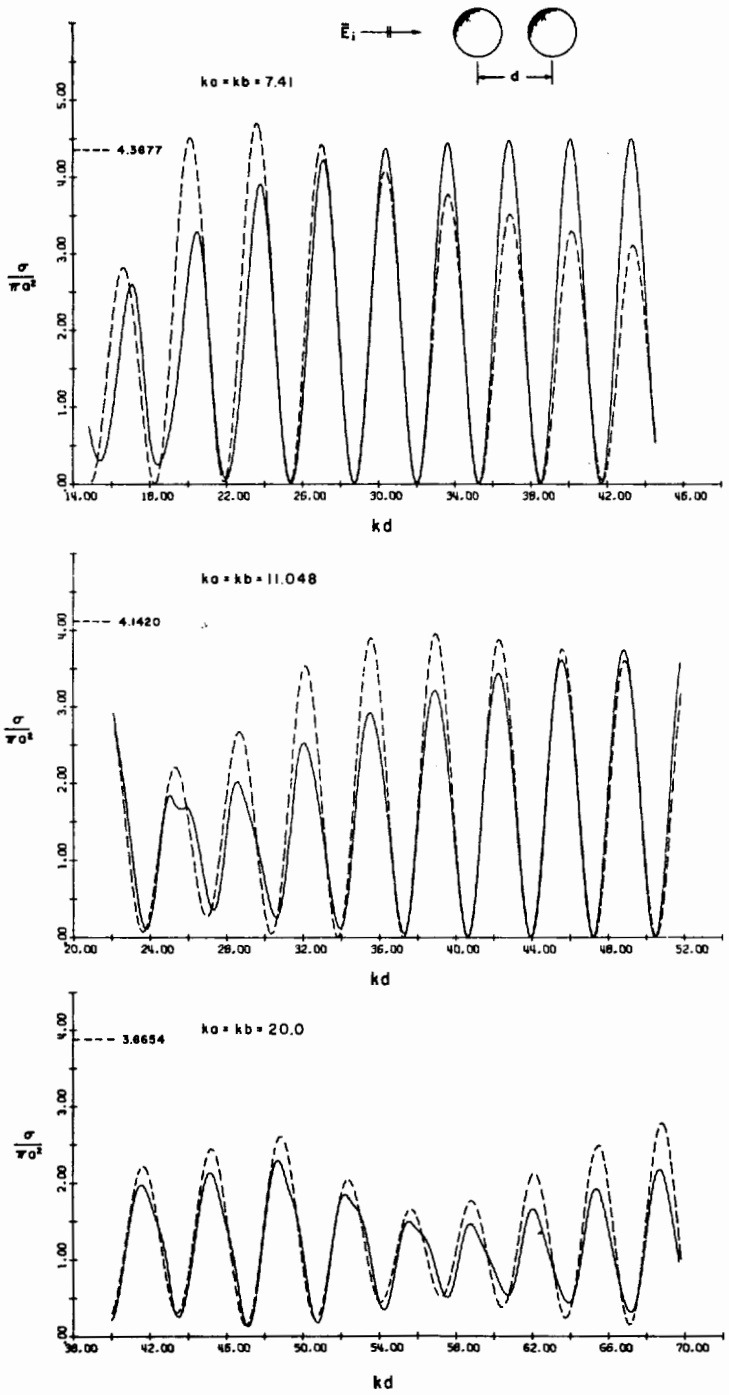

Figure 5.12 RCS of Two Equal Metallic Spheres at Endfire Incidence vs. Separation for ka = 7.41, 11.048, and 20.0 Using the Modal (———) and Ray Optics Solutions (-----).

numerical examples for endfire incidence, computations were not carried to the point where the two spheres touched (but very close) since at that point rays C_- on A and $C_-R_1C_-$ are blocked and (5.19) becomes unbounded. At very slight separation, the contribution made by (5.19) is small due to the long creeping path. Since the case of contact supports different sets of rays, we must treat it separately as shown below.

Let us consider computing the normalized RCS of two spheres in contact at endfire incidence using only the rays R_1 and $C_-R_1^NC_-$. Now the creeping wave influence on the backscattering from a single sphere is nearly absent at values of ka greater than about 10-15 since the creeping waves creep over a path length of half the circumference of the sphere. Placing an identical sphere directly behind another drastically alters that situation since the hybrid wave $C_-R_1^NC_-$ overwhelms any single sphere creeping wave C_- because its associated creeping path length is only a total of one sixth of the circumference of the first sphere — implying that the oscillations about R_1 will persist for a much larger value of ka than for the single sphere. In Figure 5.13(a) the normalized RCS of a pair of identical spheres in contact is shown computed using the exact modal approach as ka covers the range 0 to 24. It is clearly seen that there is considerable oscillation about R_1 even for ka as large as 24. It becomes somewhat costly to carry out computations much beyond this value using the modal approach. For larger ka, the ray approach should be used, with the results shown in Figure 5.13(b), plotted on a logarithmic scale in ka to ka = 150. If we compare these two curves, we find excellent agreement in the location of the peaks and nulls after ka $\approx$ 10 and also in the amplitude after

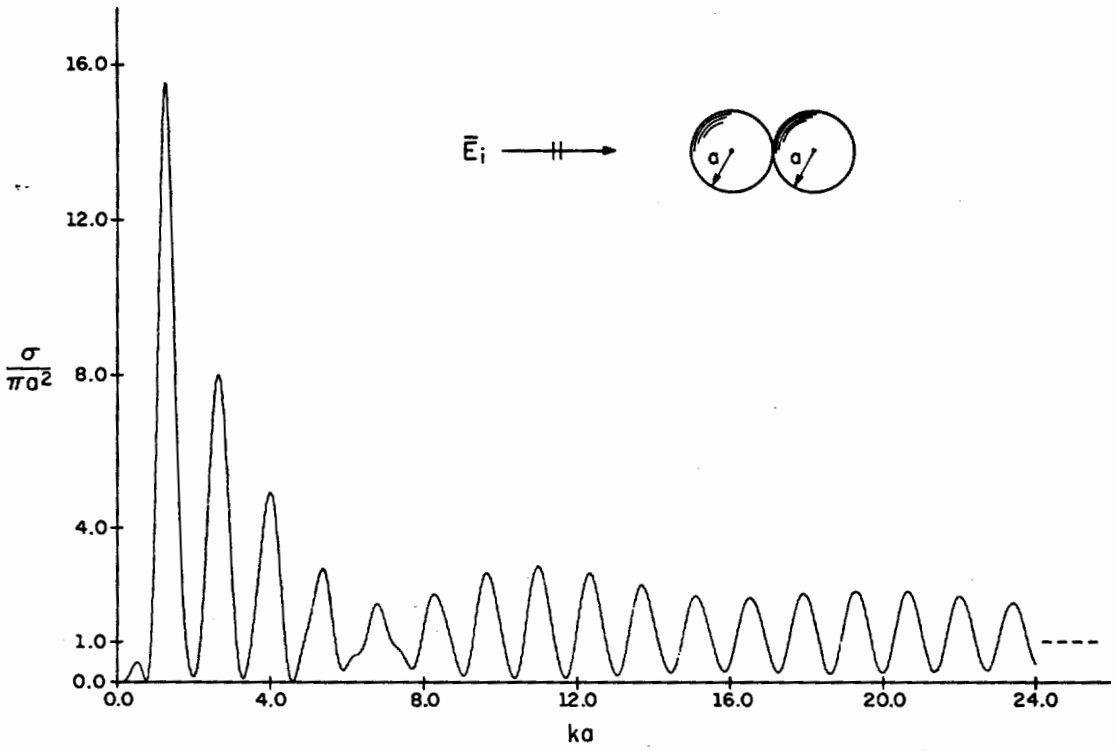

(a)

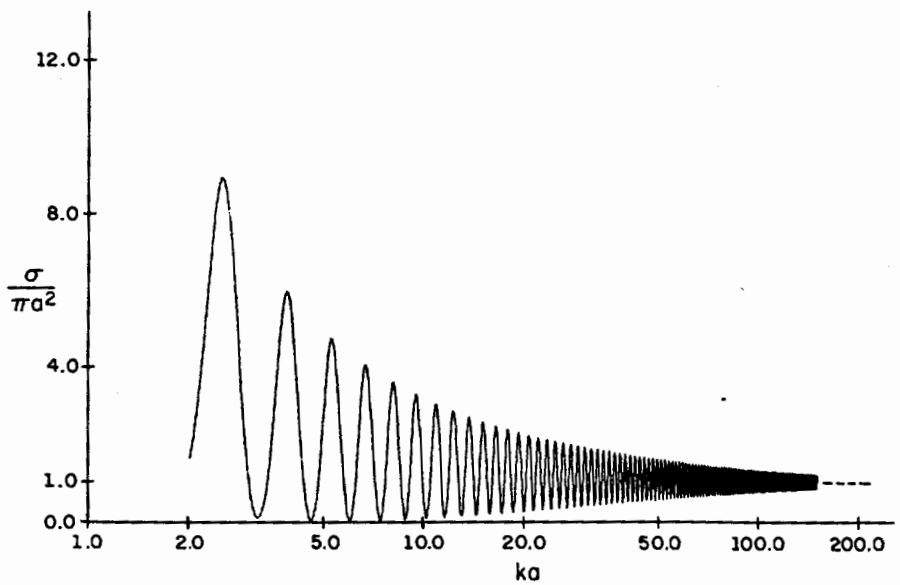

(b)

Figure 5.13 RCS of Two Equal Metallic Spheres in Contact at Endfire Incidence as They Both Grow in Size Using the (a) Modal and (b) Ray Optics Solution.

ka ≈ 16. The period of oscillation can be very simply determined. Assuming that these oscillations are caused only by the interference of R_1 and $C_- R_1^N C_-$, the period P, in ka, of the oscillation can be shown to be simply $\pi/(\pi/6 + \sqrt{3}) \approx 1.39$, with peaks at ka = nP and nulls at (2n-1)P/2 where n is a positive integer.† In the general case where a and b are of different size, the period in ka is given by:

$$P = \pi/[\csc^{-1}(1+\lambda) + 1-\lambda+\lambda\sqrt{1 + 2/\lambda}] \qquad (5.20)$$

where $\lambda = b/a$.

It is interesting to note from the above discussion and Figure 5.13 that eventually the front sphere can "hide" the back sphere — this is what geometric optics told us from the very beginning. In fact, the front sphere may even "hide" a sphere that is larger than itself. Since the attenuation of the hybrid rays $C_- R_1^N C_-$ is proportional to $e^{-2\alpha_o a \csc^{-1}(1+\lambda)}$, ka must be larger in order to hide a bigger sphere (b > a) than to hide a smaller one (b < a).

In view of the above results, it is perhaps of interest to draw some conclusion at this point. The fact that the value of ka for which the ray optics solution agrees closely with that of the modal solution is relatively small for the case of broadside incidence and considerably large in the case of endfire incidence indicates that caution must be exercised in using

---

†This may be compared with the period of oscillations in the radar cross-section curve for a single sphere (caused by the interference of R_1 and C_-) which is $2\pi/(\pi+2) \approx 1.23$. This is also evident for ka < 10 in Figure 5.10.

the ray optical approach. It would not be feasible, for example, to use this method to calculate the radar cross-section of two spheres as the incident angle (α) varies since this would require the separate consideration of different sets of rays for each angle. This kind of study would require a canonical problem which describes the smooth transition of a creeping wave ray into a reflected ray as a shadow boundary is crossed. Such a continuous ray description is presently not available even for the sphere. The ray optical method is desirable, however, in the sense that it gives us physical insight into the scattering mechanism. It can predict gross behavior in most cases and in some cases yields very good results.

The possible extension of this ray optical method to the case of two dielectric or one dielectric and one metallic sphere is certainly of interest.† Very recently, Nussenzveig (1969) in a long series of papers, considered the residue series for a single dielectric sphere and was able to interpret from the series the very complex ray geometrics when the sphere is large and lossless. His analysis is restricted to cases where the inequalities:

$$(ka)^{1/3} \gg 1$$

$$\sqrt{N-1}\ (ka)^{1/3} \gg 1 \tag{5.21}$$

hold with the exclusion of the cases where $N \gg 1$. There is a large variety of rays involved in this description of scattering by a single

†The extension to scalar scattering by two spheres with the surface conditions $u = 0$ or $\partial u/\partial n = 0$ (soft or hard) is trivial. Mention is made of these cases in connection with a parallel between the scalar and vector two sphere problem in Section 6.1.2.

dielectric sphere. There are those which undergo simple reflection and refraction, creeping waves, multiple refractions, refractions to the outside surface at the critical angle followed by creeping waves, and critical refraction of creeping waves into the sphere, called "shortcuts," of which the variety is infinite. The problems of extension to two spheres are obvious, but the physical interpretation and insight suggested appear to be most fascinating. For the case of <u>two</u> very large dielectric spheres ($ka > 100$) this appears to be the only possible means for obtaining numerical results. For smaller spheres the modal expansion technique will give the exact results for spheres of any composition (even with loss and parameters not in the ranges of (5.21)).

6. FURTHER APPLICATION OF THE GENERAL THEORY

6.1 Acoustic Scattering by Two Spheres

The geometry of the problem of acoustic scattering by two spheres is the same as given in Figure 2.1 except that the field quantity under consideration is now the acoustic pressure, a scalar quantity.

Again for simplicity the incident field is assumed to be plane and of unit strength with its propagation vector lying in the xz plane and inclined at an angle α with respect to the axis of the two spheres as in Figure 2.1. The scalar spherical wave expansion of the incident field ψ_i about origins 0 and 0' becomes, respectively:

$$\psi_i = \sum_{n=0}^{\infty} \sum_{m=-n}^{n} p_{mn} u_{mn}^{(1)}$$
$$\psi_i' = \sum_{n=0}^{\infty} \sum_{m=-n}^{n} p'_{nm} u'^{(1)}_{mn} \tag{6.1}$$

where

$$p_{mn} = i^n (2n+1) \frac{(n-m)!}{(n+m)!} P_n^m(\cos\alpha) \tag{6.2}$$

and

$$u_{mn}^{(j)} = z_n^{(j)}(kr) P_n^m(\cos\theta) e^{im\phi} \tag{2.5}$$

p'_{mn} differs from p_{mn} by the multiplicative phase factor $e^{ikd\cos\alpha}$.

As in the vector problem, in order to satisfy the boundary conditions on the two spheres simultaneously, one must be able to expand the total field alternately about the origins of spheres A and B. Such an addition theorem for scalar waves is given by (A3) and (A7) where attention is restricted to the case for $r \leq d$, d being the separation between sphere

centers. Also as in the vector problem, the scattered field of each sphere is formulated in a spherical wave expansion with unknown coefficients which are determined after the boundary conditions are applied. Let the scattered field of each sphere in the presence of the other be:

$$\psi_S^A = \sum_{nm} a_{mn} u_{mn}^{(3)}$$
$$\psi_S^{B'} = \sum_{nm} b_{mn} u_{mn}^{(3)'} \quad ; \tag{6.3}$$

then, the total field for $\bar{r}$ and $\bar{r}'$ exterior to both spheres in each coordinate system is, using the addition theorem (A25) and (A26):

$$\psi_T = \sum_{nm} \left[p_{mn} u_{mn}^{(1)} + a_{mn} u_{mn}^{(3)} + b_{mn} \sum_{\nu=m}^{\infty} \alpha_{m\nu}^{mn} u_{m\nu}^{(1)} \right] \tag{6.4}$$

$$\psi_T' = \sum_{nm} \left[p'_{mn} u_{mn}^{(1)'} + b_{mn} u_{mn}^{(3)'} + a_{mn} \sum_{\nu=m}^{\infty} (-1)^{n+\nu} \times \alpha_{m\nu}^{mn} u_{m\nu}^{(1)'} \right] \tag{6.5}$$

For $\bar{r}$ and $\bar{r}'$ interior to the spheres, the fields will have the same expressions as (6.4) and (6.5) except that the superscript (3) will be replaced by (1) since pressure and velocity are finite at all interior points. Furthermore, for the interior fields, the coefficients a_{mn} and b_{mn} must be distinguished from those in the exterior field expansion. The boundary conditions then require continuity of the pressure and radial velocity at r = a and r' = b. This requires the matching of ψ_T and ψ_T' in (6.4) and (6.5) and their radial derivitives on the interfaces of both spheres. Combining this with the orthogonality relation:

$$\int_0^{\pi} P_n^m(\cos\theta) P_\ell^m(\cos\theta) \sin\theta d\theta = \frac{2}{2\ell+1} \frac{(\ell+m)!}{(\ell-m)!} \delta_{n\ell} \tag{6.6}$$

results in the following coupled sets of simultaneous linear equations in the unknown multipole coefficients for the exterior field:

$$\begin{aligned} a_{mn} &= c_n(a)\left[p_{mn} + \sum_\nu \alpha_{mn}^{m\nu} b_{m\nu}\right] \\ b_{mn} &= c_n(b)\left[p'_{mn} + \sum_\nu (-1)^{n+\nu} \alpha_{mn}^{m\nu} a_{m\nu}\right] \end{aligned} \tag{6.7}$$

where $c_n(x)$ is the scattering coefficient for a single sphere of radius x with the appropriate impedance boundary condition (Morse and Feshbach, 1953). For a penetratable or soft sphere, $c_n(x) = j_n(kx)/h_n^{(1)}(kx)$ and a rigid or hard sphere, $c_n(x) = \frac{\partial}{\partial x}[j_n(kx)]/\frac{\partial}{\partial x}[h_n^{(1)}(kx)]$.

Once the system (6.7) is solved for a_{mn} and b_{mn}, the solution of the exterior scattered field is complete by virtue of (6.3). Of particular interest is the scattered field in the far zone. This is obtained when the asymptotic expression of $h_n^{(1)}(kr)$ for large kr is used giving for $u_{mn}^{(3)}$ and $u_{mn}^{(3)'}$:

$$\begin{aligned} u_{mn}^{(3)} &\approx i^{-n-1} \frac{e^{ikr}}{kr} P_n^m(\cos\theta) e^{im\phi} \\ u_{mn}^{(3)'} &\approx e^{ikd\cos\theta} u_{mn}^{(3)} \end{aligned} \tag{6.8}$$

Again making use of the symmetries in the associated Legendre functions, the total scattered field from (6.3) may be rewritten as a sum over only non-negative values of m giving:

$$\psi_S^{A+B} \approx \frac{e^{ikr}}{ikr} \sum_{n=0}^{\infty} \sum_{m=0}^{n} i^{-n} \epsilon_m (a_{mn} + b_{mn} e^{ikd\cos\theta}) P_n^m(\cos\theta) \cos m\phi \qquad (6.9)$$

Negative values of the index m may also be appropriately excluded from all previous equations in this section.

As in the vector problem, several simplifications result upon specialization of the geometry. When the incident plane wave is directed along the axis of the two spheres ($\alpha = 0$) only the $m = 0$ term is present since in this case (6.2) reduces to:

$$p_{mn} = i^n (2n+1) \delta_{m,o} \qquad (6.10)$$

As a result, the only translation coefficients in the scalar wave addition theorem needed are those for $m = 0$:

$$\alpha_{o\nu}^{on} = i^{\nu-n} (2\nu+1) \sum_p i^{-p} a(0,n,0,\nu,p) h_p(kd) \qquad (6.11)$$

where $a(0,n,0,\nu,p)$ is given explicitly in simple form by (A33). The series expansion of the field (6.9) in this case then involves only a single summation.

The case of a pair of identical spheres illuminated by a plane wave from the broadside direction ($\alpha = \pi/2$) yields the following simple relation between the multipole coefficients of the two spheres:

$$b_{mn} = (-1)^{n+m} a_{mn} \qquad (6.12)$$

When this is inserted into (6.7) we have the result:

$$a_{mn} = c_n(a) \left[p_{mn} + \sum_{\nu=m}^{\infty} (-1)^{\nu+m} \alpha_{mn}^{m\nu} a_{m\nu} \right] \qquad (6.13)$$

Here the only unknowns to solve for are a_{mn} which represents half the work required in solving (6.7) which may be substantial for large spheres.

6.1.1 Decoupling of Equations for Large Separation

Finally, as in the EM problem there is an asymptotic form of the addition theorem valid for large separations of the spheres when the condition $\frac{d}{a} > 0(ka)$ is satisfied. For the scalar addition theorem, as shown in (A41), the result is

$$\alpha_{m\nu}^{mn} \approx i^{n-\nu-1}(2\nu+1)\frac{e^{ikd}}{kd}\delta_{m,o}; \quad \frac{d}{a} > 0(ka). \tag{6.14}$$

From (6.7) this implies that all the coupling of the fields is contained only in the azimuthal mode m = 0. Using (6.10) and (6.14) in (6.7), the system of equations (6.7) for the m = 0 mode becomes:

$$\begin{aligned} a_{on} &= i^n(2n+1)c_n(a)\left[P_n(\cos\alpha) + (-1)^n \frac{e^{ikd}}{ikd}\sum_{\nu=0}^{\infty} i^{\nu} b_{o\nu}\right] \\ b_{on} &= i^n(2n+1)c_n(b)\left[e^{ikd\cos\alpha}P_n(\cos\alpha) + \frac{e^{ikd}}{ikd}\sum_{\nu=0}^{\infty} i^{-\nu} a_{o\nu}\right] \end{aligned} \tag{6.15}$$

The above system of equations can be solved explicitly by successive substitution since it can be demonstrated that the series obtained are geometric and hence can be summed in closed form.

First let us introduce the notation

$$S_a(r,\theta) = \frac{e^{ikr}}{ikr}\sum_{n=0}^{\infty}(2n+1)c_n(a)P_n(\cos\theta), \tag{6.16}$$

which will be recognized as the scattered field in the far zone from an isolated sphere of radius a illuminated by a plane wave of unit strength.

The observation point is located a distance r from the center of the sphere and makes an angle $\pi-\theta$ with the incident wave vector $\hat{k}$. With this notation (6.15) can be recognized as series in powers of the quantity $S_a(d,\pi)S_b(d,\pi)$. After summing these geometric series we arrive at the result:

$$a_{on} = i^n(2n+1)c_n(a)\Big[P_n(\cos\alpha) + (-1)^n \frac{e^{ikd\cos\alpha}S_b(d,\pi-\alpha) + S_a(d,\alpha)S_b(d,\pi)}{1 - S_a(d,\pi)S_b(d,\pi)}\Big]$$

$$b_{on} = i^n(2n+1)c_n(b)e^{ikd\cos\alpha}\Big[P_n(\cos\alpha) + \frac{e^{-ikd\cos\alpha}S_a(d,\alpha) + S_a(d,\pi)S_b(d,\pi-\alpha)}{1 - S_a(d,\pi)S_b(d,\pi)}\Big] \tag{6.17}$$

provided $|S_a(d,\pi)S_b(d,\pi)| < 1$. It can also be verified that (6.17) satisfies (6.12) for broadside incidence and identical spheres.

If we use these results in the expression for the scattered field (6.9), the coupled and uncoupled portions of the solution may be separated:

$$\psi_S^{A+B} \approx \frac{e^{ikr}}{ikr}\sum_{n=0}^{\infty}(2n+1)P_n(\cos\theta)\Big[(-1)^n c_n(a)\mathcal{J}_B + e^{ikd(\cos\alpha-\cos\theta)} \times c_n(b)\mathcal{J}_A\Big] + \frac{e^{ikr}}{ikr}\sum_{n=0}^{\infty}\sum_{m=0}^{n}\epsilon_m(2n+1)\frac{(n-m)!}{(n+m)!}$$

$$\times P_n^m(\cos\alpha)P_n^m(\cos\theta)\cos m\phi$$

$$\times \left[c_n(a) + e^{ikd(\cos\alpha-\cos\theta)}c_n(b)\right] \tag{6.18}$$

where

$$\mathcal{S}_B = \frac{e^{ikdcos\alpha} S_b(d,\pi-\alpha) + S_a(d,\alpha)S_b(d,\pi)}{1 - S_a(d,\pi)S_b(d,\pi)}$$

$$\mathcal{S}_A = \frac{e^{-ikdcos\alpha} S_a(d,\alpha) + S_a(d,\pi)S_b(d,\pi-\alpha)}{1 - S_a(d,\pi)S_b(d,\pi)} \quad . \tag{6.19}$$

The summation over m in (6.18) will be recognized as the addition theorem for Legendre functions which reads (Stratton, 1941):

$$P_n(\cos\xi) = \sum_{m=C}^{n} \epsilon_m \frac{(n-m)!}{(n+m)!} P_n^m(\cos\alpha) P_n^m(\cos\theta)\cos m\phi \quad . \tag{6.20}$$

The angle ξ is the space angle between the incident wave vector $\hat{k}$ and the position vector of the observation point with coordinates (r,θ,ϕ). Using this result in (6.18) gives:

$$\psi_S^{A+B} = S_a(r,\xi) + S_b(r,\xi)e^{ikd(\cos\alpha-\cos\theta)} + \mathcal{S}_B S_a(r,\pi-\theta) + \mathcal{S}_A S_b(r,\theta)e^{ikd(\cos\alpha-\cos\theta)} \tag{6.21}$$

Equation (6.21) has some rather interesting implications which can best be explained by illustration. For convenience, consider the observation point to lie in the plane $\phi = 0$; then $\xi = \theta-\alpha$. Referring to Figure 6.1 and equation (6.21) we see that the first two terms are the scattered fields from two isolated spheres individually illuminated by a unit plane wave — the incident and scattering vectors forming an angle $\theta-\alpha$ with each other. The third term $\mathcal{S}_B S_a(r,\pi-\theta)$ is the field scattered by sphere A illuminated by a plane wave of strength $\mathcal{S}_B$ originating from

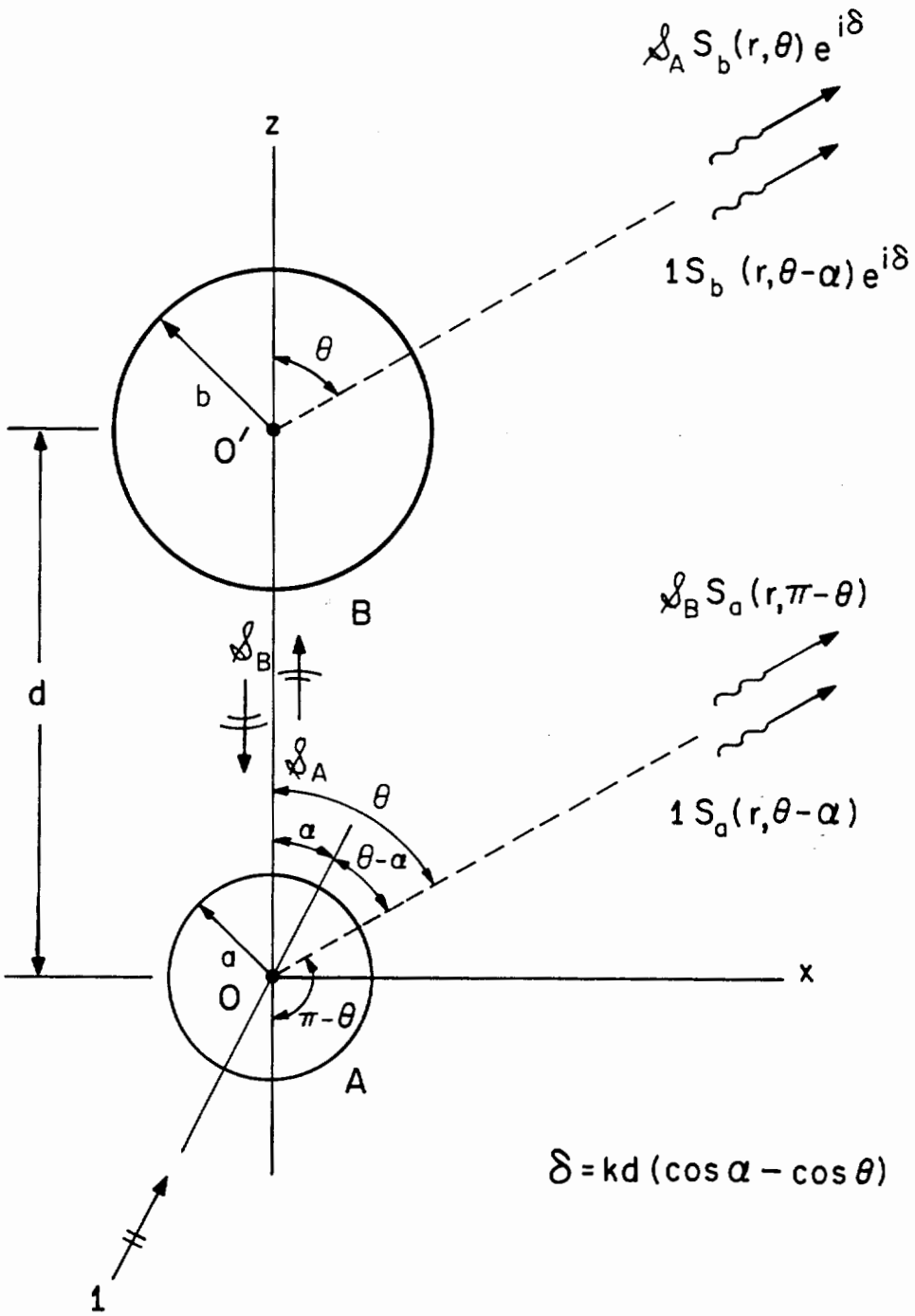

Figure 6.1 Physical Interpretation of Multiple Scattering at Large Separation.

sphere B at 0'.[†] Similarly the fourth term $\mathscr{J}_A S_b(r,\theta)e^{ikd(\cos\alpha-\cos\theta)}$ is the field scattered by sphere B due to source $\mathscr{J}_A$. The phase factor $e^{ikd(\cos\alpha-\cos\theta)}$ is present since S is always written about 0. The amplitudes $\mathscr{J}_A$ and $\mathscr{J}_B$ are also easily interpreted. From (6.19), the amplitude of $\mathscr{J}_B$ (at 0) is the sum of the field scattered by B in the direction of 0, $e^{ikd\cos\alpha}S_b(d,\pi-\alpha)$, and the field scattered by A toward B and then backscattered by B, $S_a(d,\alpha)S_b(d,\pi)$. The factor $[1 - S_a(d,\pi)S_b(d,\pi)]^{-1}$ contains the true *multiple scattering* contribution since it is the sum of the remaining infinity of contributions to $\mathscr{J}_B$ of the form $[S_a(d,\pi)S_b(d,\pi)]^n$ where n is an integer. Similar remarks follow for the interpretation of $\mathscr{J}_A$.

As a final result, consider the broadside backscattered field from a pair of identical spheres. In this case, (6.21) yields the very simple result:

$$\psi_S^{A+B} = 2\left[S_a(r,\pi) + \frac{S_a(d,\pi/2)S_a(r,\pi/2)}{1 - S_a(d,\pi)}\right] \qquad (6.22)$$

Again it is emphasized that the only assumption made in the rigorous solution to arrive at the results (6.21) and (6.22) (other than the observation point being in the far zone) was the assumption $\frac{d}{x} > 0(kx)$ in the addition theorem, where x is the larger of a and b. This assumption permits replacing the Hankel function $h_p^{(1)}(kd)$ in the addition theorem by

---

[†] The source $\mathscr{J}_B$ is, strictly speaking, a spherical wave, however, (for $b > a$) the criterion for the above analysis will be recalled as $\frac{d}{b} > 0(kb)$. This justifies considering $\mathscr{J}_A$ and $\mathscr{J}_B$ as locally plane at a distance of d.

the first term in its asymptotic expansion to $0(kd)^{-1}$. An analogous result could also be obtained using the second term in the expansion of $h_p^{(1)}(kd)$ (to $0(kd)^{-2}$) in the addition theorem, the theorem in this case being given by (A46).

The physical interpretation of the results of this approximation, shown diagrammatically in Figure 6.1, has been proposed heuristically for general multiple scattering type phenomena by many authors as long ago as 1893 (see Twersky, 1960). A result analogous to equation (6.21) was obtained by Twersky (1952) for the case of two (identical) cylinders by an identical method — i.e., by using an asymptotic form of the addition theorem (for cylindrical waves) and summing all the "orders of scattering" explicitly in a geometric series. Twersky (1960) calls this approximation in multiple scattering (where each object is in each others' far field), "far multiple scattering."

The extension of far multiple scattering (of $0(kd)^{-1}$) to arbitrary scatterers was made by Karp (1953), and to $0(kd)^{-2}$ by Zitron and Karp (1961a,b). In the general case, however, they are not able to sum up all the "orders of scattering" as in (6.21) and (6.22) so that there is not an exact correspondence with their solution to $0(kd)^{-1}$ and that given by (6.21). This has, however, been done by Twersky (1962) in operator form.

6.1.2 Numerical Results and a Comparison Study with the Electromagnetic Problem

As with the electromagnetic case we are confronted with the problem of selecting representative values for a few of the large number of parameters involved. Since the major emphasis in this thesis has been

the electromagnetic problem, no attempt will be made to be as complete for the acoustic case, however, as we will see, many of the results of the electromagnetic problem can be used in connection with the scalar problem.

To the author's knowledge, no previous results are available for the scalar problem of scattering by two spheres, numerical or experimental. We must have some means, however, of checking the numerical results. In line with this, a general program was written using the modal expansion technique of the previous section for arbitrary a, b, d, α and θ for either soft or hard spheres. Now, since the geometric optics solution for the broadside case gave such good results for the electromagnetic problem, it seemed only natural to consider the ray approach as a test for the results of the acoustic problem.

If we consider only those rays R_j at broadside, for a pair of identical spheres (see Figure 5.4), we will find the field due to these rays to be of the form:

$$\psi_j = (-1)^j c \prod_{r=1}^{j} \Delta_r e^{ikS_{rj}} \tag{6.23}$$

for the case of two soft spheres, since the Fresnel reflection coefficient for a plane boundary with the boundary condition u = 0 is -1. For hard spheres, the Fresnel coefficient is +1 so that in this case the sign preceding the constant c in (6.23) would be +1. The notation used in (6.23) was defined previously in Section 5.1. Thus we see upon comparing (6.23) with (5.3) that we will get <u>exactly</u> the same results (in the geometric optics limit) for the normalized radar cross-section of two identical spheres at broadside incidence for the EM case at vertical

polarization as we will for the acoustic case of two soft spheres, likewise for the EM case at horizontal polarization and acoustically hard spheres. This being the case, we would expect this correspondence to show up in the modal expansion solutions for the appropriate vector and scalar problems for this geometry when ka is sufficiently large. Sufficiently large is defined as that point where the backscattered field is due almost entirely to returns of the type R_j.

Numerical results using the general program for the scalar problems are shown in Figures 6.2 and 6.3 for the special cases of identical spheres, both soft and hard, at endfire and broadside incidence for ka = 2 and 10. We see by comparing Figures 6.3(c) with 5.9(d) and 6.3(d) with 5.9(c) that the correspondence is indeed remarkable, particularly in the former case. This is to be expected at ka = 10, since nearly all vestiges of creeping waves are gone at this value of ka in the backscattered field of a single soft sphere (see Senior, 1965). This is because the attenuation of the creeping waves on a soft sphere is very much higher than for the hard sphere. The comparison for the hard spheres and horizontal polarization is equally good except at contact.

The higher attenuation associated with creeping waves on an acoustically soft scatterer is quite apparent for the endfire cases, particularly that for ka = 10 in Figure 6.3(a). This behavior is easily explained on the basis of simple interference between rays R_1 and $C_-R_1^NC_-$ where the attenuation of the hybrid ray is greatest near contact since the creeping path is largest there. This claim is supported by the observation that the phase difference of these two rays from (5.18) predicts peaks in the radar cross-section at $\mu_n$ka where μ_n is the

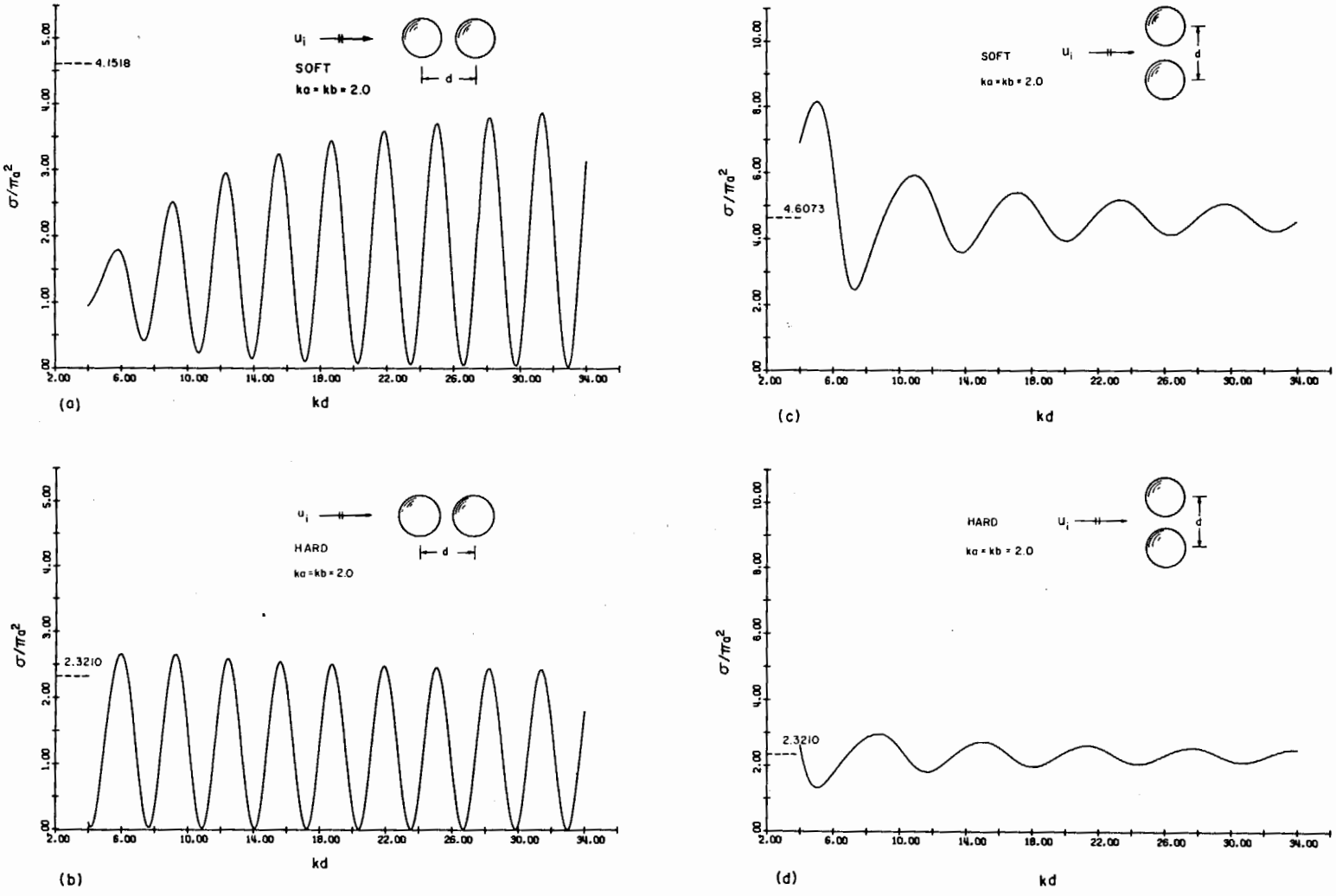

Figure 6.2 RCS of Two Equal Spheres, Hard and Soft, for ka = 2.0 at Endfire and Broadside Incidence Using the Acoustic Modal Solution.

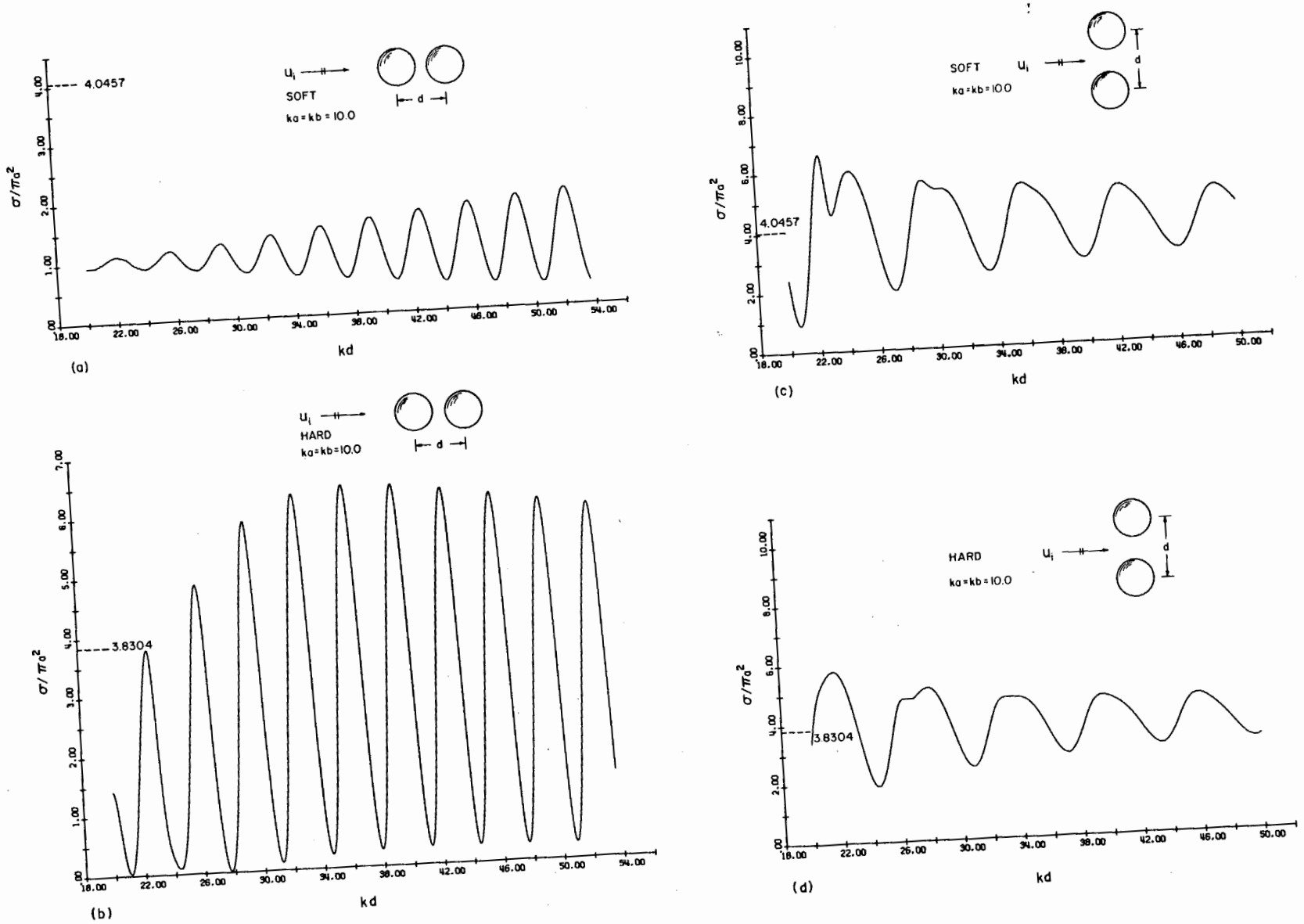

Figure 6.3 RCS of Two Equal Spheres, Hard and Soft, for ka = 10 at Endfire and Broadside Incidence Using the Acoustic Modal Solution.

solution of the equation:

$$\csc^{-1}\mu_n + \sqrt{\mu_n^2 - 1} = n\pi/ka \ .$$

From this we may also find the local period near the nth peak as $(\mu_n - \mu_{n-1})ka$. This agrees quite well with the results in Figure 6.3(a). Ultimately, for large μ_n, the above yields peaks in the cross-section at $kd = n\pi$ with period π, as we expect.

6.2 The Three Sphere Problem and Some Numerical Results

The generalization of the results for electromagnetic scattering by two spheres to the case of three,[†] is quite straightforward: therefore, most of the details will be omitted. The general procedure for the solution is again to use the addition theorem to translate the total field of the other spheres alternately into the coordinate system of each sphere and satisfy the boundary conditions on the surface. This determines the unknown multipole coefficients for each sphere in the presence of the other two in the form of coupled sets of equations. There is one major difference, however; there is no axis of symmetry for three spheres as there was for two unless all spheres are colinear. Thus, in general the more complicated general translation theorem (A20) will have to be used.

With the same configuration of the incident field as in the two sphere case (see Figure 2.1), the geometry of the three sphere problem is shown in Figure 6.4. The multipole coefficients of the incident wave about the

[†] Crane (1967) has considered the N sphere problem using matrix notation but has given no numerical or experimental results.

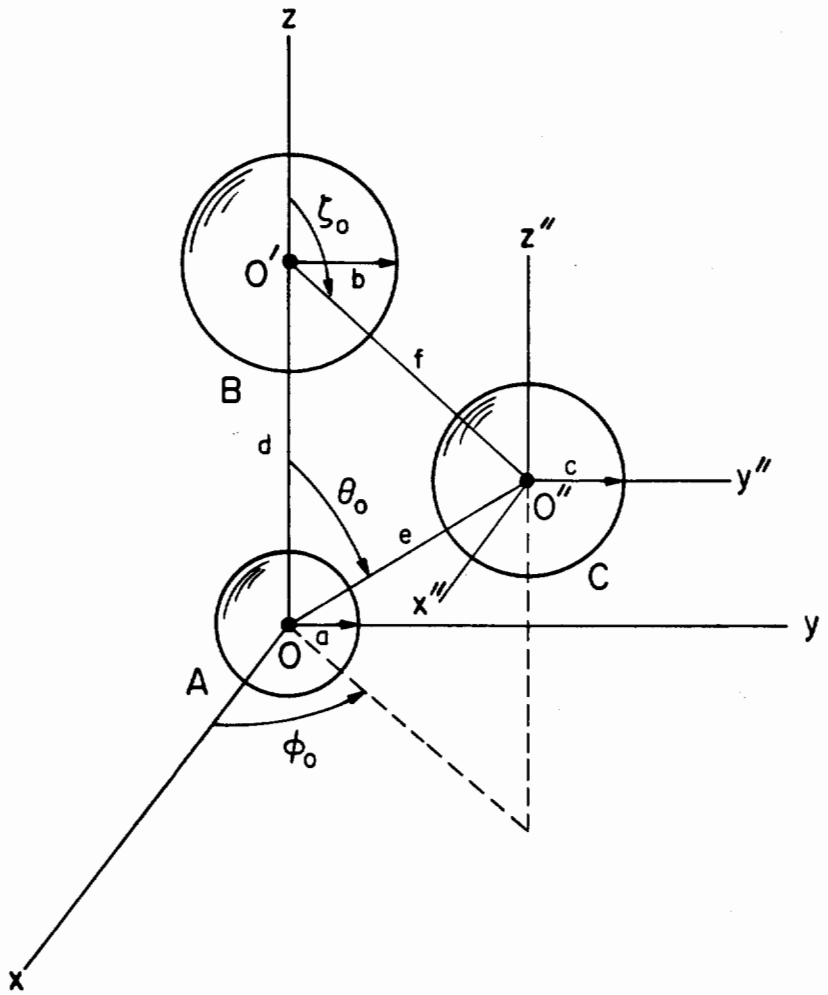

Figure 6.4 Geometry of Three Sphere Problem.

three origins 0, 0' and 0" are respectively:

$$p(m,n)$$

$$p'(m,n) = e^{ikd\cos\alpha} p(m,n)$$

$$p''(m,n) = e^{ike(\sin\theta_o \sin\phi_o \sin\alpha + \cos\theta_o \cos\alpha)} p(m,n)$$

where p(m,n) is given by (2.14). The q's follow the same form as the p's above. Using these coefficients in the incident wave expansions and combining with the scattered field expansions in terms of the unknown multipole coefficients we find in an analogous manner to the two sphere case the desired unknown multipole coefficients of each sphere in the presence of the other two after application of the boundary conditions. The results are, for the E and H modes of spheres A, B, and C, respectively:

$$A_E(m,n) = v_n(ka)\{p(m,n) + \sum_\nu [(A^{m\nu}_{mn}(d)B_E(m,\nu) + B^{m\nu}_{mn}(d)B_H(m,\nu)) + \sum_\mu (A^{\mu\nu}_{mn}(e,\theta_o,\phi_o)C_E(\mu,\nu) + B^{\mu\nu}_{mn}(e,\theta_o,\phi_o)C_H(\mu,\nu))]\}$$

$$A_H(m,n) = u_n(ka)\{q(m,n) + \sum_\nu [(A^{m\nu}_{mn}(d)B_H(m,\nu) + B^{m\nu}_{mn}(d)B_E(m,\nu)) + \sum_\mu (A^{\mu\nu}_{mn}(e,\theta_o,\phi_o)C_H(\mu,\nu) + B^{\mu\nu}_{mn}(e,\theta_o,\phi_o)C_E(\mu,\nu))]\}$$

$$B_E(m,n) = v_n(kb)\{p'(m,n) + \sum_\nu [(-1)^{n+\nu}(A^{m\nu}_{mn}(d)A_E(m,\nu) - B^{m\nu}_{mn}(d)A_H(m,\nu)) + \sum_\mu (A^{\mu\nu}_{mn}(f,\zeta_o,\phi_o)C_E(\mu,\nu) + B^{\mu\nu}_{mn}(f,\zeta_o,\phi_o)C_H(\mu,\nu))]\}$$

$$B_H(m,n) = u_n(kb)\{q'(m,n) + \sum_{\nu} [(-1)^{n+\nu}(A_{mn}^{m\nu}(d)A_H(m,\nu) - B_{mn}^{m\nu}(d)A_E(m,\nu))$$

$$+ \sum_{\mu} (A_{mn}^{\mu\nu}(f,\zeta_o,\phi_o)C_H(\mu,\nu) + B_{mn}^{\mu\nu}(f,\zeta_o,\phi_o)C_E(\mu,\nu))]\}$$

$$C_E(m,n) = v_n(kc)\{p''(m,n) + \sum_{\nu}\sum_{\mu} (-1)^{n+\nu}[A_{mn}^{\mu\nu}(e,\theta_o,\phi_o)A_E(\mu,\nu)$$

$$- B_{mn}^{\mu\nu}(e,\theta_o,\phi_o)A_H(\mu,\nu) + A_{mn}^{\mu\nu}(f,\zeta_o,\phi_o)B_E(\mu,\nu)$$

$$- B_{mn}^{\mu\nu}(f,\zeta_o,\phi_o)B_H(\mu,\nu)]\}$$

$$C_H(m,n) = u_n(kc)\{q''(m,n) + \sum_{\nu}\sum_{\mu} (-1)^{n+\nu}[A_{mn}^{\mu\nu}(e,\theta_o,\phi_o)A_H(\mu,\nu)$$

$$- B_{mn}^{\mu\nu}(e,\theta_o,\phi_o)A_E(\mu,\nu) + A_{mn}^{\mu\nu}(f,\zeta_o,\phi_o)B_H(\mu,\nu)$$

$$- B_{mn}^{\mu\nu}(f,\zeta_o,\phi_o)B_E(\mu,\nu)]\}$$

To solve these equations in general represents quite a formidable task. It will be noticed that it is necessary to calculate three different sets of translation coefficients: $A_{mn}^{m\nu}(d)$, $B_{mn}^{m\nu}(d)$, $A_{mn}^{\mu\nu}(e,\theta_o,\phi_o)$, $B_{mn}^{\mu\nu}(e,\theta_o,\phi_o)$, $A_{mn}^{\mu\nu}(f,\zeta_o,\phi_o)$ and $B_{mn}^{\mu\nu}(f,\zeta_o,\phi_o)$. Furthermore, if we truncate the multipole expansions for the fields at $\nu = n = N$ then for large N the number of coefficients $a(m,n,\mu,\nu,p)$ needed in the calculation of each of the general translation coefficients $A_{mn}^{\mu\nu}$ approaches $8N^5/15$, and $N^4/6$ for the type $A_{mn}^{m\nu}$.

No attempt was made to obtain numerical results for this very general case of three spheres, but it is relatively simple to consider the special case of a colinear array of three spheres of equal size, equally spaced.

For this case, only two sets of translation coefficients are needed, namely, $A_{mn}^{m\nu}(d)$, $B_{mn}^{m\nu}(d)$, $A_{mn}^{m\nu}(2d)$ and $B_{mn}^{m\nu}(2d)$. Numerical results for the broadside case of identical metallic spheres of size ka = 2 is shown in Figure 6.5. The general character is no different from the case of only two spheres as seen by comparison with Figure 5.8(b). The slight flattening of the left side of the peaks seems to be due to coupling between the two outside spheres. This is conjectured on the basis of additional calculations made for this case by satisfying the boundary conditions on each sphere only in the presence of its nearest neighbor (the center sphere having two nearest neighbors) with the result that this "flattening" disappeared.

Figure 6.6 shows numerical and experimental results for three equal metallic spheres in contact as the aspect angle α is changed. The agreement is excellent except near endfire. Further measurements with various combinations of three spheres (dielectric and metallic) showed a general high sensitivity to sphere allignment at and near endfire. Misalignment of sphere A or C could be easily detected as an asymmetry in the recorded scatter pattern; however, if the center sphere were positioned slightly high or low with respect to the other two, then the pattern would still retain its symmetry. This type of misalignment (if indeed there was any) could not be detected at the time of the measurement.

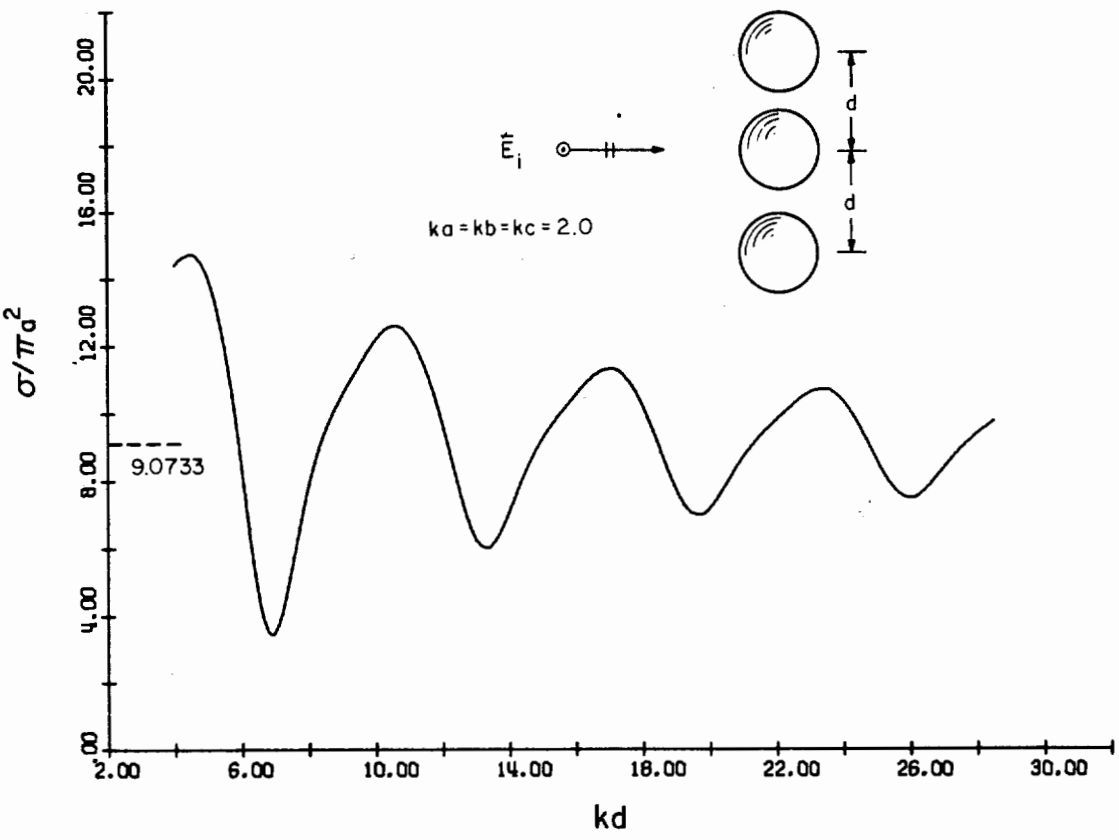

Figure 6.5 RCS of Three Equally Spaced Identical Metallic Spheres, at Broadside Incidence, for ka = 2.0 vs. Separation Using the Modal Expansion Solution.

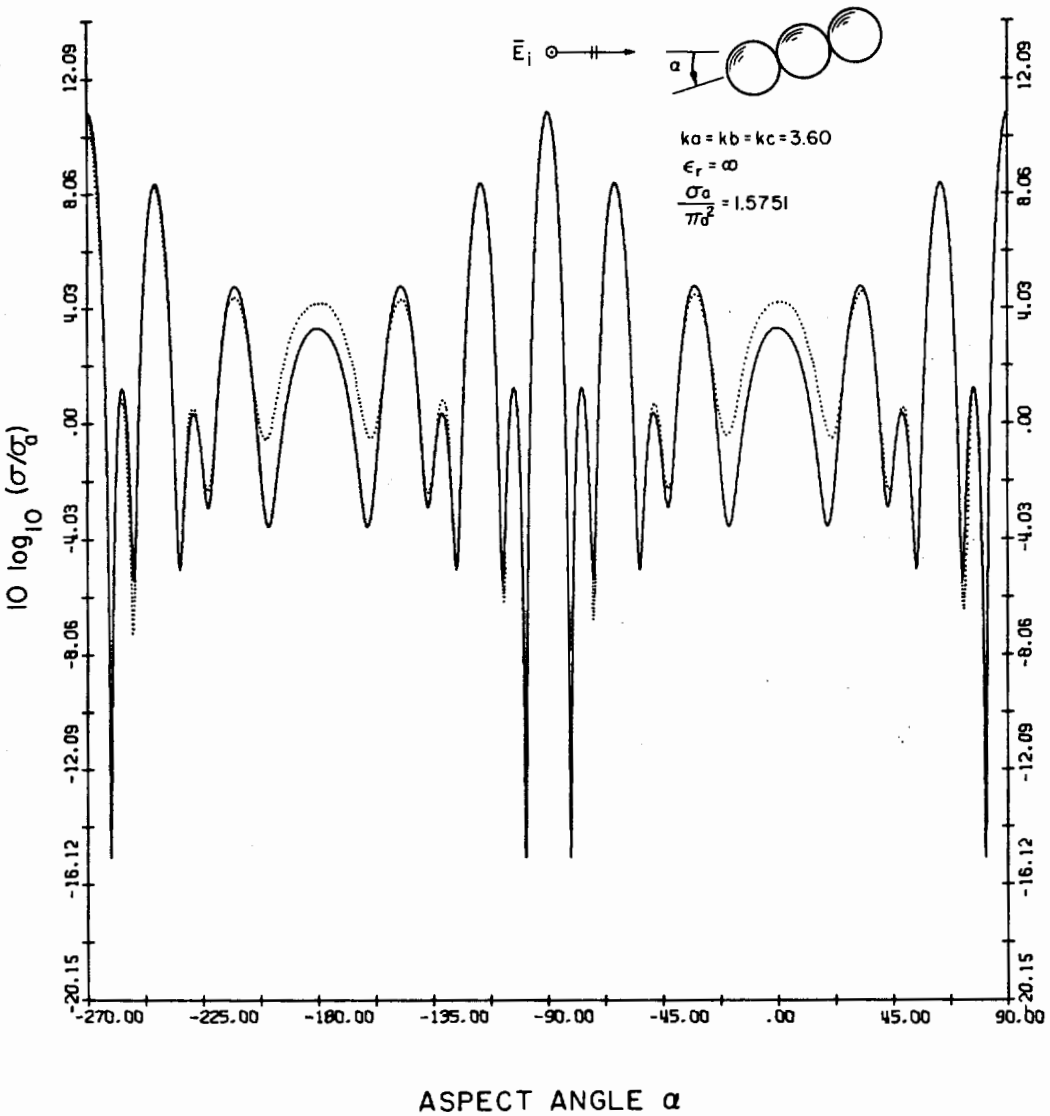

Figure 6.6 RCS of Three Equal Metallic Spheres in Contact vs. Aspect Angle Using the Modal Expansion Solution.

7. EXPERIMENTAL INVESTIGATION

The need for experimental confirmation of the theoretical predictions of multiple scattering behavior of two spheres is great in view of the complexity of the solution. The modal expansion solution to the two sphere problem is formally exact, but its usefulness is questionable unless we can obtain reliable numerical results from it. In a previous chapter various procedures were used to check numerical accuracy and consistency of the programs, including comparison with different theoretical approaches. Still, the most convincing check is direct experimental measurement.

A practical quantity for measurement and comparison is the radar cross-section. The requirements on the equipment and environment for accurate measurements of this type are, however, quite stringent. A lot of time and money is required to set up a radar scattering range. Since the laboratory under which this research was conducted had no scattering measurement facility, it was thought that it would be best to conduct the measurements elsewhere, at a well established facility. The CIC program provides for such arrangements between the big ten universities of which the University of Illinois is a part. It was indeed fortunate that such an arrangement could be made to use the excellent scattering facility at the Radiation Laboratory of the University of Michigan.

In what follows, a brief description of this scattering range is given. The problems associated with supporting the two spheres and making dynamic RCS measurements are also discussed and the equipment constructed for this purpose is described.

The scattering range is an indoor anechoeic chamber approximately 105' long, 15' high and 30' wide with 2" hairflex microwave absorber lining the floor, walls and ceiling, with VHP-18 absorber on the rear wall (both B. F. Goodrich products). The physical layout of the chamber may be seen in the photographs to follow (see also Knott, 1964).

The microwave equipment is located outside of the chamber and is shown pictorially in Figure 7.1 and schematically in Figure 7.2. This corresponds to a rather typical CW system for RCS measurements. There are frequency capabilities in the K_u, X, C and S bands; the appropriate equipment for each band is contained on its own stand. The C band cart is shown in position in Figure 7.1.

The ideal system with perfectly matched loads at each arm of a completely symmetrical hybrid junction or "magic tee" would totally isolate the transmitter and receiver. In practice, however, the termination is purposely mismatched (by the tuners shown in Figure 7.2) in order to reflect just that amount of signal into the receiver arm to balance or cancel out the unwanted background signals. These background signals come from extraneous reflections due to imperfect absorption by the anechoeic chamber and any other obstacles present. The ratio of the power remaining in the receiver arm *after cancellation* to the power in the transmitting arm is referred to as the isolation of the system. The accuracy of the system depends on the isolation obtainable. For an accuracy of $\pm$ 1/2 db in the RCS measurements shown in Figures 4.4 to 4.9 at the lowest level, the required isolation would typically have to be in excess of 100 db (Blacksmith, et al., 1965). This means that with the spheres removed,

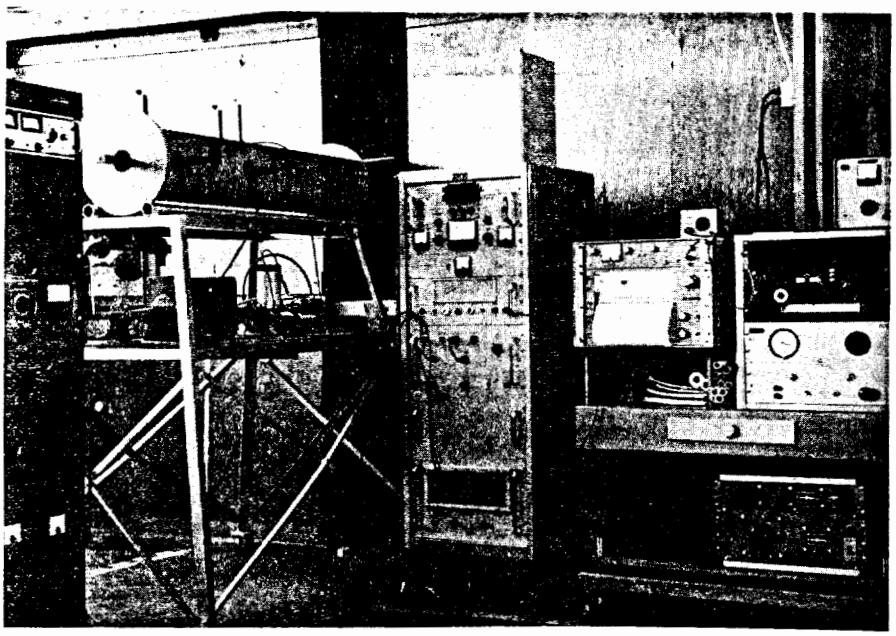

Figure 7.1 Photograph of C Band RCS Measurement System.

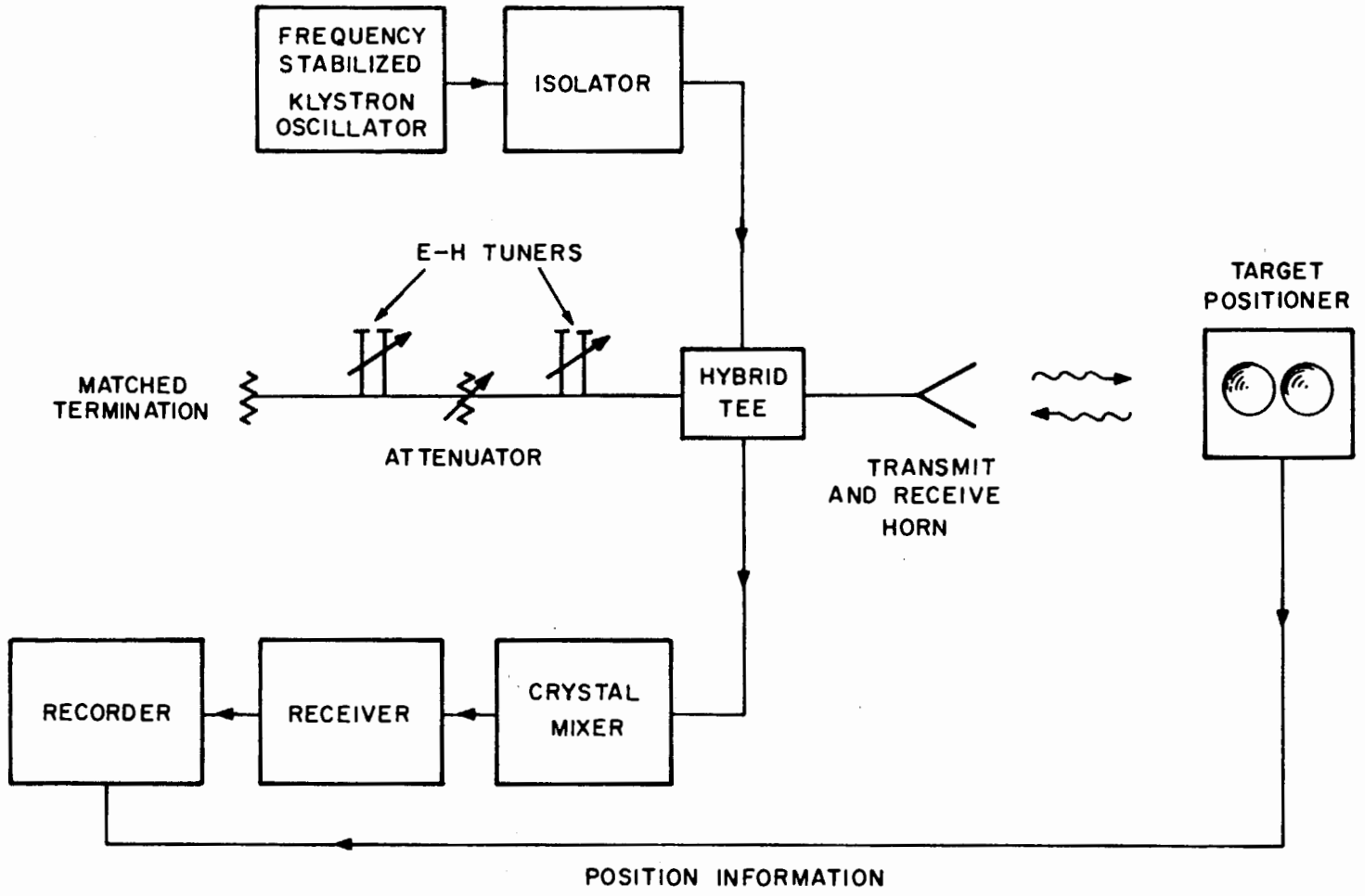

Figure 7.2 Schematic Diagram of CW System for RCS Measurements.

the power in the receiver arm must be 100 db below that in the transmitter arm. This requires extreme mechanical and frequency stability since this isolation must be maintained throughout the time required for the measurement which could be quite long.

Backscattering measurements have been made on two spheres for endfire and broadside incidence vs. separation by Angelakos and Kumagai (1964) and Mével (1960). Their measurements were made at discrete spacings. Many points must be measured to faithfully reproduce the RCS behavior vs. separation, particularly for the endfire case. This would require a great deal of time and patience for investigation of more than just a few cases. Since the scattering facility was available only for a short time, a more expedient method was sought.

A preliminary trip was made to the scattering facility to determine such essentials as characteristics of the equipment and electrical connections that would have to be made. The device for supporting and separating the spheres was designed and constructed prior to succeeding trips.

Size and weight of the spheres to be measured are factors which influence the choice of supporting technique. Extremely accurate spheres are readily and economically available from ball bearing manufacturers in sizes up to 4" in diameter and with surface tolerances to 10 millionths of an inch, but the weight of these spheres is quite high. Supporting technique utilizing very thin suspension lines are superior to most others in regard to unwanted background radiation, however, excessively heavy spheres may not be used. Hollow aluminum spheres 3 and 5 inches in

diameter, ball bearing balls less than 1 1/2 inch, and solid dielectric spheres about 3 inches in diameter were used and could be suspended safely by .005" monofilament line. Many different commerical fishing lines were tested for this application and Stren† was found to be the strongest for its diameter and had the highest tensile strength without stretching permanently. The 2 lb. line is .005" diameter and for the sphere sizes mentioned should introduce a signal no larger than -40 db with respect to the return from the two spheres under test (Freeny, 1965). "Cages" were made of this line in order to suspend the spheres from the ceiling of the chamber. The sphere separation was changed by pulling them apart using lines connected to a servo controlled "winch." This had to be accomplished differently for the endfire and broadside cases. The method employed for these two configurations is shown schematically in Figures 7.3(a) and (b), respectively. As seen in 7.3(a) there are unique problems associated with keeping the rear sphere level as the separation is changed. Clearly the broadside configuration does not have this problem. Figure 7.4 shows the motorized winch which reels in the line, thereby separating the spheres. This winch is motor driven and is connected to a servo which senses and transmits the sphere separation information to the RCS chart recorder. Between the winch and servo is a variable ratio drive (which may be recognized from the picture as a ball-disc integrator). This allows any desired expansion or contraction of the horizontal scale (kd) on the recorded RCS pattern. We see that the above mechanism allows *continuous*

†Registered tradename of E. I. duPont de Nemours.

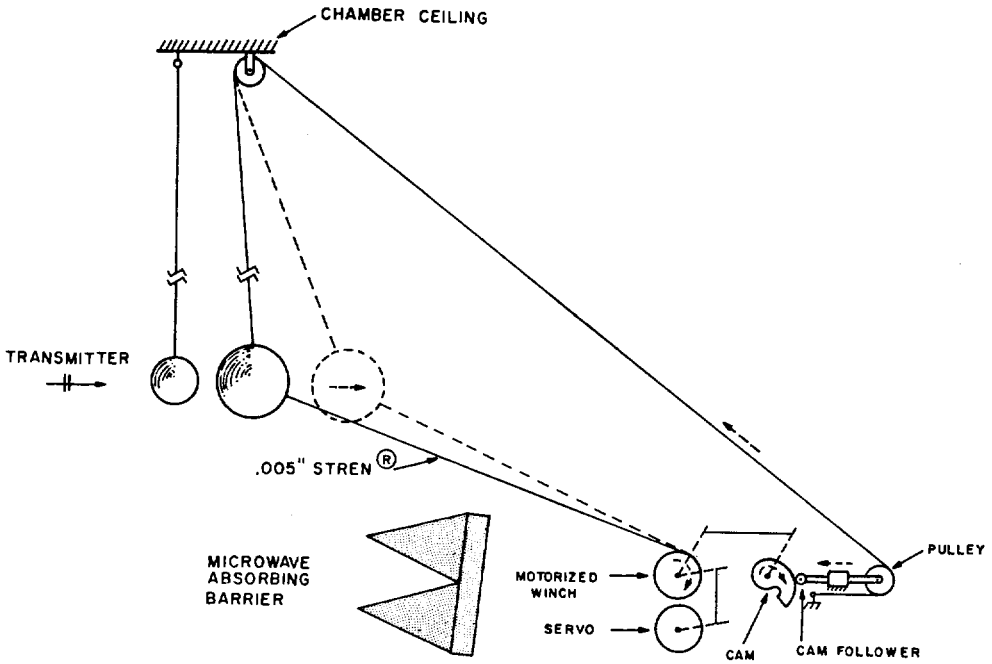

(a)

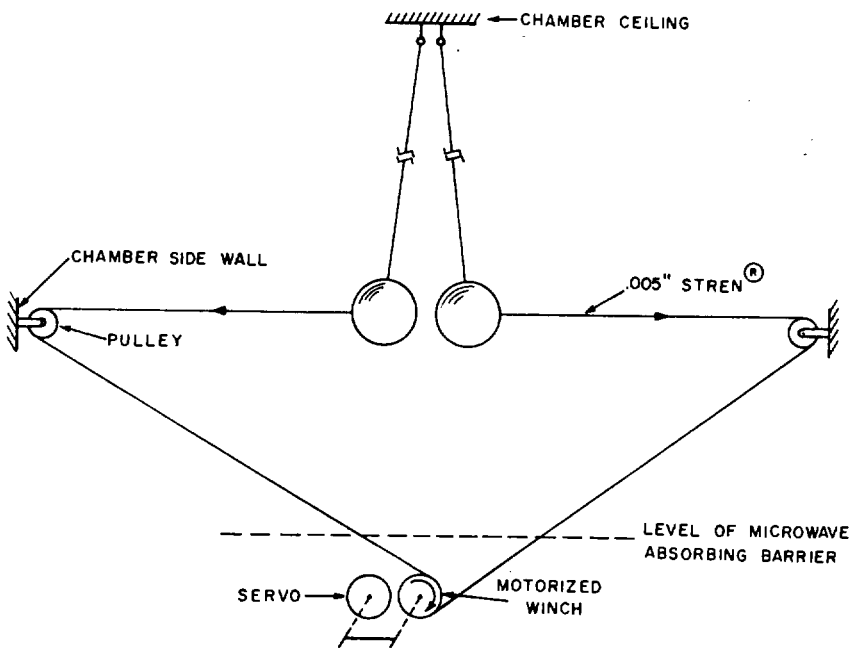

(b)

Figure 7.3 Schematic Diagram of First Suspension Technique for RCS Measurements of Two Spheres at (a) Endfire and (b) Broadside Incidence.

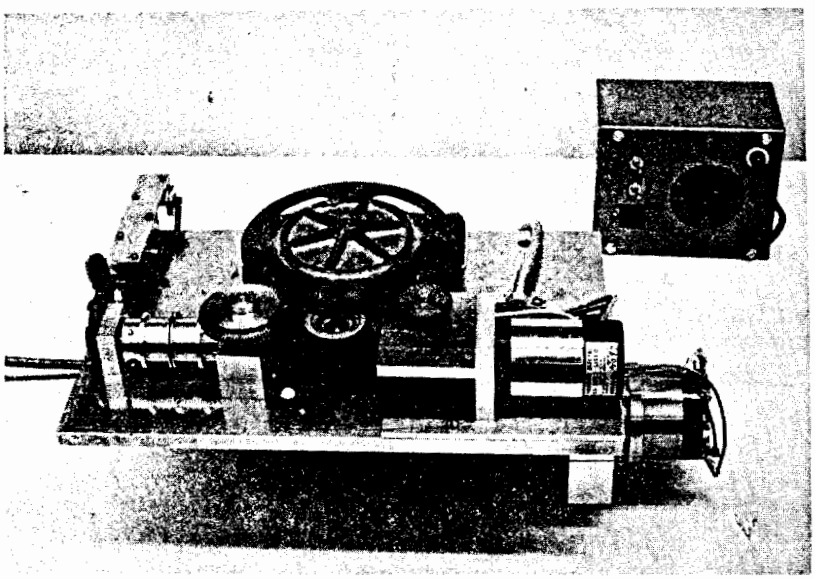

Figure 7.4 Motorized Winch Used for Separating the Spheres for Endfire and Broadside RCS Measurements.

recording of RCS vs. separation. Once the system is balanced and the spheres are set in the proper position, the actual time required for the measurement is very short. Figure 7.5 shows the actual setup of the suspended spheres in their "cages" for the endfire (left photo) and broadside configurations (right photo) at the completion of the measurements. The mechanism shown in Figure 7.4 is "hidden" behind the absorbing barrier shown on the floor in both photos. One possible drawback of this dynamic RCS measurement scheme is that before the system can be balanced, the spheres must be removed, and replaced again after balancing. Proper alignment of the spheres before the measurement may take considerable time, hence, balance must be checked before and after the measurement. Since the spheres in the above two geometries are essentially suspended each from a single point by rather long lengths of line, vibrations were completely undetectable. Any swinging of the spheres that resulted from pendulum type motion could be easily eliminated by "bouncing" the spheres together a few times. To avoid inducing any swinging or oscillatory motion as the spheres are drawn apart (or together), the winch is driven at a *nonuniform* rate.

Cases involving measurements with the two 3" hollow aluminum spheres for the broadside geometry presented a slight problem because of their extremely light weight (a few ounces). At close spacing, the amount of tension in the horizontal lines is so small that the lines tend to sag. This explains the departure of the horizontal scale in Figure 4.1(a). In 4.1(b), the larger (and heavier) spheres were used, minimizing the effect. The experimental results using this suspension technique are shown in Figures 4.1 through 4.6.

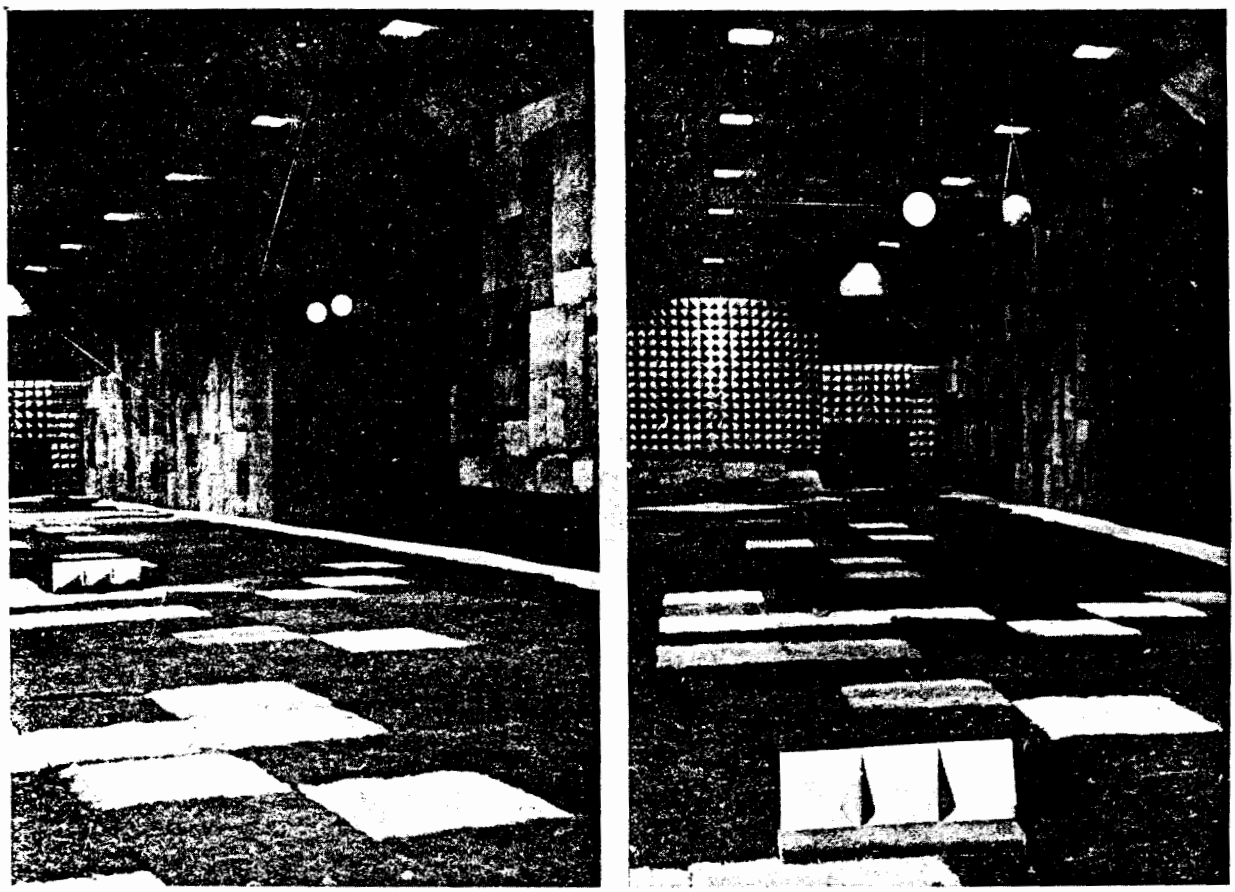

Figure 7.5 Photo of Spheres in Position at Endfire (left) and Broadside (right) Using First Suspension Technique.

RCS measurements of two spheres for variable angle of incidence and fixed separation requires yet a third supporting structure. This is shown in Figure 7.6 and consists of a rotary table with a polystyrene foam column. This is the typically used supporting structure for most RCS measurements and no modification was necessary. This structure was used for the measurements appearing in Figures 4.7 through 4.9.

Another sphere supporting technique was conceived and the equipment constructed to achieve the same results as the previous three configurations but with a single apparatus. Furthermore, it was desired to have the capability to make all adjustments from outside of the anechoeic chamber including a method for withdrawing the spheres in order to balance the system. The design arrived at is shown schematically in Figure 7.7. As seen, the rotary table provides for aspect angle changes; another motor and servo allow the spheres to be separated at will, and small motorized winches allow both spheres to be moved up and down independently. All these motions can be controlled at will from outside of the chamber. This unit is covered with microwave absorbing material to minimize extraneous scattering effects. The hardware and associated controls are shown in Figure 7.8.

Measurements for any of the previous configurations could be made quite rapidly with this system since the balancing and positioning of the spheres can be done from outside of the chamber. With this, the spheres could be separated at any angle or rotated at any separation. Since the same basic drive mechanism was used for separation of the spheres, the horizontal scale expansion or compression feature for the recorded RCS

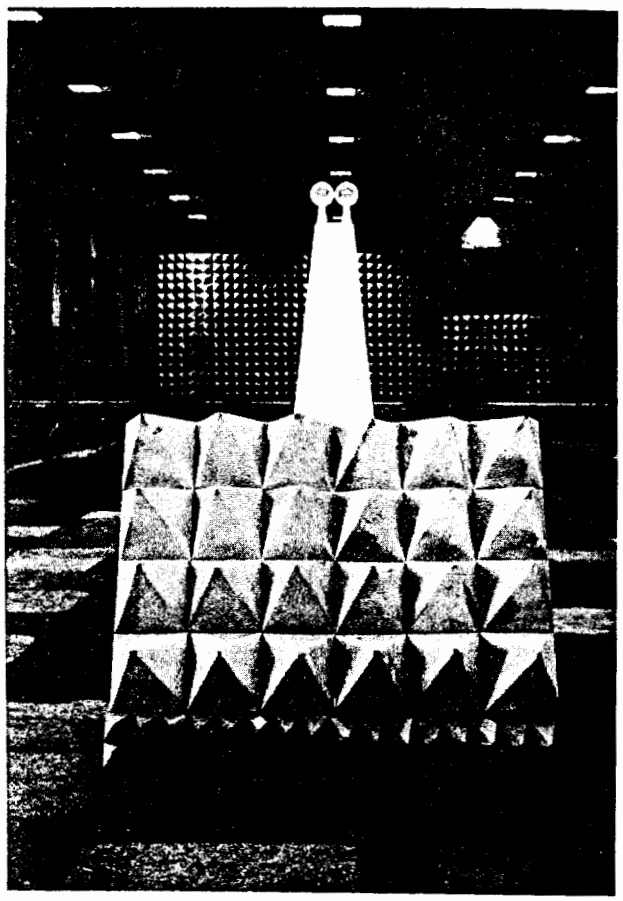

Figure 7.6 Supporting Structure for Fixed Separation, Variable Angle of Incidence.

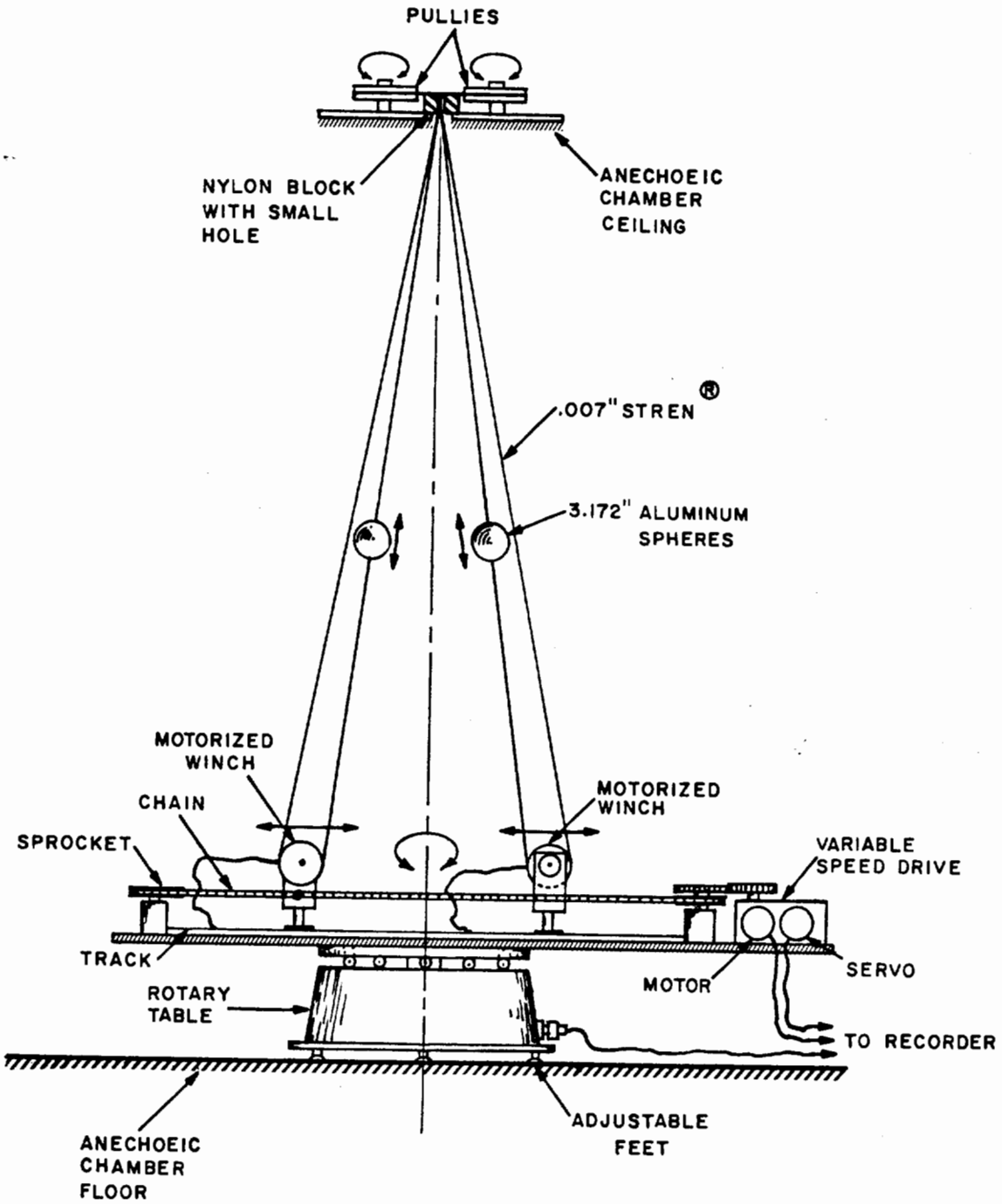

Figure 7.7 Schematic Diagram of Final Suspension Technique for all Orientations of Two Spheres.

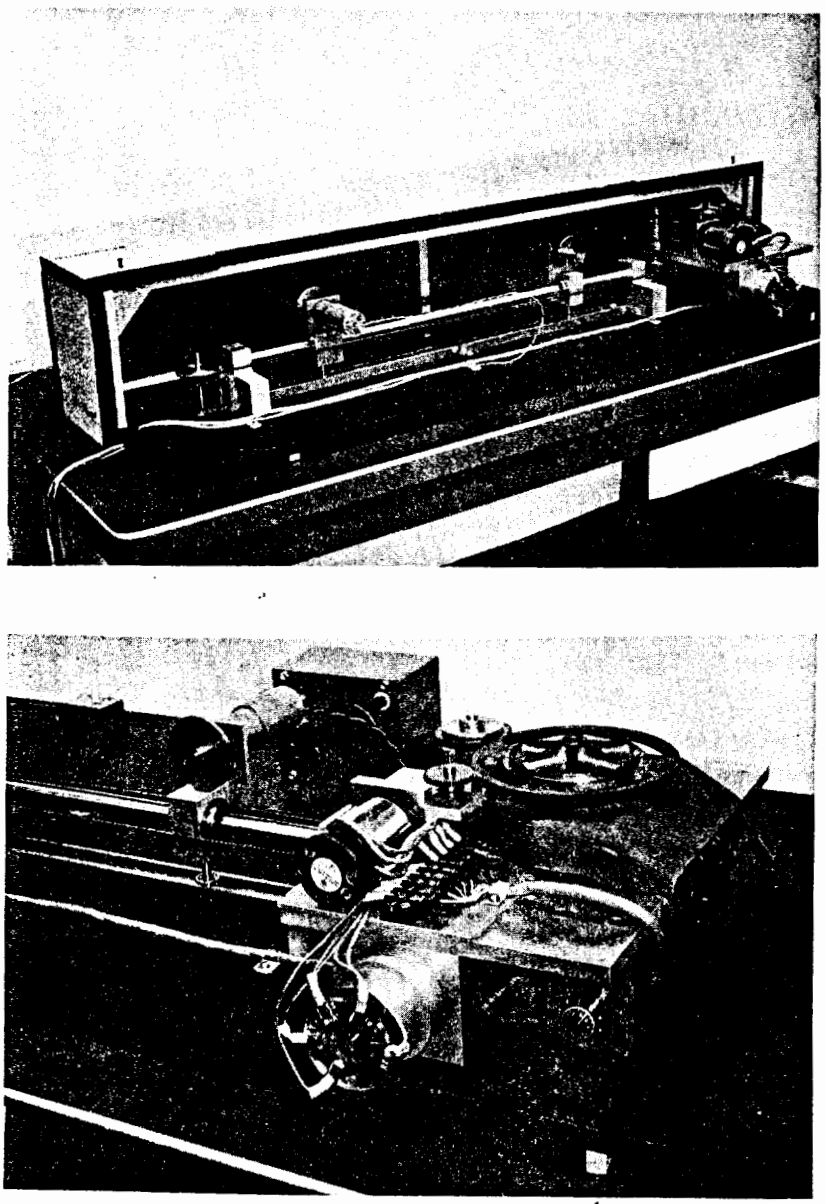

Figure 7.8 Associated Hardware for General Suspension Technique.

pattern was also available. Figure 7.9 (bottom) shows the two spheres withdrawn below the absorbing barrier in position for balancing of the system. The upper figure shows the same spheres raised and aligned in position for the start of the measurement. Since the spheres in this setup are essentially supported both from above and below, they are more susceptible to vibration and oscillations. This was detectable most when the spheres were rotated. Therefore great caution had to be exercised during the measurement.

In summary, the results consistently showed excellent agreement with the theory indicating that the supporting structure and suspension lines were indeed "invisible" to the receiver. This of course also indicates the caliber of the microwave equipment and the chamber itself.

To aid in identification of some of the parameters associated with the experimental results, the sphere sizes and materials and frequency of operation[†] are associated with the results presented in the previous chapter by the figure number in the table on the following page. In all of the above cases, the distance from the transmitter to the spheres was about 19 feet.

Many other measurements were made, all showing the same excellent agreement with the theory. These are not included to prevent added confusion.

[†]Size is inches of diameter; Al. signifies aluminum, Cu - copper plated steel and Rx. - Rexolite ($\epsilon_r \approx 2.56$). The frequency is given in GHz.

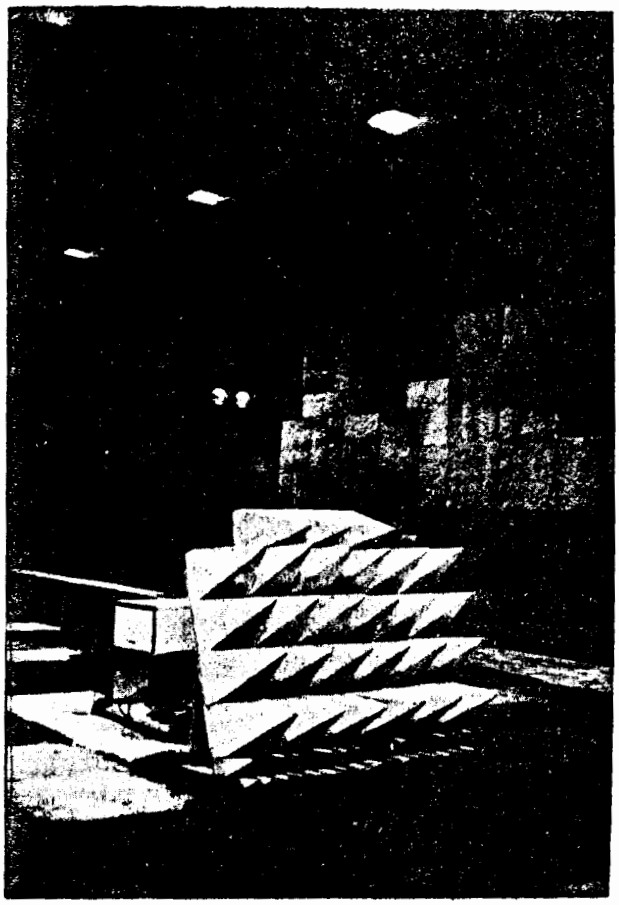

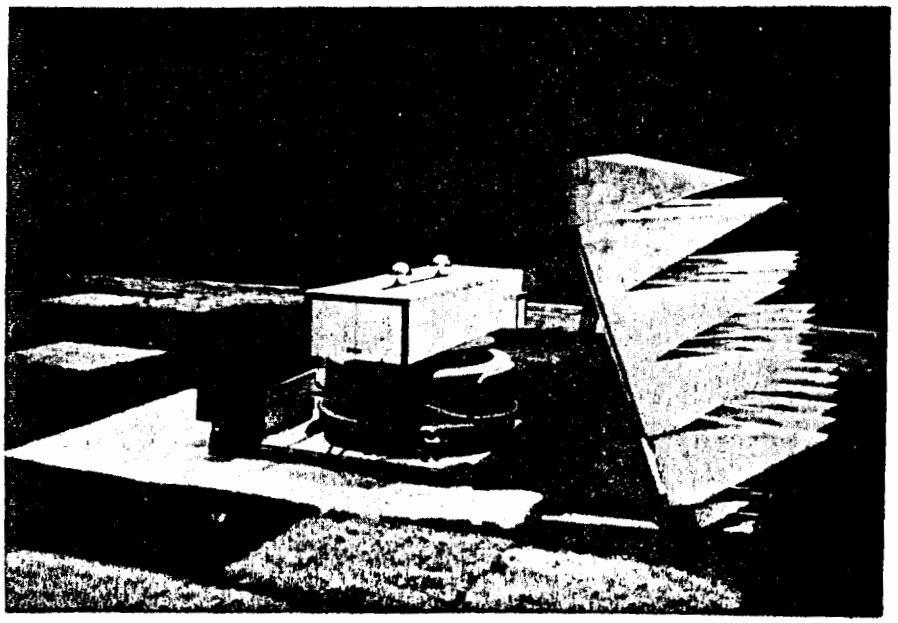

Figure 7.9 Final Suspension Technique Showing Spheres in the Lowered Position for Balancing of the Chamber (bottom) and in the Raised, Aligned, Position Ready for Measurement (top).

Table 7.1

Physical Parameters of the Spheres Used in the RCS Measurements

Figure #	Sphere A	Sphere B	Frequency
4.1(a)	3.173 - Al.	3.173 - Al.	4.9645
4.1(b)	4.750 - Al.	4.750 - Al.	4.9645
4.2	3.187 - Rx.	3.187 - Rx.	4.9645
4.4(a)	3.173 - Al.	3.173 - Al.	8.7810
4.4(b)	4.750 - Al.	4.750 - Al.	8.7810
4.5(a)	3.173 - Al.	4.750 - Al.	8.7810
4.5(b)	4.750 - Al.	3.173 - Al.	8.7810
4.6(a),4.9(a)	3.187 - Rx.	3.187 - Rx.	8.7810
4.6(b),4.7	3.187 - Rx.	3.173 - Al.	8.7810
4.8(a)	3.173 - Al.	3.173 - Al.	4.2650
4.8(b)	3.187 - Rx.	3.173 - Al.	4.2650
4.9(b)	1.000 - Cu.	1.000 - Cu.	10.202

8. CONCLUSIONS

In this thesis, multiple scattering of electromagnetic or acoustic waves by two or three spheres has been studied in great detail using three different approaches: multipole expansion, ray optics, and experiments. The results of these approaches were compared whenever possible. Except for a very few cases, nearly perfect agreement was found.

In the multipole expansion approach, the translational addition theorem for spherical wave functions is required. Due to the complexity of this theorem, previous computations by other authors have been restricted to spheres of radii less than 3/4 wavelength and large separations. In this investigation, an important recursion relation pertaining to the translation coefficients has been obtained. With this relation and other symmetry properties, not only has computation time been reduced by several orders of magnitude, but the range of computation was also extended to spheres of radii as large as 10 wavelengths and separations as small as physical contact. In addition, results were also extended to spheres of different materials.

Solutions in closed forms are obtained for two special cases: the Rayleigh approximation and the far multiple scattering approximation. The former is applicable to spheres of radii small compared to a wavelength while the latter applies to spheres at large separation.

The ray optical approach, which is particularly useful for large spheres, is also studied in some detail. The scattered field is attributed to purely geometric optics rays, creeping wave rays, and hybrid rays which creep and reflect. It is shown that this approach yields excellent results

for spheres even as small as 1/2 wavelength in radius and spaced as close as physical contact. However, at present, this approach is confined only to conducting spheres due to the lack of a tractable creeping wave theory for dielectric spheres. Cases involving rays that come close to shadow boundaries also require more investigation. This situation causes problems even in the ray description of the single sphere. In spite of these limitations, this approach provides much insight into the multiple scattering mechanism, backscattering behavior in particular. The strength of the multiple scattering contributions at broadside incidence for large spheres depend only on the separation to radius ratio of the two spheres whereas at endfire for the same separation the dependency is more complicated. The multiple scattered rays are shown to be purely geometric optics rays in the first case and hybrid rays in the second.

The value of any theory must be questioned if it cannot accurately predict and explain experimental results. Due to the large number of parameters in this problem, an extensive experimental program was undertaken. For convenience, the experimental work has been restricted to backscattering measurements. In almost all the cases, nearly perfect agreement has been obtained.

Because of symmetry, the backscattered field of a single sphere, and thus of two uncoupled spheres, will not be depolarized. Therefore, depolarization from scattering by two spheres is a consequence of multiple scattering. The polarization ellipse of the backscattered field has been examined in this context.

Acoustic scattering by two spheres has also been studied and numerical results were given. The analysis is considerably simpler, but

numerical convergence for many cases is often slower than in the electromagnetic problem. A unique relation between the acoustic two sphere problem and its electromagnetic counterpart was discussed. Finally, the problem of scattering by three spheres has also been formulated and some numerical and experimental results were presented.

There are many aspects of this problem which have been dealt with only briefly here but which deserve a more thorough investigation. These include multiple scattering by resonant dielectric spheres, and a creeping wave theory valid near and at a shadow boundary, not to mention the many additional numerical results that can be obtained.

A class of other related problems may now be readily solved because of the more tractable form of the addition theorem presented. This includes the non-concentric spherical cavity and scattering by a sphere with a non-concentric dielectric coating to name but a few.

APPENDIX

TRANSLATIONAL ADDITION THEOREMS FOR SPHERICAL WAVE FUNCTIONS

A.1 General Scalar Addition Theorem

In this section the translational addition theorems for scalar and vector spherical waves are examined and the work of previous authors is reviewed and discussed. Recursion formulas are derived which greatly simplify numerical computation of the coefficients involved and an asymptotic form for the translation theorem for large translational distances is presented.

The addition theorem for spherical waves finds its use in problems involving more than one coordinate origin where it may be necessary to express spherical waves in one spherical coordinate system in terms of spherical waves about another "translated" coordinate system. The geometry describing such a translation is shown in Figure A1.

This problem has received the attention of many investigators, however there seems to have been a considerable lack of communication among them. The first known appearance of the addition theorem (both vector and scalar) was due to Trinks (1935) who developed it specifically for the two sphere boundary value problem. Perhaps this is why his work went unnoticed by present day authors of the subject. His form of the addition theorem, however, lacked the elegance of the more recent treatments. The coefficients in the addition theorem were given in operator form rather than in an explicit form and translation was restricted to the z axis ($\theta_o = 0,\pi$). Independently Sato (1950) derived the scalar addition theorem again only valid for translation along the

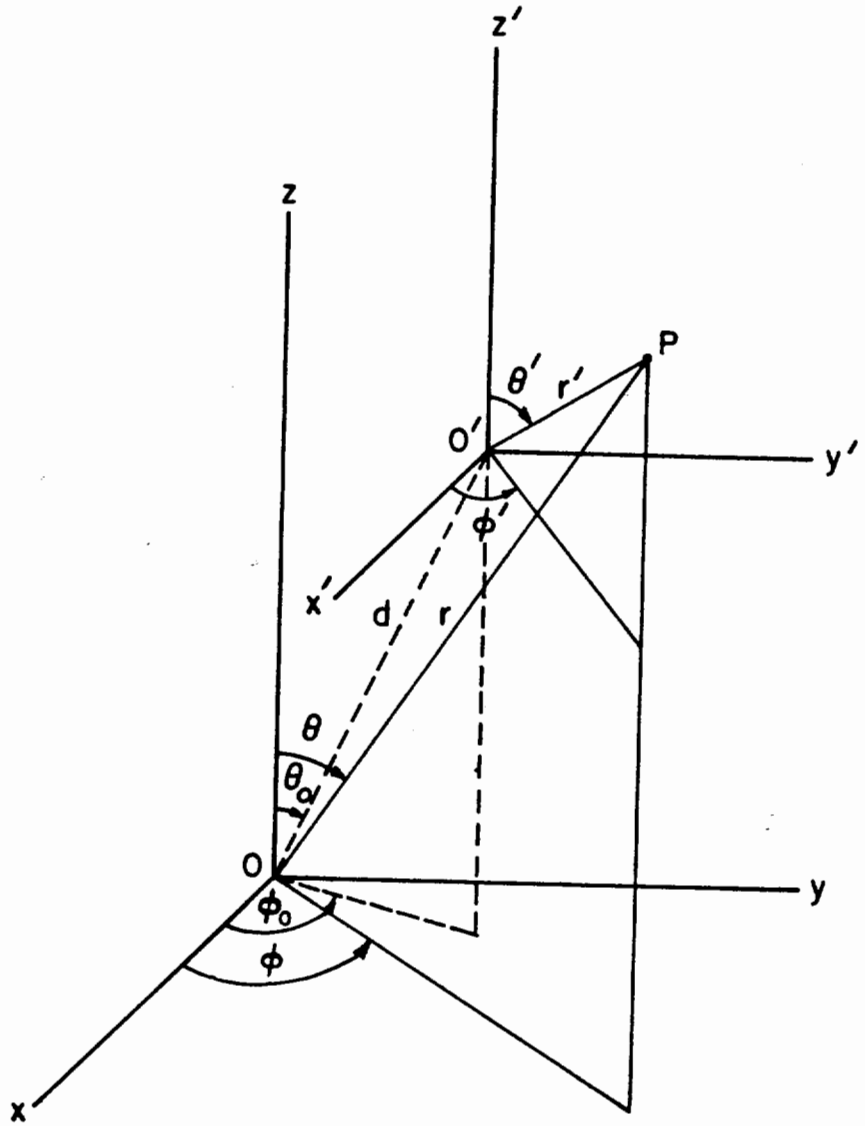

Figure A1. Geometry for General Rigid Coordinate Translation.

z axis. The coefficients for his expansion were not given explicitly but in a recurrent form. Eyges (1957) presents a still different form for translation along the z axis. Ament (1959) tabulated some of the coefficients involved in the vector translation theorem only for low orders of the wave functions, however, no explicit form was given for all orders.

The most significant contributions to the general addition theorem include the work on the scalar addition theorem by Friedman and Russek (1954) and the extension to the vector case by Stein (1961), and Cruzan (1962). Recent related work includes that of Danos and Maximon (1965) and Sack (1964).

Scalar spherical waves are solutions to the Helmholtz equation in spherical coordinates:

$$\nabla^2 u + k^2 u = 0 \tag{A1}$$

k being the wave number $2\pi/\lambda$. The set of characteristic solutions with suppressed time factor $e^{-i\omega t}$ is given by:

$$u_{mn}^{(j)} = z_n^{(j)}(kr) P_n^m(\cos\theta) e^{im\phi} \quad |m| \leq n, \; 0 \leq n < \infty. \tag{A2}$$

$z_n^{(j)}(kr)$ is any of the spherical radical functions j_n, n_n, $h_n^{(1)}$, and $h_n^{(2)}$ which refer respectively to the superscripts j = 1,2,3,4. The defintions of the functions follow those given by Stratton (1941). The translation of the spherical wave u_{mn} from origin 0 to origin 0' a distance d is given by (Stein, 1961)

$$u_{mn}^{(j)'} = \sum_{\nu=0}^{\infty} \sum_{\mu=-\nu}^{\nu} \alpha_{\mu\nu}^{mn} \, u_{\mu\nu}^{(1)} \tag{A3}$$

where the prime indicates only that the coordinate variables refer to origin 0' (see Figure A1) and

$$\alpha_{\mu\nu}^{mn} = (-1)^{\mu} i^{\nu-n}(2\nu+1) \sum_{p} i^{-p} a(m,n,-\mu,\nu,p) z_p^{(j)}(kd) P_p^{m-\mu}(\cos\theta_o) \times e^{i(m-\mu)\phi_o} \quad r \leq d$$

$$\alpha_{\mu\nu}^{mn} = (-1)^{m-\mu} i^{\nu-n} \sum_{p} i^{-p}(2p+1) a(m,n,\mu-m)p,\nu) j_p(kd) P_p^{m-\mu}(\cos\theta_o) \times e^{i(m-\mu)\phi_o} \quad r \geq d \tag{A4}$$

The coefficient $a(m,n,\mu,\nu,p)$ is defined by the following linearization expansion:

$$P_n^m(x) P_\nu^\mu(x) = \sum_{p} a(m,n,\mu,\nu,p) P_p^{m+\mu}(x) \tag{A5}$$

where $p = n+\nu, n+\nu-2, \ldots, |n-\nu|$; the coefficient $a(\cdot)$ vanishes for all other values. From the orthogonality properties of the associated Legendre functions and equation (A5), the following identity results:

$$a(m,n,\mu-m,p,\nu) = (-1)^m \frac{2\nu+1}{2p+1} a(m,n,-\mu,\nu,p) \tag{A6}$$

If this is used in (A4) above, a new more symmetric form of the coefficient $\alpha_{\mu\nu}^{mn}$ results

$$\alpha_{\mu\nu}^{mn} = (-1)^{\mu} i^{\nu-n}(2\nu+1) \sum_{p} i^{-p} a(m,n,-\mu,\nu,p) \begin{bmatrix} z_p^{(j)}(kd) \\ j_p(kd) \end{bmatrix} \times P_p^{m-\mu}(\cos\theta_o) e^{i(m-\mu)\phi_o} \begin{bmatrix} r \leq d \\ r \geq d \end{bmatrix} \tag{A7}$$

If now translation is desired from 0' to 0, the primed and unprimed quantities in (A3) trade places and $\alpha_{\mu\nu}^{mn}$ is preceded by the factor $(-1)^{n+\nu}$. This is evident upon replacing θ_o by $\pi-\theta_o$ and ϕ_o by $\phi_o+\pi$ which introduces a $(-1)^p$ factor under the summation; this may be removed as $(-1)^{n+\nu}$ since p cycles in jumps of 2.

As will soon become evident, the computation of these coefficients presents the major difficulty in any application of the scalar or vector translation theorem (see Section 3.2). From the orthogonality properties of the associated Legendre functions, it is clear that the coefficient $a(\cdot)$ can be written as an integral of the product of three associated Legendre functions. This integral has quite a long history† and has been evaluated in various forms by Gaunt (1929), Infeld and Hull (1951) and others as rather cumbersome summations of factorials. This has been identified as a generalized hypergeometric series by Hardy (1923) and Rose (1955). Stein and Cruzan, among others, recognized that the coefficient $a(m,n,\mu,\nu,p)$ could be written in terms of a product of two Wigner 3-j coefficients which are associated with the coupling of two angular momentum vectors (see, for example, Edmonds, 1957). This was regarded as an elegant formulation as there are available extensive tables involving these coefficients (Rotenberg, et al., 1959). With this representation, the coefficients $a(\cdot)$ are given by (Cruzan, 1962):

---

†The product expansion for Legendre polynomials ($m = \mu = 0$) dates back to 1878 in a paper by Adams.

$$a(m,n,\mu,\nu,p) = (-1)^{m+\mu}(2p+1)\left[\frac{(n+m)!\,(\nu+\mu)!\,(p-m-\mu)!}{(n-m)!\,(\nu-\mu)!\,(p+m+\mu)!}\right]^{1/2}$$

$$\times \begin{pmatrix} n & \nu & p \\ 0 & 0 & 0 \end{pmatrix} \begin{pmatrix} n & \nu & p \\ m & \mu & -m-\mu \end{pmatrix} \qquad \text{(A8)}$$

where $\begin{pmatrix} j_1 & j_2 & j_3 \\ m_1 & m_2 & -m_1-m_2 \end{pmatrix}$ is the Wigner 3-j symbol. The 3-j coefficient has many different representations (Rotenberg, et al., 1959) but the Van der Waerden definition is most convenient for the present discussion; it is given by:

$$\begin{pmatrix} n & \nu & p \\ m & \mu & -m-\mu \end{pmatrix} = (-1)^{n-\nu-m-\mu}$$

$$\times \left[\frac{(n+\nu-p)!\,(n-\nu+p)!\,(-n+\nu+p)!\,(n+m)!\,(n-m)!\,(\nu+\mu)!\,(\nu-\mu)!\,(p+m+\mu)!\,(p-m-\mu)!}{(n+\nu+p+1)!}\right]^{1/2}$$

$$\times \sum_k (-1)^k [k!\,(n+\nu-p-k)!\,(n-m-k)!\,(\nu+\mu-k)!\,(p-\nu+m+k)!\,(p-n-\mu+k)!]^{-1}$$

(A9)

The special coefficient $\begin{pmatrix} n & \nu & p \\ 0 & 0 & 0 \end{pmatrix}$ has a simpler form not involving a summation but still a large number of factorials. Nevertheless, one can appreciate the difficulty in trying to compute a single coefficient $a(m,n,\mu,\nu,p)$. Furthermore, any computation involving the translation theorem, for all but the smallest orders, would require a prohibitive storage capacity for the 3-j coefficients if tabulated values were used (see Section 3.2). What is really needed is an efficient and systematic method of generating the $a(\cdot)$'s. In particular it would be highly

desirable to have a recursion formula for the $a(\cdot)$'s which involves only a cycling of the index p since the $\alpha_{\mu\nu}^{mn}$'s in (A7) involve a summation of the $a(\cdot)$'s with p as the cycling index. Cruzan listed nine recursion formulas involving the $a(\cdot)$'s which he stated should be useful for computational purposes; however, by themselves they are quite clumsy since within a single recursion formula as many as six terms or three different indices are involved. Curiously enough, all the information for obtaining a single recursion formula in the index p alone is nevertheless contained in six of these nine formulas. These six formulas with slight rearrangement of the indices are shown in matrix form[†] in Table AI, and can be reduced, after very tedious elimination, to the following pair of three-term recursion formulas in the two indices ν and p:

$$(2p+1)(2p-3)(\nu-\mu+1)[(m-\mu)p(p-1)-m_3(n-\nu)(n+\nu+1)]a(m,n,\mu,\nu+1,p-1)$$

$$+ (2p+1)(p-m_3-1)(-n+\nu+p-1)(n+\nu+p)[\mu(p-\nu-1)-m(\nu+1)]a(m,n,\mu,\nu,p-2)$$

$$+ (2p-3)(p+m_3)(n+\nu-p+1)(n-\nu+p)[\mu(p+\nu)+m(\nu+1)]a(m,n,\mu,\nu,p) = 0 \qquad \text{(A10)}$$

[†] Table AI gives six recursion formulas, each row corresponding to one. A recursion formula is read by preceding each of the coefficients $a(\cdot)$ in the top row by the factors in the columns below them, adding together and setting the result to zero. For example, the last row in the table corresponds to the following recursion formula:

$$(\nu+\mu)(\nu-\mu+1)a(m,n,\mu-1,\nu,p-2) + (p+m_3-1)(p-m_3-2)a(m,n,\mu+1,\nu,p-2)$$

$$+ [(n+\nu-p+2)(n-\nu+p-1)-2\nu(p-1)+2\mu m_3]a(m,n,\mu,\nu,p-2) = 0.$$

Table A1

The Six Essential Recursion Formulas for the Coefficient $a(m,n,\mu,\nu,p)$

$a(m,n,\mu+1,\nu,p)$	$a(m,n,\mu-1,\nu,p)$	$a(m,n,\mu-1,\nu,p-2)$	$a(m,n,\mu+1,\nu,p-2)$	$a(m,n,\mu,\nu-1,p-1)$	$a(m,n,\mu,\nu+1,p-1)$	$a(m,n,\mu,\nu,p-2)$	$a(m,n,\mu,\nu,p)$
$-(2p-3)(p+m_3)(p+m_3+1)$	$(2p-3)(\nu+\mu)(\nu-\mu+1)$	$-(2p+1)(\nu+\mu)(\nu-\mu+1)$	$(2p+1)(p-m_3-1)(p-m_3-2)$	0	0	$2\mu(2p+1)(p-m_3-1)$	$2\mu(2p-3)(p+m_3)$
$(2p-1)(p+m_3)(p+m_3+1)$	$(2p-1)(\nu-\mu)(\nu-\mu+1)$	0	0	$-(2p+1)(-n+\nu+p-1)$ $\cdot(n+\nu+p)$	0	0	$2(2p-1)(p+m_3)(\nu-\mu)$
0	$-2\mu(2p-1)(2\nu+1)$	0	0	$-(2p+1)(-n+\nu+p-1)$ $\cdot(n+\nu+p)$	$-(2p+1)(n+\nu-p+2)$ $\cdot(n-\nu+p-1)$	0	$2(2p-1)(2\nu+1)(p+m_3)$
0	0	$2\mu(2p-1)(2\nu+1)$	0	$-(2p-3)(n+\nu-p+1)$ $\cdot(n-\nu+p)$	$-(2p-3)(-n+\nu+p)$ $\cdot(n+\nu+p+1)$	$2(2p-1)(2\nu+1)$ $\cdot(p-m_3-1)$	0
0	0	$(2p-1)(\nu+\mu)(\nu+\mu+1)$	$(2p-1)(p-m_3-1)(p-m_3-2)$	0	$-(2p-3)(-n+\nu+p)$ $\cdot(n+\nu+p+1)$	$2(2p-1)(p-m_3-1)$ $\cdot(\nu+\mu+1)$	0
0	0	$(\nu+\mu)(\nu-\mu+1)$	$(p+m_3-1)(p-m_3-2)$	0	0	$(n+\nu-p+2)(n-\nu+p-1)$ $-2\nu(p-1)+2\mu m_3$	0

and

$$-(2p+1)(2p-3)(\nu+\mu)[(m-\mu)p(p-1)-m_3(n-\nu)(n+\nu+1)]a(m,n,\mu,\nu-1,p-1)$$

$$+(2p+1)(p-m_3-1)(n+\nu-p+2)(n-\nu+p-1)[\mu(p+\nu)+m\nu]a(m,n,\mu,\nu,p-2)$$

$$+(2p-3)(p+m_3)(n+\nu+p+1)(-n+\nu+p)[\mu(p-\nu-1)-m\nu]a(m,n,\mu,\nu,p)=0 \qquad (A11)$$

where $m_3 = m+\mu$. These can in turn be reduced to a single three-term recursion formula in the index p alone, but for this case it is computationally more efficient to simultaneously generate two sets of coefficients using the above two formulas.

Any recursion formula used for the purpose of generating special functions or coefficients is of questionable value unless the starting values are readily obtainable. For the present case this is very easily accomplished by matching coefficients in the highest powers of the argument from equation (A5) with the results:

$$a_{n+\nu} = \frac{(2n-1)!!(2\nu-1)!!}{(2n+2\nu-1)!!}\ \frac{(n+\nu-m_3)!}{(n-m)!(\nu-\mu)!}$$

$$a_{n+\nu-2} = -\frac{(2n+2\nu-3)}{2(2n-1)(2\nu-1)(n+\nu-m_3)(n+\nu-m_3-1)}$$

$$\times\{(n+\nu-1)[n\nu+m\mu(2n+2\nu-1)]-m_3[\nu m(2\nu-1)+n\mu(2n-1)]\}a_{n+\nu} \qquad (A12)$$

where $a_q \equiv a(m,n,\mu,\nu,q)$. This of course implies backward recursion.

These same starting values could also be determined from equation (A9) since in this case the Van der Waerden definition of the 3-j coefficient reduces to a single term for $p = n+\nu$ and three terms for

$p = n+\nu-2$, which can be easily combined; however, the coefficient matching procedure is preferable because of its simplicity. Several other useful recursion relations may be obtained. From (A5) and the product derivative

$$\frac{d}{d\theta}\left(P_n^m P_\nu^\mu\right) = P_n^m \frac{dP_\nu^\mu}{d\theta} + P_\nu^\mu \frac{dP_n^m}{d\theta} \tag{A13}$$

and the associated Legendre function derivative relations:

$$\frac{dP_n^m}{d\theta} = \frac{m\cos\theta}{\sin\theta} P_n^m - P_n^{m+1} \tag{A14}$$

and

$$\frac{dP_n^m}{d\theta} = -\frac{m\cos\theta}{\sin\theta} P_n^m + (n+m)(n-m+1)P_n^{m-1}\,, \tag{A15}$$

one may obtain the following relations (Cruzan, 1962):

$$a(m,n,\mu,\nu,p) = a(m+1,n,\mu,\nu,p) + a(m,n,\mu+1,\nu,p)\,, \tag{A16}$$

$$\begin{aligned}(p+m+\mu)(p-m-\mu+1)a(m,n,\mu,\nu,p) &= (\nu+\mu)(\nu-\mu+1)a(m,n,\mu-1,\nu,p) \\ &+ (n+m)(n-m+1)a(m-1,n,\mu,\nu,p)\,,\end{aligned} \tag{A17}$$

$$\begin{aligned}&[(p+m+\mu)(p-m-\mu+1)+(\nu-\mu)(\nu+\mu+1)-(n+m)(n-m+1)]a(m,n,\mu,\nu,p) \\ &= (\nu+\mu)(\nu-\mu+1)a(m,n,\mu-1,\nu,p) \\ &+ (p+m+\mu+1)(p-m-\mu)a(m,n,\mu+1,\nu,p)\,,\end{aligned} \tag{A18}$$

and

$$[(p+m+\mu)(p-m-\mu+1)+(n-m)(n+m+1)-(\nu+\mu)(\nu-\mu+1)]a(m,n,\mu,\nu,p)$$

$$= (n+m)(n-m+1)a(m-1,n,\mu,\nu,p)$$

$$+ (p+m+\mu+1)(p-m-\mu)a(m+1,n,\mu,\nu,p) \qquad \text{(A19)}$$

To this point it has been demonstrated that the coefficients $a(\cdot)$ can be determined in a considerably more efficient and systematic manner than appeal to the 3-j formulation.

A.2 General Vector Addition Theorem

Armed with the results in A.1, the vector spherical wave addition theorem can be more simply presented. This is obtained as a superposition of scalar spherical waves from equation (2.3) and the scalar addition theorem (A3) and (A7). The theorem reads:

$$\begin{aligned} \overline{M}_{mn}^{(j)'} &= \sum_{\nu=1}^{\infty}\sum_{\mu=-\nu}^{\nu}(A_{\mu\nu}^{mn}\,\overline{M}_{\mu\nu}^{(j)} + B_{\mu\nu}^{mn}\,\overline{N}_{\mu\nu}^{(j)}) \\ \overline{N}_{mn}^{(j)'} &= \sum_{\nu=1}^{\infty}\sum_{\mu=-\nu}^{\nu}(A_{\mu\nu}^{mn}\,\overline{N}_{\mu\nu}^{(j)} + B_{\mu\nu}^{mn}\,\overline{M}_{\mu\nu}^{(j)}) \end{aligned} \qquad \text{(A20)}$$

with

$$A_{\mu\nu}^{mn} = (-1)^{\mu} i^{\nu-n}\,\frac{2\nu+1}{2\nu(\nu+1)}\sum_{p} i^{-p}[n(n+1)+\nu(\nu+1)-p(p+1)]$$

$$\times\, a(m,n,-\mu,\nu,p)\,z_p^{(j)}(kd)\,P_p^{m-\mu}(\cos\theta_o)\,e^{i(m-\mu)\phi_o} \qquad \text{(A21)}$$

and

$$B_{\mu\nu}^{mn} = (-1)^{\mu} i^{\nu-n} \frac{2\nu+1}{2\nu(\nu+1)} \sum_{p} i^{-p} \times b(m,n,-\mu,\nu,p,p-1) z_p^{(j)}(kd) P_p^{m-\mu}(\cos\theta_o) e^{i(m-\mu)\phi_o} \quad (A22)$$

for $r \geq d$ where:

$$b(m,n,-\mu,\nu,p,p-1) = \frac{2p+1}{2p-1} [(\nu-\mu)(\nu+\mu+1) a(m,n,-\mu-1,\nu,p-1) - (p-m+\mu)(p-m+\mu+1) a(m,n,-\mu+1,\nu,p-1) + 2\mu(p-m+\mu) a(m,n,-\mu,\nu,p-1)]. \quad (A23)$$

The form given here for $A_{\mu\nu}^{mn}$ incorporates a factorization in which the factor $2\nu+1$ was extracted — this was apparently overlooked by Cruzan. Without this factorization, the obviousness of the asymptotic form of $A_{\mu\nu}^{mn}$ (Section A.4) for large translational distances is obscured. It was not noted by Stein or Cruzan that the theorem for $r \leq d$ could be obtained from that for $r \geq d$ by simply replacing $z_p^{(j)}(kd)$ by $j_p(kd)$. In addition, the form given here for $B_{\mu\nu}^{mn}$ (Cruzan, 1962) is not in the most desirable for computational purposes since three different coefficients of the type $a(m,n,-\mu,\nu,p-1)$ (see A23) preceeded by factors containing the index p must be available at the time of each summation in p. Furthermore, this form does not show explicitly the simplifications that result when translation is confined to the z-axis. Instead, the form given by Stein (1961) for $B_{\mu\nu}^{mn}$ is preferred which is:

$$B_{\mu\nu}^{mn} = -\frac{ikd\cos\theta_o}{2\nu(\nu+1)}\ 2\mu\ \alpha_{\mu\nu}^{mn}$$

$$-\frac{ikd\sin\theta_o}{2\nu(\nu+1)}\left[e^{i\phi_o}(\nu-\mu)(\nu+\mu+1)\alpha_{\mu+1,\nu}^{mn}+e^{-i\phi_o}\alpha_{\mu-1,\nu}^{mn}\right] \qquad \text{(A24)}$$

where $\alpha_{\mu\nu}^{mn}$ are the scalar wave addition theorem coefficients given by (A7).

For the case of vector translation from 0' to 0 (A20) remains the same except the unprimed quantities become primed and vice versa; the coefficient $A_{\mu\nu}^{mn}$ is preceded by the factor $(-1)^{n+\nu}$ and $B_{\mu\nu}^{mn}$ by $(-1)^{n+\nu+1}$.

A.3 Translation Along the z-Axis

There are cases (such as the two sphere problem) in which the origins 0 and 0' may be restricted to lie along the z-axis with no attendent loss in generality. As will become evident, this specialization admits many simplifications. Some of these are obvious but will be stated for clarity. Considering first the scalar case, one sees from (A7) that for z axis translation ($\theta_o = 0$ or π) the coefficient $\alpha_{\mu\nu}^{mn}$ vanishes for all values of μ except $\mu = m$ since $P_p^{m-\mu}(\pm 1)$ is non-zero only in such a case; hence (A7) becomes[†]

$$\alpha_{m\nu}^{mn} = (-1)^m i^{\nu-n}(2\nu+1)\sum_p i^{-p} a(m,n,-m,\nu,p) \begin{bmatrix} z_p^{(j)}(kd) \\ j_p(kd) \end{bmatrix}, \begin{bmatrix} r \le d \\ r \ge d \end{bmatrix} \qquad \text{(A25)}$$

[†] The scalar addition theorem for translation along the z axis for $r \ge d$ and $r' \ge d$ appears incorrectly in Liang and Lo (1967).

and since $u_{m\nu}^{(j)} = 0$ when $\nu < m$, (A3) becomes

$$u_{mn}^{(j)'} = \sum_{\nu=m}^{\infty} \alpha_{m\nu}^{mn} u_{m\nu}^{(1)} \tag{A26}$$

Similarly, it is easily seen that the vector addition theorem reduces to:

$$\begin{aligned} \bar{M}_{mn}^{'(j)} &= \sum_{\nu=(1,m)}^{\infty} \left[A_{m\nu}^{mn} \bar{M}_{m\nu}^{(1)} + B_{m\nu}^{mn} \bar{N}_{m\nu}^{(1)}\right] \\ \bar{N}_{mn}^{'(j)} &= \sum_{\nu=(1,m)}^{\infty} \left[A_{m\nu}^{mn} \bar{N}_{m\nu}^{(1)} + B_{m\nu}^{mn} \bar{M}_{m\nu}^{(1)}\right] \end{aligned} \tag{A27}$$

where $(1,m)$ denotes the larger of 1 and m, and

$$A_{m\nu}^{mn} = (-1)^m i^{\nu-n} \frac{2\nu+1}{2\nu(\nu+1)} \sum_p i^{-p[n(n+1)+\nu(\nu+1)-p(p+1)]} \times a(m,n,-m,\nu,p) \begin{bmatrix} z_p^{(j)}(kd) \\ j_p(kd) \end{bmatrix}, \begin{bmatrix} r \geq d \\ r \leq d \end{bmatrix} \tag{A28}$$

$$B_{m\nu}^{mn} = -\frac{imkd}{\nu(\nu+1)} \alpha_{m\nu}^{mn} \tag{A29}$$

Perhaps most significant are the simplifications involved in the calculation of the coefficients $a(m,n,-m,\nu,p)$. The recursion formulas (A10) and (A11) may be easily combined to yield:

$$\alpha_{p-3} a_{p-4} - (\alpha_{p-2}+\alpha_{p-1}-4m^2) a_{p-2} + \alpha_p a_p = 0 \tag{A30}$$

where $a_p \equiv a(m,n,-m,\nu,p)$

$\alpha_p = C(p)C(-p)$

and

$$C(p) = \frac{1}{2p+1}\,(n+\nu+p+1)(n-\nu+p).$$

The two starting values are

$$a_{n+\nu} = \frac{(2n-1)!!(2\nu-1)!!}{(2n+2\nu-1)!!}\;\frac{(n+\nu)!}{(n-m)!(\nu+m)!}$$

$$a_{n+\nu-2} = \frac{(2n+2\nu-3)}{(2n-1)(2\nu-1)(n+\nu)}\,[\nu n - m^2(2n+2\nu-1)]a_{n+\nu}. \tag{A31}$$

Clearly then, all coefficients can be generated without calculating a single 3-j coefficient.† Furthermore if these coefficients are generated in the proper sequence with regard to n, ν, and m, then no explicit factorials need be calculated. In other words, the starting coefficients can also be generated in a recurrent fashion (see Section 3.2).

A striking feature of the three term formula (A30) is that for m = 0 it reduces to the two term formula:

$$\alpha_p a(0,n,0,\nu,p) - \alpha_{p-1} a(0,n,0,\nu,p-2) = 0 \tag{A32}$$

which by successive application yields:

---

†It is worth noting that these new recursion formulas (A10), (A11), (A30) and the result (A6) could be used to obtain new recursion formulas for the 3-j coefficients. This is possible by simply using the definition of $a(\cdot)$ in terms of the 3-j symbols (A8) and extracting the special 3-j symbol for $m = \mu = 0$. The latter coefficient may always be extracted since it is known explicitly and never vanishes for $n+\nu+p$ an even integer.

$$a(0,n,0,\nu,p) = \frac{2p+1}{(n+\nu+p+1)} \frac{\binom{-n+\nu+p}{\frac{-n+\nu+p}{2}} \binom{n-\nu+p}{\frac{n-\nu+p}{2}} \binom{n+\nu-p}{\frac{n+\nu-p}{2}}}{\binom{n+\nu+p}{\frac{n+\nu+p}{2}}} \tag{A33}$$

This agrees with the formula given by Adams (1878), Hylleraas (1962), and could also have been obtained by using the special form for the 3-j coefficient for $m_1 = m_2 = 0$ (Edmonds, 1957).

By combining (A16) and (A17) one can obtain the following recursion formula in the azimuthal index m for the case $\mu = -m$ (which is useful for recursion in m):

$$\begin{aligned}[p(p+1)-(n+m)(n-m+1)-(\nu-m)(\nu+m+1)]a(m,n,-m,\nu,p) \\ = (\nu-m)(\nu+m+1)a(m+1,n,-m-1,\nu,p) \\ + (n+m)(n-m+1)a(m-1,n,-m+1,\nu,p),\end{aligned} \tag{A34}$$

and when m is set to zero, the above yields:

$$a(1,n,-1,\nu,p) = \frac{[n(n+1)+\nu(\nu+1)-p(p+1)]}{2\nu(\nu+1)} a(0,n,0,\nu,p) \tag{A35}$$

or

$$a(1,n,-1,\nu,p) = -\frac{2p+1}{2\nu(\nu+1)} \frac{[n(n+1)+\nu(\nu+1)-p(p+1)]}{(n+\nu+p+1)} \times \frac{\binom{-n+\nu+p}{\frac{-n+\nu+p}{2}} \binom{n-\nu+p}{\frac{n-\nu+p}{2}} \binom{n+\nu-p}{\frac{n-\nu+p}{2}}}{\binom{n+\nu+p}{\frac{n+\nu+p}{2}}} \tag{A36}$$

This situation corresponds to the case of axial symmetry which admits only the $m = \pm 1$ azimuthal modes in the vector theorem and in the two-sphere electromagnetic scattering problem, results when the source is incident along the common axis of the two spheres. The corresponding azimuthially symmetric case in the scalar problem requires only the $m = 0$ mode; hence the coefficients for this case are given by (A33).

Unfortunately there do not seem to be any further simple or closed forms for the $a(\cdot)$'s of great practical importance. Gaunt (1929) has shown that the coefficients may be reduced to more elementary forms when certain restrictions are placed on the indices. One special value of the coefficient $a(m,n,-m,\nu,p)$ useful for checking the stability of the recursion formula (A30) is:

$$a(m,n,-m,n,0) = (-1)^m/(2n+1). \qquad \text{(A37)}$$

Friedman and Russek (1954) give a short table of the coefficients $a(m,n,\mu,\nu,p)$ for some low orders of the index n.†

A.4 Asymptotic Forms

It would seem reasonable that one should be able to simplify the addition theorems when the translational distance kd is sufficiently large. It is shown below that indeed such a simplification exists; in fact, they can be reduced to a particularly simple form for the case when translation is restricted to the z-axis.

---

† The entry $a(1,2,\mu,\nu,\nu)$ in their Appendix II appears incorrectly and should read $\dfrac{3(2\mu+1)}{(2\nu+3)(2\nu-1)}$.

Working first with the scalar addition theorem, we have, as in (A7):

$$\alpha_{\mu\nu}^{mn} = (-1)^{\mu} i^{\nu-n}(2\nu+1) \sum_{p} i^{-p} a(m,n,-\mu,\nu,p) \begin{bmatrix} z_p^{(j)}(kd) \\ j_p(kd) \end{bmatrix} \times P_p^{m-\mu}(\cos\theta_o) e^{i(m-\mu)\phi_o} \qquad \text{(A7)}$$

for $\begin{bmatrix} r \geq d \\ r \leq d \end{bmatrix}$. What is sought is a simpler form for the above valid for large values of kd. It may be assumed in what follows that $z_p(kd) = h_p^{(1)}(kd)$, since if a simpler form can be found for the above case, then it is also known for $h_p^{(2)}(kd)$ and hence also for $j_p(kd)$ and $n_p(kd)$. If $kd > 0(p^2)$ where $p \leq n+\nu$, then:

$$h_p^{(1)} \approx i^{-p-1} \frac{e^{ikd}}{kd} \qquad \text{(A38)}$$

and (A7) reduces to

$$\alpha_{\mu\nu}^{mn} \approx (-1)^{\mu} i^{\nu-n}(2\nu+1) \frac{e^{ikd}}{ikd} e^{i(m-\mu)\phi_o} \sum_{p} (-1)^{p} a(m,n,-\mu,\nu,p) \times P_p^{m-\mu}(\cos\theta_o) \qquad \text{(A39)}$$

and since $p = n+\nu, n+\nu-2, \ldots, |n-\nu|$, the $(-1)^p$ factor may be removed as $(-1)^{n+\nu}$. The remaining summation may then be identified as just the linearization expansion (A5) and we obtain as a result:

$$\alpha_{\mu\nu}^{mn} \approx (-1)^{\mu} i^{n-\nu-1}(2\nu+1) \frac{e^{ikd}}{kd} P_n^m(\cos\theta_o) P_\nu^{-\mu}(\cos\theta_o) e^{i(m-\mu)\phi_o}, \quad kd > 0(n+\nu)^2 \qquad \text{(A40)}$$

For z-axis translation (say $\theta_o = 0$), the above simplifies to:

$$\alpha_{\mu\nu}^{mn} \approx i^{n-\nu-1}(2\nu+1)\,\frac{e^{ikd}}{kd}\,\delta_{m,o}\delta_{\mu,o} \tag{A41}$$

For the vector case, applying (A38) to (A21) yields

$$A_{\mu\nu}^{mn} \approx (-1)^{\mu} i^{n-\nu-1}\,\frac{2\nu+1}{2\nu(\nu+1)}\,\frac{e^{ikd}}{kd}\,e^{i(m-\mu)\phi_o}\sum_{p}$$

$$\times\,[n(n+1)+\nu(\nu+1)-p(p+1)]\;a(m,n,-\mu,\nu,p)P_p^{m-\mu}(\cos\theta_o)\,. \tag{A42}$$

The summation in (A42) cannot be formed as in (A39) due to the presence of the factor $p(p+1)$. This can be summed, however, by combining (A16) and (A17) with the result.

$$\sum_{p}[n(n+1)+\nu(\nu+1)-p(p+1)]a(m,n,-\mu,\nu,p)P_p^{m-\mu}$$

$$= 2\mu m P_n^m P_\nu^{-\mu} - (\nu-\mu)(\nu+\mu+1)P_n^{m+1}P_\nu^{-\mu-1}$$

$$- (n+m)(n-m+1)P_n^{m-1}P_\nu^{-\mu+1} \tag{A43}$$

With this, (A42) becomes:

$$A_{\mu\nu}^{mn} \approx (-1)^{\mu} i^{n-\nu-1}\,\frac{2\nu+1}{2\nu(\nu+1)}\,\frac{e^{ikd}}{kd}\,e^{i(m-\mu)\phi_o}[2\mu m P_n^m(\cos\theta_o)P_\nu^{-\mu}(\cos\theta_o)$$

$$- (\nu-\mu)(\nu+\mu+1)P_n^{m+1}(\cos\theta_o)P_\nu^{-\mu-1}(\cos\theta_o)$$

$$- (n+m)(n-m+1)P_n^{m-1}(\cos\theta_o)P_\nu^{-\mu+1}(\cos\theta_o)]. \tag{A44}$$

If now (A38) is used in (A24), $B_{\mu\nu}^{mn}$ is identically zero, in which case, the next higher order expansion for $h_p^{(1)}(kd)$ must be used:

$$h_p^{(1)}(kd) \approx i^{-p-1}\,\frac{e^{ikd}}{kd}\left[1 + \frac{i}{2kd}\,p(p+1)\right] \tag{A45}$$

To this order, (A43) and (A45) are combined with (A39) to yield:

$$\alpha_{\mu\nu}^{mn} \approx (-1)^{\mu} i^{n-\nu-1}(2\nu+1)\,\frac{e^{ikd}}{kd}\,e^{i(m-\mu)\phi_o}$$

$$\times\left(P_n^m P_\nu^{-\mu} + \frac{i}{2kd}\left\{\left[n(n+1)+\nu(\nu+1)-2\mu m\right]P_n^m P_\nu^{-\mu}\right.\right.$$

$$\left.\left. + (\nu-\mu)(\nu+\mu+1)P_n^{m+1}P_\nu^{-\mu-1} + (n+m)(n-m+1)P_n^{m-1}P_\nu^{-\mu+1}\right\}\right) \qquad \text{(A46)}$$

Using this in (A24) gives the asymptotic form for $B_{\mu\nu}^{mn}$ to the same order as $A_{\mu\nu}^{mn}$. Finally for z-axis translation ($\theta_o = 0$) it is clear from (A24), (A46), and (A44) that we get

$$A_{\mu\nu}^{mn} = B_{\mu\nu}^{mn} \approx i^{n-\nu-1}\,\frac{2\nu+1}{2\nu(\nu+1)}\,\frac{e^{ikd}}{kd}\,\delta_{m\mu}\left[\nu(\nu+1)\delta_{m,-1}+n(n+1)\delta_{m,1}\right]. \qquad \text{(A47)}$$

LIST OF REFERENCES

Adams, J. C. (1878), On the expression for the product of any two Legendre's coefficients by means of a series of Legendre's coefficients, Proc. Roy. Soc. (London), Vol. 27, 63.

Aden, A. L. and M. Kerker (1951), Scattering of electromagnetic waves by two concentric spheres, J. Appl. Phys., 22, 1242.

Ament, W. S. (1959), Wave propagation in suspensions, U. S. Naval Research Laboratory Report No. 5307.

Angelakos, D. J. and K. Kumagai (1964), High-frequency scattering by multiple spheres, IEEE Trans. Ant. Prop., AP-13, No. 1, 105.

Beckmann, P. (1968), The depolarization of electromagnetic waves (The Golem Press, Boulder, Colorado).

Blacksmith, P., R. E. Hiatt and R. B. Mack (1965), Introduction to radar cross-section measurements, Proc. IEEE, 53, No. 8, 901.

Bonkowski, R. R., C. R. Lubitz and C. E. Schensted (1953), Studies in radar cross-section VI: cross sections of corner reflectors and other multiple scatters at microwave frequencies, Rept. No. UMM-106, E.R.I., Univ. of Mich., Ann Arbor, Mich.

Born, M. and E. Wolf (1964), Principles of Optics (Pergamon Press, New York, N. Y.).

Bruning, J. and Y. T. Lo (1967), Electromagnetic scattering by two spheres, 1967 Fall URSI Meeting, Ann Arbor, Mich.

Bruning, J. and Y. T. Lo (1968), Electromagnetic scattering by two spheres, Proc. IEEE 56, No. 1, 119.

Burke, J. E. and V. Twersky (1964), On scattering of waves by many bodies, Radio Science, 680, 500.

Corbató, F. J. and J. L. Uretsky (1959), Generation of spherical Bessel functions in digital computers, J. Assoc. Comp. Mach., 6, 366.

Crane, R. K. (1967), Cooperative scattering by dielectric spheres, Technical Note 1967-31, Lincoln Laboratory, M.I.T., Lexington, Massachusetts.

Cruzan, O. R. (1962), Translational addition theorems for spherical vector wave functions, Quart. Appl. Math., 20, 33.

Danos, M. and L. C. Maximon (1965), Multipole matrix elements of the translation operator, J. Math. Phys., 6, No. 5, 766.

Deschamps, G. A. (1967), Matrix methods in geometrical optics, 1967 Fall URSI Meeting, Ann Arbor, Mich.

Edmonds, A. R. (1957), Angular Momentum in Quantum Mechanics (Princeton University Press, Princeton, N. J.).

Eyges, L. (1957), Some nonseparable boundary value problems and the many-body problem, Annals of Physics, 2, 101.

Fahlen, T. S., H. C. Bryant (1968), Optical back scattering from single water droplets, J. Optical Soc. Am., 58, No. 3, 304.

Franz, W. (1954), Über die Greenschen funktionen des zylinders und der kugel, Z. fur Naturforschung, 9, 705.

Franz, W. and K. Depperman (1952), Theorie der beugung am zylinder unter berücksichtigung der kriechwelle, Ann. Phys. Dtsch., 10, 361.

Freeny, C. C. (1965), Target support parameters associated with radar reflectivity measurements, Proc. IEEE, 53, No. 8, 929.

Friedman, B. and J. Russek (1954), Addition theorems for spherical waves, Quart. Appl. Math., 12, No. 1, 13.

Gaunt, J. A. (1929), On the triplets of helium, Philos. Trans. Roy. Soc. (London), Ser. A228, 151.

Gautschi, W. (1967), Computational aspects of three-term recurrence relations, SIAM Rev., 9, No. 1, 24.

Germogenova, O. A. (1963), The scattering of a plane electromagnetic wave by two spheres, Akad. Nauk SSSR, Izvestiia, Ser. Geofiz, No. 4, 648.

Hardy, G. H. (1923), A chapter from Ramanujan's note-book, Proc. Camb. Phil. Soc., Vol. 21, 492.

Hylleraas, E. A. (1962), Linearization of products of Jacobi polynomials, Math. Scand., 10, 189.

Infeld, L. and T. E. Hull (1951), The factorization method, Reviews Modern Physics, 23, 54.

Jones, D. S. (1964), The Theory of Electromagnetism (Pergamon Press, New York, N. Y.).

Karp, S. N. (1953), Diffraction by combinations of obstacles, Proc. McGill Symp. Microw. Opt., 198.

Kattawar, G. W. and G. N. Plass (1967), Resonance scattering from absorbing spheres, Appl. Optics, 6, No. 9, 1549.

Knott, E. F. (1964), An indoor radar scattering range, Radar Reflectivity Measurements Symposium, Rome Air Development Center, New York, Tech. Doc. Rept. RADC-TDR-64-25 (April), Vol. II: AD 601 365.

Levine, S. and M. Kerker (1963), Scattering of electromagnetic waves from two concentric spheres, when outer shell has a variable refractive index. Published in Electromagnetic Scattering, edited by M. Kerker (Pergamon Press, Oxford).

Levy, B. R. and J. B. Keller (1959), Diffraction by a smooth object, Comm. Pure Appl. Math., XII, No. 1, 159.

Levy, B. R. and J. B. Keller (1960), Diffraction by a spheroid, Can. J. Phys., 38, 128.

Liang, C. and Y. T. Lo (1967), Scattering by two spheres, Radio Science, 2, No. 12, 1481.

Lillesaeter, O. (1964), Scattering of microwaves by adjacent water droplets in air, Proc. of the World Conference on Radio Meteorology (incorporating the 11th Weather Radar Conference), Boulder, Colorado, September 14-18.

Logan, N. A. (1962), Early history of the Mie solution, J. Opt. Soc. Am., 52, 342.

Logan, N. A. (1965), Survey of some early studies of the scattering of plane waves by a sphere, Proc. IEEE, 53, No. 8, 773.

Mével, J. (1960), Contribution de la diffraction des ondes electromagnetiques par les spheres, Annales de Physique, 265.

Mie, G. (1908), Beiträge zur optik trüber medien, speziell kolloidaler metallosungen, Ann d. Physik, Vol. 25, 377.

Morse, P. and H. Feshbach (1953), Methods of Theoretical Physics, Vol. II (McGraw-Hill Book Co., Inc., New York, N. Y.).

Nuzzenzveig, H. M. (1969), High-frequency scattering by a transparent sphere. Parts I and II, J. Math. Phys., 10, No. 1, 125.

Rose, M. E. (1955), Multipole Fields (John Wiley & Sons, Inc., New York, N. Y.).

Rotenberg, M. R., R. Bivins, N. Metropolis and J. K. Wooten, Jr. (1959), The 3-j and 6-j symbols (Technology Press, M.I.T., Cambridge, Massachusetts).

Row, R. V. (1955), Theoretical and experimental study of electromagnetic scattering by two identical conducting cylinders, J. Appl. Phys., 26, No. 6, 666.

Sack, R. A. (1964), Three-dimensional addition theorem for arbitrary functions involving expansions in spherical harmonics, J. Math. Phys., 5, No. 2, 252.

Sato, Y. (1950), Transformation of wave-functions related to transformations of coordinate systems, Bull. Earthquake Research Inst. Tokyo, 28, 1 and 175.

Senior, T. B. A. (1965), Analytical and numerical studies of the back scattering behavior of spheres, Tech. Rept. No. 7030-1-T, AF 04(694)-683, Univ. of Mich., Ann Arbor, Mich.

Senior, T. B. A. and R. F. Goodrich (1964), Scattering by a sphere, Proc. IEE (London), Vol. III, 907.

Stein, S. (1961), Addition theorems for spherical wave functions, Quart. Appl. Math., 19, No. 1, 15.

Stratton, J. A. (1941), Electromagnetic Theory (McGraw-Hill Book Co., Inc., New York, N. Y.).

Todd, J. (1962), Survey of Numerical Analysis (McGraw-Hill Book Co., Inc., New York, N. Y.).

Trinks, W. (1935), Zur vielfachstreuung an kleinen kugeln, Ann. Phys. Dtsch., 22, 561.

Twersky, V. (1952), Multiple scattering of radiation by an arbitrary planar configuration of parallel cylinders and by two parallel cylinders, J. Appl. Phys., 23, 407.

Twersky, V. (1960), On multiple scattering of waves, J. Res. NBS 640 (Radio Prop.), No. 6, 715.

Twersky, V. (1962), Multiple scattering by arbitrary configurations in three dimensions, J. Math. Phys., 3, 83.

Twersky, V. (1967), Multiple scattering of electromagnetic waves by arbitrary configurations, J. Math. Phys., 8, No. 3, 589.

Van de Hulst, H. C. (1957), Light Scattering by Small Particles (John Wiley & Sons, Inc., New York, N. Y.).

White, F. P. (1922), The diffraction of plane electromagnetic waves by a perfectly reflecting sphere, Proc. Roy Soc. (London), Vol. 100, 505.

Zitron, N. R. and S. N. Karp (1961a), Higher-order approximations in multiple scattering; I. Two-dimensional scalar case, J. Math. Phys., 2, 394.

Zitron, N. R. and S. N. Karp (1961b), Higher-order approximations in multiple scattering; II. Three-dimensional scalar cases, J. Math. Phys., 2, 402.